UNIVERSITÀ degli STUDI di CATANIA
Dipartimento di Agricoltura, Alimentazione e Ambiente
Di3A

UNIVERSITÀ DEGLI STUDI DI CATANIA

PH.D. IN "AGRICULTURAL, FOOD, AND ENVIRONMENTAL SCIENCE"

Wind-driven natural ventilation in a semi-open free-stall barn for dairy cows: CFD simulation and analysis of alternative barn design

Nicoletta Tomasello

Advisor:
Prof. Giovanni Cascone

Coordinator:
Prof. Cherubino Leonardi

Ph.D. attended during 2016/2019

Index

1. Abstract and sommario

Natural ventilation is the most common passive cooling system in livestock buildings. The aim of this research was to assess airflow distribution inside a free-stall barn for dairy cows by computational fluid dynamics (CFD) modelling and simulation. The barn and the closer context were modelled in Autodesk Autocad 2016® and, by using Ansys ICEM 17.1®, the related mesh was built and the boundary conditions assigned. Then, by using Ansys Fluent 17.1® software tool, indoor natural ventilation was simulated taking into account as simulation parameters airflow velocities typical for the reference period and collected by the closest meteorological station. Simulations were carried out in steady-state conditions, and simulated data were validated by the average values of air velocity measurements. Since the modelled air velocity distribution in the barn fits the real one well, the CFD model was considered validated. The air velocity inside the barn, both simulated and measured, was too low, a condition that leads to discomfort in cows. To confirm the result, the dairy cow behaviour in the reference period was studied through visual examination of time-lapse video-recordings obtained from a multi-camera system. Therefore, alternatives design configurations of the barn were evaluated in order to find the best condition for the well-being of animals. The case study was considered relevant because it is located in a region characterised by hot climate conditions during the summer that could induce animal heat stress and by the presence of many similar cases. Therefore, the methodology applied in this thesis can represent an example to study the wind driven natural ventilation of barns having similar characteristics.

La ventilazione naturale è il sistema più comune di ventilazione passiva utilizzato negli edifici zootecnici. Lo scopo della presente ricerca è stato quello analizzare la distribuzione del flusso d'aria all'interno di una stalla per l'allevamento a stabulazione libera di vacche da latte adoperando la metodologia CFD (computational fluid dynamics). La stalla e l'immediato contesto sono stati modellati adoperando Autodesk Autocad 2016® e, utilizzando Ansys ICEM 17.1®, la relativa mesh è stata costruita e le condizioni al contorno assegnate. Successivamente, adoperando Ansys Fluent 17.1®, la ventilazione naturale interna è stata simulata adottando come parametri le velocità del flusso d'aria tipiche del periodo di riferimento e misurate dalla stazione metereologica più prossima alla stalla. Le simulazioni sono state condotte in condizioni stazionarie e i dati simulati sono stati validati dai valori medi delle velocità medie sperimentali acquisite. Dal momento che la distribuzione della velocità dell'aria simulata rispecchia quella reale, il modello CFD è stato considerato validato. La velocità dell'aria, sia simulata che misurata, è risultata troppo bassa, condizione che comporta discomfort alle vacche. Per confermare quanto riscontrato, il comportamento delle vacche da latte allevate all'interno della stalla è stato studiato nel periodo di riferimento attraverso l'esame visivo delle registrazioni video time-lapse ottenute da un sistema multicamera. Di conseguenza, diverse alternative progettuali della stalla sono state valutate al fine di trovare quella migliore dal punto di vista del benessere per gli animali. Il caso studio è stato considerato di interesse in quanto localizzato in una regione caratterizzata da un clima estivo molto caldo – che può indurre stress agli animali – e dalla presenza di molti edifici simili a quelli in esame. Di conseguenza, la metodologia applicata in questa tesi può

rappresentare un esempio al fine di studiare la ventilazione naturale generata per effetto del vento in stalle aventi caratteristiche similari a quella oggetto di studio.

2. Introduction

2.1 Introduction to natural ventilation

2.1.1 General definition and advantages of natural ventilation

Natural ventilation is the process of providing air to and removing air from an indoor space without using mechanical systems. Therefore, it represents a sustainable design strategy.

Natural ventilation depends on different factors, i.e. the number of openings in the envelope, the internal distribution of flow pattern and the air pressure difference between internal and external. In a naturally ventilated building envelope, the ventilation occurs through the opening thanks to two phenomena: the action of the wind and the buoyancy (Etheridge, 2015), as reported in the paragraph 2.3.2.

Today, natural ventilation represents an intensive research field. After a considerable decrease during to the 20th century on behalf of mechanical ventilation, the studies on natural ventilation increased again during the 21th century thanks to the advantages that it gives, such as:

- the reduction of energy consumption (Alloca et al., 2003; Bournet and Boulard, 2010; Bjerg et al., 2013);
- the well-being improving of users and animals, obtained more easily compared to air-conditioned buildings (Zhiqiang et al., 2015); in fact, "sick building syndrome" is often associated with HVAC (heating, ventilating and air-conditioning) systems;
- the lack of environmental impact (Energy efficiency Best Practice Programme, 1998);
- the lower construction, operation and maintenance cost required (Asfour, 2015);

Regarding the energy consumption, the energy cost of a naturally ventilated building is typically 40% lower than that of mechanically ventilated building (Alloca et al., 2003; CISBE, 1997).
Many agricultural buildings are naturally ventilated in order to reduce energy cost addressed to indoor climate control (Bournet and Boulard, 2010; Bjerg et al., 2013a).
It represents one of the most used strategies for passive cooling of livestock buildings and is generally preferred for dairy barns (Shen et al., 2013).

2.1.2 The development of natural ventilation study

Natural ventilation studies started from the first necessity to have thermal comfort and to supply the air in the dwellings. The first studies related to natural ventilation focused on the recognition of connection between well-being, air exchange and minimum ventilation rate.
Natural ventilation through windows was the only way to ventilate buildings before the development of the electric power industry in the late 19th century. In 1925, a code of "Minimum Requirements for Heating and Ventilation of Buildings" was published in the ASHVE Guide, providing a minimum ventilating rate for the 1946 American Standards Association (ASA) lighting standard.
The last important researches studies can be identified in the past fifty years. Based on the ASHVE research, ASHRAE Standard 55 for thermal comfort and Standard 62 for ventilation were developed. The first one, called "*ANSI/ASHRAE Standard 62-1973, Standards for Natural and Mechanical Ventilation*", reported minimum and recommended ventilation rates for 266 applications and was the basis for many state codes. "*Standard 62-1989, Ventilation for Acceptable Indoor Air Quality*" was later

taken as a reference because it was based on the latest research on odour. Many papers refer to this period: Tiller (1973) based his research on the cost/benefit of outdoor air for ventilation; Cain et. al (1983), Fanger et. al, (1984) and Janssen (1986) studied minimum ventilation rates necessary to dilute occupant odour; Janssen et. al (1982) studied the response of school children to CO_2-controlled ventilation.
Until 1973, the use of mechanical ventilation was much more common than the use of natural ventilated system, because the energy was cheap and the results in thermal comfort acceptable. In these years, the study of mechanical ventilation increased and the ventilation approach lost its importance in building research, also because mechanical ventilation was more predictable and satisfied very well thermal comfort and indoor air quality standards (da Graça and Linden, 2016).
After the oil crisis of 1973, and the awareness of the limit of energy availability, the development of energy policies addressed to reduce the global energy consumption was observed.
In this period, building researches in Western countries developed. With the new guidelines, buildings needed less energy thanks to the use of construction techniques based on innovative envelope, equipped with an insulation layer and designed in order to reduce air infiltration. Infiltrations cause an uncontrolled movement of air to and from the building (Asfour, 2015). The infiltration topic - as international problem - was object of a Conference in the 1980 organized by the Air Infiltration Centre (AIC, 1980). On the other hand, these new solutions – addressed only to a reduction of energy – lead to an increase of humidity condensation and growth of mould, so to a proliferation of building related sickness of the occupants. This fact leads to consider not only the energy needs but also the quality of indoor and outdoor environment:

"Energy efficiency" was born. Research studies focused on this topic, started in 1990s, are still in progress and implementation, and a new design approach can be observed together with some changes in HVAC systems, i.e. the prohibition to use CFCs (chlorofluorocarbons).
Many international competitions, like the ZEPHYR European Architectural Ideas Competition held in Dublin in 1994, were characterized by the exposure of projects based on the use of passive cooling systems

2.1.3 Comparison with mechanical ventilation

Mechanical ventilation is based on a mechanically generated power to drive airflow. It is divided in mechanical extract, mechanical supply and mechanical balanced ventilation, according to the purpose of the mechanical ventilation system (CIBSE, 1997).
Obviously, in addition to the mentioned advantages, the natural ventilation energy is preferred to the mechanical energy also because is totally renewable and has no impact on the environment. In fact, it can provide thermal comfort without (or almost without) using air conditioning system, with consequent reduction or elimination of energy use for active air conditioning and associated costs (Hawendi and Gao, 2017; da Graça and Linden, 2016; Ahmed, 2017).
Although the advantages of natural ventilation are considerable, there are some disadvantages. The pressure difference relative to the natural ventilation, and in general the forces that drive it, are difficult to study because of their variability (Linden, 1999). In fact, the term "natural" can be associated with the term "random", and its control in a building can be problematic and uncertain.

2.1.4 General design rules

Natural ventilation effectiveness of buildings strongly depends on the design phase: contrary to mechanical ventilation, it cannot be integrated in a second step.

Table 1. Qualitative and quantitative information about the interactions between building characteristics and natural ventilation

QUALITATIVE INFORMATIONS	QUANTITATIVE INFORMATIONS
Design context background	Calculations techniques to define climate parameters
Design criteria	Sizing openings
Design concepts	Estimating airflow rate
	Evaluation method

Below are reported some design rules that should be follow in the design phase.

1. In the rural site (object of this thesis), i.e. located not in an urban area but surrounded by some buildings and vegetative barriers, the **best location** should be the one that allow the cross ventilation through the shortest section of the building. Regarding the **distance from the other buildings**, the building should be positioned with a distance that is bigger than the depth of their wake, so that they will not shelter it from summer winds (Santamouris et al., 1998). If it is not possible, the longitudinal axis should be perpendicular to the prevalent summer wind exposure.
2. **Internal spaces** should be distributed to allow the best configuration for the natural ventilation, so to permit the

cross ventilation. The partitions perpendicular to the flow should be reduced to minimum in order to reduce the obstructions to airflow path.

3. The **size of the openings** should be estimated depending on climate conditions, local obstructions and windows characteristics. Two types of sizing methods are usually applied:

- simplified empirical methodologies, applied to calculate inlet and outlet areas for cross-ventilation in a single room, by neglecting the buoyancy forces;
- computerized iterative methods, based on network models reported below.

4. The **shape and inclination of the roof** should be accurately studied because, depending on the type of roof and the inclination of the roof, the shape and the size of downwind eddy is different, as well as the air pressure distribution on the surfaces.

2.2 Mathematical concepts and fundamentals of natural ventilation

2.2.1 Wind structure near the ground and the concept of "turbulence"

Wind represents an irregular physical phenomenon. The "irregularity" – that decreases with the height - can be described by the term "*turbulence*", that is generated in the low atmospheric layer by the variation of thermal airflow and by the presence of obstacles.

Figure 1. The typical measured wind velocity time history (image from "Multisensors On-Site Monitoring and Characteristic Analysis of UHV Transmission Tower")

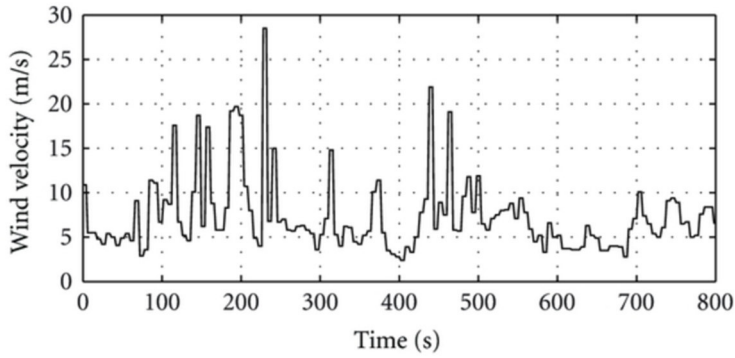

So, the instantaneous wind velocity can be calculated using a statistical approach, i.e.:

Instantaneous wind velocity u(t) =
average velocity $\bar{u}$ *+ fluctuating velocity* $u'(t)$
(Reynold decomposition of a velocity vector)

where: $\bar{u} = \frac{1}{T}\int_{t_0}^{t_0+T} u(t)dt$ and T, in the lower part of the atmosphere, is 10-60 minutes. It is assumed that the average process is independent of time and period T is the average operator should converge in a quadratic mean.
Due to adherence and non-permeability conditions, the vertical and lateral mean velocity components of a homogenous flow over a flat surface are 0.
The components of instantaneous velocity vector V(t) are:

- $\bar{u} + u'(t)$, with $u'(t)$=longitudinal fluctuation;
- $\bar{v} + v'(t)$, with $v'(t)$=lateral fluctuation;

- $\bar{w} + w'(t)$, with $w'(t)$=vertical fluctuation.

In general case for building applications, we should consider two factors to understand the assumption made to express the air velocity:

1. The effects of thermal stratification of the wind velocity can be neglected, so the flow direction can be assumed as a constant in a layer near to the ground (about 100 m).
2. The terrain contains an aggregate of obstacles (such as hills and buildings) called *roughness elements*, that affect the variables within the atmosphere. The dynamical effect of this complex rough surface affects the transfer of momentum from the wind to the ground, so the mean atmospheric flow field should be adjusted according to the local roughness. In general, the average velocity decreases for an increasing roughness of the ground.

As consequence, the nature of the ground surface and the presence of obstacles must be classified and taken into account, because the roughness height is a function of the nature of the ground and the geometry of existing obstacles.

There are two mathematical expressions used to represent the atmospheric boundary layer: the *power-law* and the *log-law*. The power-law has no theoretical justification but fits the profile of the mean velocity well when the correct parameters are defined. The log-law is based on physical principles and can represent the lower regions of the atmospheric boundary layer.

As reported below, these laws are used to calculate the wind speed as a function of wind velocity measurements from meteorological data at a fixed height, generally 10 m above the ground level.

2.2.1.1 Log-law

The log-law is represented by the Equation 1 (Richards and Hoxey, 1993):

$$U_z = \frac{u_*}{K_v} ln \left[\frac{z + z_0}{z_0}\right] \quad (1)$$

where:

- U_z is the average wind speed at the height z above the ground;
- z_0 is the surface roughness;
- u_* is the friction velocity;
- K_v is the von Karman's constant, equal to 0.35-0.42.

With regard to the surface roughness, it is classified by tables (Wieringa, 1992; Wu et al., 2012).

With regard to friction velocity, it is calculated from a specified velocity U_{ref} at a reference height h as reported in the Equation 2:

$$u_* = \frac{K_v U_{ref}}{\ln(\frac{h + z_0}{z_0})} \quad (2)$$

2.2.1.2 Power-law

Wind power law can be used to calculate the air inflow velocity profile. It is represented by the Equation 3:

$$\frac{U_y}{U_{ref}} = \left(\frac{Y}{Y_{ref}}\right)^{\alpha} \quad (3)$$

where:

- U_{ref} is the mean velocity at reference height;
- Y_{ref} is the reference height;

- α is the power law exponent.

With regard to the power law exponent, for an open rural field and for a building located in an open farmland with few trees and buildings, the exponent α=0.14 should be utilized (Shen et al., 2013; Sullivan and Greeley, 1993; Schlichting, 1979; Wu et al., 2012; Wieringa, 1992).

2.3. The effect of wind on buildings

Airflow inside buildings can affect different factors, i.e. environmental ones (temperature, pressure, etc.), pollutants emissions and animals' well-being.

2.3.1. Wind pressure distribution on buildings: the pressure coefficient C_p on building envelope

Wind creates a pressure distribution around buildings. In particular, positive pressure is created on building windward side (generally, the inflow) and suction areas are generated on the sidewalls and on the leeward sides (generally, the outflow), so – inside the building – negative pressure that lead to the development of airflow is generated.

Bernoulli's equation expresses the relation between velocity and pressure at different points of flow field. After the assumption of constant density along a streamline at a given height, it is written as reported in the Equation 4:

$$Pstat + 0.5\rho v^2 = Costant \quad (4)$$

where P_{stat} = static pressure.

The pressure distribution created by the wind is calculated by correcting the wind average dynamic pressure coefficient called pressure coefficient C_p, so:

$$wind\ induced\ pressure\ =\ \Delta P_w\ =\ 0.5 C_p \rho v^2 \qquad (5)$$

Considering a reference dynamic pressure P_{dyn} at a height equal to z_{ref}, for a given direction θ, the pressure coefficient C_p in a point A (x, y, z) is given by:

$$Cp_s(z_{ref};\ \theta) = [P - P_0(z)] \cdot \left[P_{dyn}(z_{ref})\right]^{-1} \qquad (6)$$

where:

- $P_{dyn}(z_{ref}) = 0.5 \rho_{out} v^2(z_{ref})$
- ρ_{out} = outdoor air density
- P=measured pressure
- P_0=reference atmospheric pressure

Figure 2. An example of contours of statistical values of local wind pressure coefficients (http://www.wind.arch.tkougei.ac.jp/info_center/windpressure/lowrise/Introductionofthedatabase.pdf)

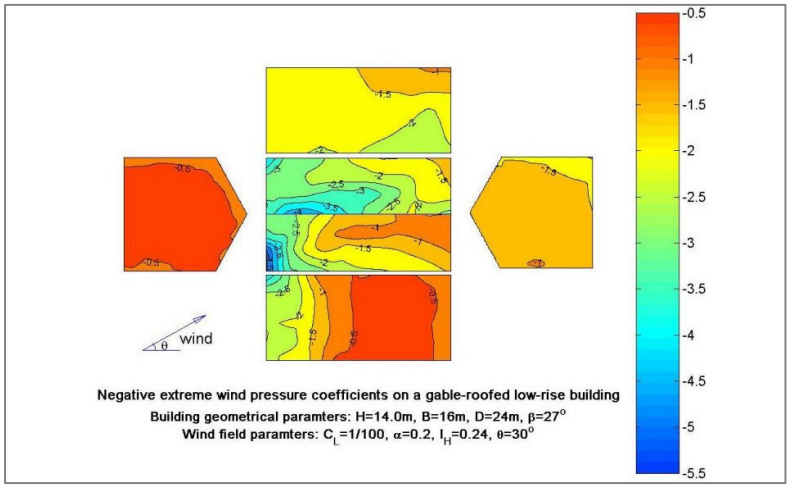

The parameters that affect the distribution of C_p can be grouped as reported in the Table 2:

Table 2: Parameters affection C_p distribution (Santamouris et al., 1998)

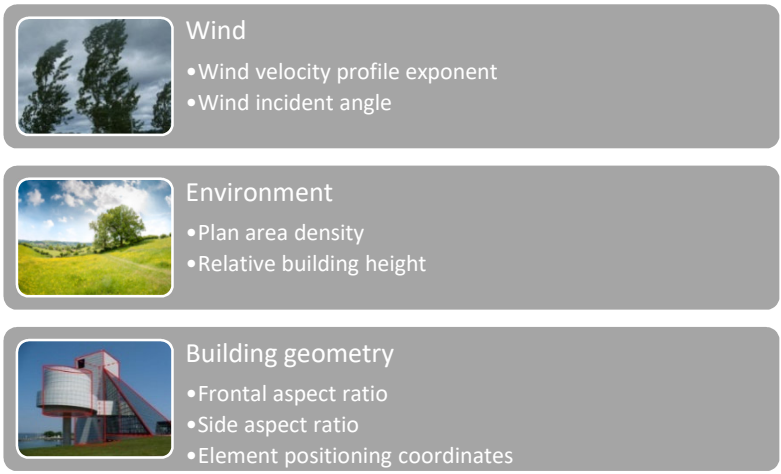

To calculate C_p it is possible to use table that correlate façade characteristics (i.e. nature, aspect ratio and exposure) with pressure coefficient C_p (Clarke et al., 1990) or use models as the one of Grosso (1992), based on climate, environmental and building parameters.

2.3.2 The mass transfer prediction: the driving forces in the environment

For steady, incompressible and non-viscous flow, the Navier-Stokes equations are integrated and reduced, obtaining the Bernoulli equation that is the fundamental equation to understand the behaviour of airflows in a building:

$$\frac{1}{2}\rho V^2 + P + \rho g z = costant \quad (7)$$

This equation combines:
- the transport effect upon a field of density of the flow velocity;
- the pressure gradient effect;
- the gravity effect.

Natural ventilation is generated by pressure differences due to wind (wind-driven natural ventilation) and buoyancy forces (stack-driven natural ventilation) that act on the openings in the building envelope (da Graça and Linden, 2016), i.e. pressure difference results from the combined action of two different mechanisms: wind and temperature difference.

Wind driven natural ventilation

Wind driven natural ventilation is the internal ventilation induced by the external wind entering from the openings. As discussed previously, the wind creates a pressure distribution around the building given by:

$$P_s = Cp\frac{1}{2}\rho V_H^2 \quad (8)$$

where:
- V_H = mean velocity at upwind building height;
- ρ = outdoor air density as function of atmospheric pressure, temperature and humidity.

Buoyancy or stack-driven natural ventilation

The buoyancy or stack effect influences the ventilation rate of a building and is due to air density differences between inside and outside or between two zones, so to the temperature differences:

$$\rho = \rho_0 \frac{T_0}{T} \quad (9)$$

where T is the absolute temperature (K), T_0 = 273.15 K and ρ_0 = 1.29 kgm^{-3}.

By considering two points A and B belong to two different zones (Figure 3), the pressure difference between two sides of an opening $P_i - P_j$ is:

$$\Delta P = P_i - P_j = P_A - P_B + P_{st} \quad (10)$$

with:

- P_A, P_B = pressure at point A, B
- $P_{st} = \rho_A g(z_A - z_i) - \rho_B g(z_B - z_j)$ = pressure difference created by buoyancy or stack effect, where:
    - ρ_A, ρ_B = air density at point A, B
    - z_i, z_j = relative heights of the leakage in each zone
    - z_A, z_B = reference height at point A, B

The air density, in this context, is mainly a function of the moisture content of the air (Feustel et al., 1990).

Figure 3. The stack effect

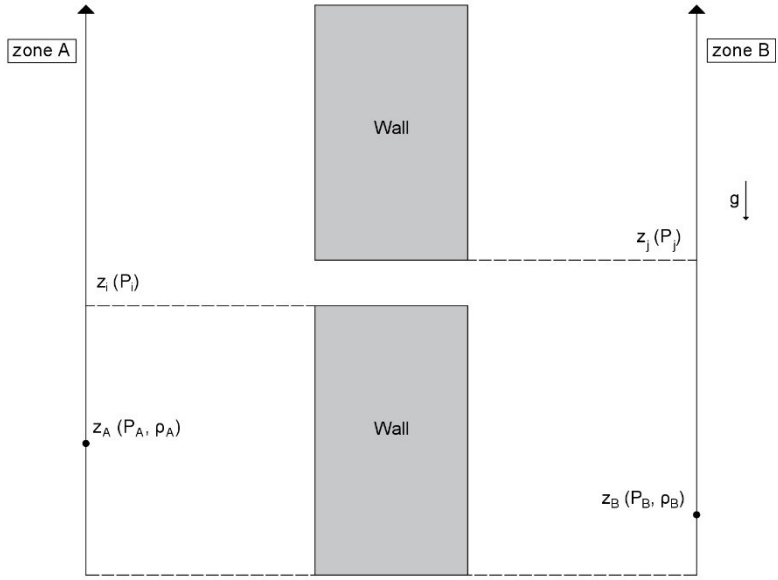

2.4. Assessment of natural ventilation: prediction methods

The physical processes related to natural ventilation are difficult to describe. Canonically, the description of the flow is obtained under specific initial and boundary conditions by combining Navier-Stokes equation and equations that describe the turbulence effects. As a description of the conditions is difficult to obtain, it is difficult to describe the airflow behaviour in a proper way.
There are multiple models able to describe in a simplified way the airflow behaviour, different from each other according to the type of information requested and to the level of modelling complexity.

2.4.1. Empirical models: analytical and/or semi-empirical formulae

A first estimation of airflow natural ventilation is often generalized and reduced in empirical or simplified formulas addressed to calculate airflow or air velocity, that combine airflow with temperature difference, wind velocity and fluctuant term. As reported in the following table, there are two typologies of methods, different from each other for their purpose.

Table 3: Simplified methods for the prediction of airflow rates and for the estimation of air velocity within natural ventilated buildings

Simplified methods for the prediction of airflow rates within natural ventilated building	
British standard method (BS 5925, 1980)	The method calculates – for single-side and cross-ventilation – air infiltration and ventilation, assuming two-directional flow through a building and omitting internal partitions.
ASHRAE method (1985)	In this method, the calculation of the airflow rate depends on leakage area of the building, to the stack and wind coefficient (respectively calculated by using table according to the number of storey of the building and to the building heights and local shielding classes), to the average indoor-outdoor temperature difference and to the meteorological wind speed.

Aynsley method (1977)	Imposing mass conservation between two openings, the Aynsley method calculates airflow for cross-ventilation assuming two main openings on two opposite facades of the building characterized by two different pressure coefficients. The method takes into account openings area and configuration and the wind velocity.
De Gidds and Phaff method (1982)	Differently from the other methods, the De Gidds and Phaff method takes into account fluctuating term. In particular, with the application of this method the effective velocity depends on meteorological wind velocity, vertical size of the opening and constants depending on wind, boundary and turbulence.
Simplified methods for the estimation of air velocity within natural ventilated building	
Givonni's method (Givonni, 1978)	The method proposed a formula to calculate the average velocity inside a room with square floor plan and equal upwind and downwind openings located in opposite walls. With this method, the average indoor velocity depends on the ratio of opening's area to wall area and reference wind speed.
Method based on tabulated data	Thanks to studies in wind tunnel, this method proposed values of average and maximum indoor velocity for two different ratios of aperture width to

(Melaragno, 1982)	wall width for naturally ventilated spaces under different wind directions and with different number of apertures and location. Another use of tabulated data is addressed to find values of the mean indoor air speed for cross-ventilation configuration without internal partitions as function of inlets and outlets.
CSTB methodology (CSTB, 1982)	Based on data obtained from architectural scale models in a wind tunnel for the prediction of indoor air motion induced by wind, the method is based on the evaluation of a "Global Ventilation Coefficient" that depends on: - the characteristics of the site (i.e. topography, characteristics of the surrounding environment and urban plan of the site); - the orientation of the building and of the wind (i.e. the angle between the axis of openings and the axis of wind, the angle between the orientation of the urban plan and the axis of the wind and the nature and characteristics of the urban plan); - the exterior characteristics of the building (i.e. the nature and characteristics of the openings the architecture of the roof, the

	existence of an open roof, the existence of concrete stilts and the presence of wings walls); - the interior architecture and the interior aerodynamics of the building (i.e. the internal partitions and furniture).
The Ernest methodology (Ernest, 1991)	By using data derived from architectural scale models in a boundary-layer wind tunnel, the model proposed by this method is addressed to predict wind-induced indoor air motion by using climatic input (i.e. wind direction and pressure distribution around the building) and building related data (i.e. size and characteristics of the windows and interior partition configuration).

2.4.2. Network models: simulations with zonal and multizone network models

The interaction of various zones through internal openings is of great importance, so network models were developed. They are based on two assumptions:

- the air temperature field in the studied zone is uniform;
- the airflow through an opening is inviscid and incompressible.

A building can be approximated to a grid composed by different nodes representing the correlation between inside and outside and through which the flow path develops. All nodes have the related pressure value.

According to the network approach, a building with N zones is represented by a network of N pressure nodes and boundary

nodes are used to represent the environment outside the building.
Because the airflow rate through an opening is connected to the difference of pressure value, and pressure at exterior node is known, the pressure at the interior node should be determined by applying the mass balance equations.
Application of the mass balance to a zone *i* with *j* flow paths gives:

$$\sum_{k=1}^{j} \rho_i Q_{ik} = 0 \qquad (11)$$

By applying mass balance for each node, a set of simultaneous non-linear equation is obtained, which solution gives the internal node pressure.

2.4.3. Zonal modelling and Computational Fluid Dynamics (CFD) modelling

Overcoming the not always valid assumption of fully mixed zones and increasing the interest for indoor air quality and comfort, new methods able to predict airflow patterns and temperature were developed, i.e. the zonal and the CFD modelling approach. These approaches are based on the following passage:

1. discretization of the building volume into small sub-volumes;
2. application of mass, energy and momentum conservation for each sub-volume;
3. derivation of temperature and air velocity fields.

2.4.3.1 Zonal models

They are an intermediate approach between network and CFD models and are based on two points to predict indoor patterns of temperature and air velocity:

- the analysed enclosure is split into different macroscopic subzones;
- it should be established the mass and energy conservation equations, together with momentum equations or identification of main flows.

In a first approach, momentum equations are not formulated and only mass and energy equations are established in each subzone, so the number of unknowns is more than the equation. Consequently, temperature and pressure models can be applied:

- temperature model: the air movement inside the building is imposed;
- pressure model: simple formulations of the missing momentum equations are added.

2.4.3.2 Introduction to CFD models

Different computational tools analyse the natural ventilation environments, but the most important are represented by CFD softwares which offer a scientific and accurate approach to the problems related to the natural ventilation in the building and in the urban environment (Shuzo, 2007).

CFD programs involve different fields concerning principally fluid mechanics, computing methods and computer graphics (Shuzo, 2007; Yang et al., 2014). Through CFD programs, fluid characteristics - i.e. temperatures, velocities, particle concentrations, pressure and pressure coefficients - can be calculated based on the principles of mass conservation, energy and momentum in the space and time domain. In fact, they solve the governing Navier-Stokes equations - i.e. mass,

momentum and energy conservation equations - to solve the fluid dynamic properties governing airflow movement (Anderson, 1995).
One of the most important advantage of CFD method is that it can analyse complex air flow patterns for naturally ventilated buildings (Hong et al., 2017) providing a detailed description of them, although CFD simulation are often computationally expensive (Omrani et al., 2017).

2.5. Type of openings

As expressed previously, the ventilation inside the building naturally occurs through the openings, due to the pressure difference between outside and inside induced by wind and buoyancy (Etheridge, 2015).
The openings were classified by Etheridge (2015), as reported in the following table:

Table 4: Five types of ventilation opening (Etheridge, 2015)

Type	Description	Still-air Cd	Examples
1–Small	Adventitious	Depends strongly on Re_0	Cracks in door, window frames, wall joints
2–Small	Purpose-provided, short	Independent of Re_0	Air vents, small windows
3–Large	Purpose-provided, long	Weakly dependent of Re_0	Chimney, stacks, ducts
4–Large	Purpose-provided, short	Cd independent of Re_0, but value probably not relevant	Large open windows, internal doors
5–Very large	Purpose-provided, short	Cd independent of Re_0, but value probably not relevant	Very large open windows, internal doors

The types of openings depend differently on the Reynolds coefficient Re_0 and from the still-air discharge coefficient, C_d. They can be "Adventitious", i.e. that are not purpose-provided, or "Purpose provided".

2.5.1 "Problems" of large openings

This problem is due to the fact that turbulence can greatly affect airflow and bidirectional flow is difficult to analyse.
Generally, wind induced pressure is due to the assumption that wind induced pressure is created from the transfer of kinetic energy of the wind when it strikes a solid body. When an opening is large, the transfer is not totally developed to generate a surface pressure, so the wind "drives" through the opening.
In addition to the previous classification of openings depending on their size, a large opening is an opening characterized by a two-way flow. In the absence of wind, light warm airflow outgoing through the upper part of the opening and cool airflow through the lower part in the opposite direction can occur. The level characterized by no air movement is called "neutral plan".

Figure 4. A representation of a two-way flow through a large opening

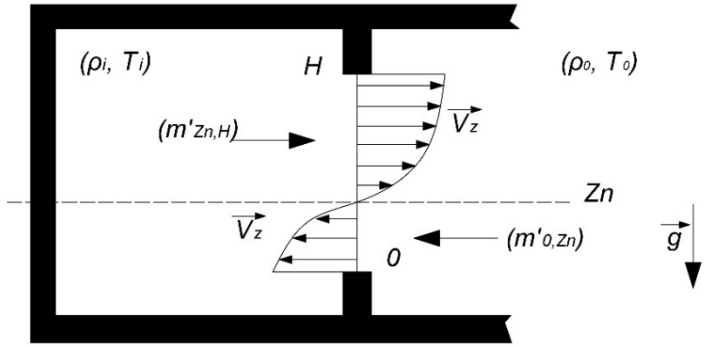

In order to describe the "behaviour" of a large opening, a set of non-linear equations can be used. For an incompressible, inviscid and steady flow, the horizontal velocity V_z along a streamline is:

$$V_z = \sqrt{2\left(\frac{\rho_0 - \rho_i}{\rho_0}\right)} \qquad (12)$$

Considering the neutral plan with a height equal to Z_N, its position is given by the mass conservation equation through the opening:

$$\frac{Z_N}{H - Z_N} = \sqrt[3]{\frac{\rho_i}{\rho_0}} \qquad (13)$$

By considering a discharge coefficient C_d, that contemplates the local contraction of the flow through the opening and the

friction effects along its solid limits, the mass flow rate below the neutral plane is:

$$m'_{0,Z_N} = C_d \int_0^{Z_N} \rho_0 V_z W dz \quad (14)$$

A direct integration gives the value of incoming airflow:

$$m'_{0,Z_N} = C_d \frac{W}{3} \sqrt{8gH^3 \rho'_i \Delta\rho} \quad (15)$$

where:

$$p'_i = \frac{p_i}{\left[1 + \sqrt[3]{\frac{\rho_i}{\rho_0}}\right]^3} \quad (16)$$

In this model, air density is function of air humidity and temperature.

2.6 Barriers

In a building, the natural ventilation performance is affected by:

- external factors that affect wind velocity and direction, such as vegetation and external building;
- internal factors, such as openings, walls and internal rooms.

Their presence can induce effects in the airflow due to the increase or decrease in turbulence, the change in the direction of the airflow and the increase or decrease of the average air speed.

2.7 Airflow rate

For openings larger than 10 mm, the airflow rate can be found by applying the equation:

$$Q = K(\Delta P)^n \quad (17)$$

where:
- ΔP=pressure difference across an opening;
- K= flow coefficient, function of the geometry of the opening;
- n=flow exponent, function of the flow characteristics (0.5 for fully turbulent flow and 1 for laminar flow).

For large openings, considering two point 1 and 2 starting from the Bernoulli equation, the airflow rate is given by:

$$dQ = C_d \sqrt{\frac{2(p_1 - p_2)}{\rho}} W dz \ (m^3/s) \quad (18)$$

where:
- p=air pressure;
- ρ=air density;
- W=width of the opening;
- Z=height of the opening;
- C_d=discharge coefficient, that depends on function temperature, difference, wind speed and opening geometry. Many researches were conducted to find the relation able to describe C_d (Santamouris, 1992; Pelletret et al., 1991; Limam et al., 1991; Darliel and Lane-Serff; 1991; Khodr Mneimne, 1990).

2.8 The theory behind the model: CFD theoretical background

2.8.1 Governing equations

CFD approach is based on the resolution of Navier-Stokes equations, i.e. mass, momentum and energy conservation equations. By solving these equations, CFD can quantitatively calculate various air distribution parameters.

1. *Mass conservation* imposes that the net rate of density in a control volume *dxdydz* is equal to the net rate of mass influx to the control volume:

$$\frac{\partial \rho}{\partial t} + \frac{\partial}{\partial x}(\rho U) + \frac{\partial}{\partial y}(\rho V) + \frac{\partial}{\partial z}(\rho W) = 0 \qquad (19)$$

   By taking into account the effect of turbulence, the air velocity is:

$$U = u + u' \qquad V = v + v' \qquad W = w + w' \qquad (20)$$

   where:

- u, v, w = time-mean components;
- u', v', w' = fluctuating term.

Conservation of Momentum imposes that the net force on the control volume *dxdydz* in any direction is equal to the outlet momentum flux minus the inlet momentum flux in the same direction:

x direction:

$$\frac{\partial}{\partial t}(\rho U)+\frac{\partial}{\partial x}(\rho UU)+\frac{\partial}{\partial y}(\rho UV)+\frac{\partial}{\partial z}(\rho UW) = -\frac{\partial P}{\partial x}+\frac{\partial}{\partial x}\left(\mu\frac{\partial U}{\partial x}\right)+\frac{\partial}{\partial y}\left(\mu\frac{\partial U}{\partial y}\right) +\frac{\partial}{\partial z}\left(\mu\frac{\partial U}{\partial z}\right) +\frac{1}{3}\frac{\partial}{\partial x}\left[\mu\left(\frac{\partial U}{\partial x}+\frac{\partial V}{\partial y}+\frac{\partial W}{\partial z}\right)\right]+\rho g_x$$

y direction:

$$\frac{\partial}{\partial t}(\rho V)+\frac{\partial}{\partial x}(\rho UV)+\frac{\partial}{\partial y}(\rho VV)+\frac{\partial}{\partial z}(\rho VW) = -\frac{\partial P}{\partial x}+\frac{\partial}{\partial x}\left(\mu\frac{\partial V}{\partial x}\right)+\frac{\partial}{\partial y}\left(\mu\frac{\partial V}{\partial y}\right) +\frac{\partial}{\partial z}\left(\mu\frac{\partial V}{\partial z}\right) +\frac{1}{3}\frac{\partial}{\partial y}\left[\mu\left(\frac{\partial U}{\partial x}+\frac{\partial V}{\partial y}+\frac{\partial W}{\partial z}\right)\right]+\rho g_y \qquad (21)$$

z direction:

$$\frac{\partial}{\partial t}(\rho W)+\frac{\partial}{\partial x}(\rho UW)+\frac{\partial}{\partial y}(\rho VW)+\frac{\partial}{\partial z}(\rho WW) = -\frac{\partial P}{\partial x}+\frac{\partial}{\partial x}\left(\mu\frac{\partial W}{\partial x}\right)+\frac{\partial}{\partial y}\left(\mu\frac{\partial W}{\partial y}\right) +\frac{\partial}{\partial z}\left(\mu\frac{\partial W}{\partial z}\right) +\frac{1}{3}\frac{\partial}{\partial z}\left[\mu\left(\frac{\partial U}{\partial x}+\frac{\partial V}{\partial y}+\frac{\partial W}{\partial z}\right)\right]+\rho g_z$$

where, by taking into account the effect of turbulence, the air velocity is as expressed by Equation 20 and P = p + p'.

2. The *Conservation of thermal energy* imposes that the net increase in internal energy in a control volume is equal to

the net flow of energy by convection plus the net inflow by thermal and mass diffusion:

$$\frac{\partial}{\partial t}(\rho T) + \frac{\partial}{\partial x}(\rho UT) + \frac{\partial}{\partial y}(\rho VT) + \frac{\partial}{\partial z}(\rho WT) = \frac{\partial}{\partial x}\left(\Gamma \frac{\partial T}{\partial x}\right) + \frac{\partial}{\partial y}\left(\Gamma \frac{\partial T}{\partial y}\right) + \frac{\partial}{\partial z}\left(\Gamma \frac{\partial T}{\partial z}\right) \quad (22)$$

where, by taking into account the effect of turbulence, the air velocity is as expressed by Equation 20 and T = t + t'. $\Gamma = \mu/\sigma$ stands for the diffusion coefficient.

As reported by Rong (2016), CFD refers to two parts:

- *Solving the right equations*, that means select correctly physical properties, boundary conditions, turbulence models, etc.
- *Solving the equations right*, that means select correctly numerical methods i.e. discretization schemes, computational grid, convergence etc.

2.8.2 Solving the right equations

2.8.2.1 Turbulence models

It is not possible to describe mathematically the effects of turbulence, so it is necessary to adopt an approximate method. The choice is generally the result of a compromise, because no method can describe exactly the turbulence. The choice depends on the needed accuracy and on the computing costs.

CFD predicts turbulent flows through three approaches:

- direct numerical simulation (DNS)
- Reynolds-averaged Navier-Stokes (RANS) equation simulation
    - eddy-viscosity models
    - Zero-Equation Eddy-Viscosity Models
    - One-Equation Eddy-Viscosity Models
    - Two-Equations Eddy-Viscosity Models
        - k–ε turbulence model
            - Standard
            - RNG
            - Realizable
        - k–ω turbulence model
        - Reynolds-stress models
            - large-eddy simulation (LES)
            - detached-eddy simulation models (DES)

2.8.2.2 Standard k- ε models

This sub-section reports a formulation of the turbulence model used in this thesis, i.e. the Standard k- ε model.

This model (Launder and Spalding, 1974) is the most used one, and was adopted in this thesis due to its simple format and robust performance. It describes well the fully developed turbulent flow (Rong et al., 2016).

All the k-ε models predict the Reynolds stresses by adopting the Boussinesq hypothesis (Boussinesq, 1877) that relates the Reynolds stresses to the mean rate of deformation.

In this model, two transport equations for kinetic energy k and dissipation rate ε are introduced. In detail:

- The turbulent kinetic energy k is a measure of the energy associated with the turbulent fluctuations in the flow.
- The dissipation rate ε is caused by the work done by the smallest eddies in the flow against viscous stresses.

They are related each other through the equations:

$$\varepsilon = \frac{C_\mu \rho k^{1.5}}{L} \qquad \mu_t = \rho L \sqrt{k} \mu_t = \frac{C_\mu \rho k^2}{\varepsilon} \tag{23}$$

Where:
- C_μ= constant = 0.09;
- L = length scale;
- μ_t = turbulence viscosity.

The two transport equation – called "closure equation" because they allow to complete the system of equation to calculate air velocity and temperature fields – are:

For k:

$$\begin{aligned} &\frac{\partial}{\partial t}(\rho K) + \frac{\partial}{\partial x}(\rho u k) + \frac{\partial}{\partial y}(\rho v k) + \frac{\partial}{\partial z}(\rho w k) \\ &= \frac{\partial}{\partial x}\left(\Gamma_k \frac{\partial k}{\partial x}\right) + \frac{\partial}{\partial y}\left(\Gamma_k \frac{\partial k}{\partial y}\right) \\ &+ \frac{\partial}{\partial z}\left(\Gamma_k \frac{\partial k}{\partial z}\right) \\ &+ \mu_t \left\{ 2\left[\left(\frac{\partial u}{\partial x}\right)^2 \right.\right. \\ &\left.\left. + \left(\frac{\partial v}{\partial y}\right)^2 + \left(\frac{\partial w}{\partial z}\right)^2\right] + \left(\frac{\partial u}{\partial y} + \frac{\partial v}{\partial x}\right)^2 \right. \\ &\left. + \left(\frac{\partial u}{\partial z} + \frac{\partial w}{\partial x}\right)^2 + \left(\frac{\partial w}{\partial y} + \frac{\partial v}{\partial z}\right)^2 \right\} \\ &+ C_\mu \rho \frac{k^{1.5}}{L} + \beta g \frac{\mu_t}{\sigma_t} \frac{\partial T}{\partial y} \end{aligned} \tag{24}$$

where:
- $\Gamma_k = \mu_e/\sigma_k$, with $\sigma_k \approx 1$;
- μ_e=effective viscosity;

- σ_t is the Turbulent Prandtl, with $0.5< \sigma_t<0.9$;
- β is the coefficient of volumetric expansion;
- the last term is the buoyancy.

For Ɛ:

$$\frac{\partial}{\partial t}(\rho\varepsilon)+\frac{\partial}{\partial x}(\rho u\varepsilon)+\frac{\partial}{\partial y}(\rho v\varepsilon)+\frac{\partial}{\partial z}(\rho w\varepsilon) = \frac{\partial}{\partial x}\left(\Gamma_\varepsilon\frac{\partial\varepsilon}{\partial x}\right)+\frac{\partial}{\partial y}\left(\Gamma_\varepsilon\frac{\partial\varepsilon}{\partial y}\right) + \frac{\partial}{\partial z}\left(\Gamma_\varepsilon\frac{\partial\varepsilon}{\partial z}\right) + C_1\frac{\varepsilon}{k}\mu_t\left\{2\left[\left(\frac{\partial u}{\partial x}\right)^2+\left(\frac{\partial v}{\partial y}\right)^2+\left(\frac{\partial w}{\partial z}\right)^2\right]+\left(\frac{\partial u}{\partial y}+\frac{\partial v}{\partial x}\right)^2 + \left(\frac{\partial u}{\partial z}+\frac{\partial w}{\partial x}\right)^2+\left(\frac{\partial w}{\partial y}+\frac{\partial v}{\partial z}\right)^2\right\} + C_2\rho\frac{\varepsilon^2}{k}+C_1\beta g\frac{\varepsilon}{k}\Gamma_t\frac{\partial T}{\partial y} \quad (25)$$

where:
- C_1=1.44;
- C_2=1.92.

2.8.3 Solving the equations right

Solving the equation right means to choose accurately the numerical schemes (first order upwind, second order upwind or QUICK scheme, depending on the needed accuracy), the near wall treatment (i.e. taking into account near wall effect) and the convergence criteria. The iteration steps and the residuals should be defined before the simulation, in order to

obtain an appropriate convergence of the simulation. In addition:

- values of important variables should be monitored during the simulation;
- conservation of energy and mass should be checked after the simulation.

Great importance is given to the discretization of space, the explanation of which requires further study in the following sub-section.

2.8.3.1 Space discretization

When numerical method is used, the space is discretized to solve the partial differential equations. Mesh generation is the pre-processing step for the computational simulation and consists in the discretization of the domain.

Mesh generation is a fundamental and critical problem in geometric data modelling and processing involved in numerical computations or simulations (e.g. solving partial differential equations (PDE) using finite difference methods (FDM), finite element methods (FEM), or finite volume methods (FVM)). Generally, the commercial CFD codes uses the Finite Volume method, which results are strongly influenced by the computational grid. Mesh generation requires geometric data discretization by using polygonal or polyhedral elements. Meshing procedure failure is a relevant problem for numerical simulations. For this reason, meshing process, especially of geometrically complex three-dimensional fluid flows, has attracted much attention in recent times because most engineering configurations involve critical issues that do not make it possible an easy mesh processing due to the time consuming and the difficult procedure of blocking complex domains.

There are three different types of simulations. The first one, called *structured*, is defined as a group of hexahedral elements with an implicit connectivity of the points in the mesh. The second one, called *unstructured*, consists in a group of elements, generally tetrahedrons, with an explicitly defined connectivity. The third one, called *hybrid*, where the viscous region is filled with prismatic or hexahedral cells while the rest of the domain is filled with tetrahedral cells.

2.8.3.2 Convergence criteria

In order to obtain a convergent solution, a low residual value should be set together with an adequate number of iterations. In parallel, in order to evaluate the solution accuracy, values of relevant variables have to been monitored. In addition, conservation of the mass should be checked after the simulation is done.

2.9 CFD researches applied on livestock buildings and introduction to the present research

In the current state of research, mainly addressed to domestic building, more studies should be developed to improve design strategies for simulating natural ventilation in non-domestic buildings (da Graça and Linden, 2016).

In livestock buildings, in particular in those for dairy cows, natural ventilation is the most common passive cooling system (Shen et al., 2013; Rong et al., 2016) and, in the last decade, the number of related research studies increased because of the necessity to improve operators and animal well-being (Zhiqiang et al., 2015). In fact, natural ventilation of livestock buildings could decrease air temperature, gas emissions, air pollutant concentration (Wathes, 1994) and dust concentration (Zhang, 1999) inside the building

environment. Moreover, natural ventilation could reduce energy consumption for cooling livestock buildings (Alloca et al., 2003; Bournet and Boulard, 2010; Bjerg et al., 2013a) giving a contribute to the sustainability of livestock productions.

Natural ventilation depends on different factors, i.e. the number of openings in the envelope, the internal distribution of flow pattern and the pressure difference between indoor and outdoor environment.

Researches regarding models used for the study of natural ventilation in livestock building – addressed to quantify ventilation rate – have been carried out over the past forty years.

A comprehensive collection of theoretical models of natural ventilation was included in a report authored by J.M. Bruce "The design of livestock buildings for natural ventilation: the theoretical basis and a rational design method" (Down et al., 1985). The book made it possible to enlarge knowledge about the ventilation rate and the wind-driven natural ventilation in livestock buildings (Bruce, 1974, 1977a, 1977b, 1978, 1982; Down et al., 1990; Foster and Down, 1987).

More recent studies have used computational software tools to analyse the ventilation rate, study the influence of external conditions on building environment and find suitable design solutions. Gurdil et al. (2009) developed a simulation software for controlling the natural ventilation rates in a laying hen house in Black Sea region (Turkey). They found that a combination of natural and mechanical ventilation systems is required in order to guarantee the animal's well-being during the hottest months of the year. Liberati and Zappavigna (2007) developed a software tool to simulate transient environmental conditions inside closed animal buildings, that was applied to a case study, i.e. a barn for

fattening pigs, and made it possible to optimize the thermal performance of the building during the whole year by finding the best compromise between summer and winter requirements. Sapounas et al. (2013) used a 3D simulation model to analyse the airflow inside commercial dairy cow houses having different roof types and side ventilators; the configurations have been studied by considering different external conditions and the results showed that both uniformity of indoor climate and ventilation rate were influenced by the roof shape. Norton et al. (2009) developed a CFD model to study the natural ventilation of a commercial naturally ventilated calf housing under different wind incidences for three different inlet openings. They showed that the highest ventilation homogeneity is obtained when the wind has a direction normal to the building and that the maximum level of environmental heterogeneity is obtained with a wind angle equal to 10-40°. In a next study, Norton et al. (2010) investigated the thermal environment and the performance of natural ventilation in a calf barn under the effect of variation of both permeable windbreak materials and height of eave openings. By considering a case of wind driven natural ventilation, they showed that the ventilated cladding offered the most efficient ventilation system and thermal comfort. Moreover, by increasing the height of the eave opening, they found that the mean air velocity at animal level decreases. Seo et al. (2009) analysed, thanks to a previously developed CFD model, airflow, internal air temperature distribution and ventilation efficiency of a conventional ventilation system installed in a broiler house and different modified ventilation systems. The best result in terms of energy saving and animal welfare was obtained for the configuration with a diffuser beneath the chimney inlet which mixed the incoming cold air with the warm air. By using a

CFD methodology, Wu et al. (2012) studied the performances of three techniques used to estimate the ventilation rate of a naturally ventilated dairy cattle building in order to find the best solution to calculate the emissions measured by a Photo-acoustic Multi-gas Monitor, model 1312 and by a multiplexer, model 1303 (Innova air Tech Instruments A/S, Denmark).

Nowadays only few researches regarded the study of natural ventilation through large openings which often characterize semi-open buildings for dairy cows in hot climate regions because they can ensure an air change adequate to guarantee the animal's well-being (Shen et al., 2013). This kind of research studies are still challenging in the field of CFD application because of bidirectional flows through large openings.

In this thesis, by using a CFD specifically put forward methodology, wind driven natural ventilation (i.e. an internal ventilation induced by the external wind entering from the openings) was studied in a semi-open free-stall barn for dairy cows, located in Southern Italy, in a region highly characterised by hot climate conditions during summer that could induce animal heat stress.

Firstly, all the building components of the barn which had an influence on the airflow were 3D modelled by using Autodesk Autocad 2016®. Next, Ansys ICEM 17.1® software tool was used in order to obtain the mesh of both the modelled objects and other elements outside the barn (i.e., trees and rural buildings). The same software tool made it possible to set boundary conditions. Then, Ansys Fluent 17.1® software tool was used to simulate indoor natural ventilation by using as simulation parameters airflow velocities collected by a meteorological station nearby the barn. Finally, alternatives design configurations, based on the first results, have been

evaluated in order to find the best condition for the well-being of animals.
Due to the difficulty of the modelling phase, this study focused on a relevant cross-section of the barn which intercepted the resting area of the animals, where they spend 8-10 hours a day. This cross-section is also significant for the analysis of the internal microclimatic conditions.
Simulations were carried out both by considering hourly data, in order to compare simulated data to those obtained from a measuring system previously installed within the barn, both for the basis configuration, i.e. the configuration that considers as input the average data taken from the weather station. After the simulation of the basis configuration, average air velocities of the two areas considered more "relevant", i.e. those addressed to animals, were analysed. During the hours for which simulations were carried out in the validation phase (see paragraph 4.3), dairy cow behaviour was studied by visual examination of time-lapse video-recordings provided by a multi-camera system composed of ten cameras positioned in the resting area. Through the visual analysis, five different cow behaviours were identified and analysed because of their high relation to the comfort of the animals. Basing on the validated model obtained as first results of the study, alternative design configurations were analysed with the aim to discover the best condition for the well-being of animals.
This case study was considered significant for the position and for the high number of similar cases in hot climate regions, so the methodology applied in this thesis could represent an example to study the natural ventilation of livestock buildings with similar characteristics.

2.10 Why to study natural ventilation of livestock buildings?

The study of natural ventilation of livestock buildings is of utmost importance, since it removes heat, moisture and contaminant gases from indoor space (Rong et al., 2016), contributing to the well-being of workers and animals. Moreover, high ambient temperature and heat waves highly influence the well-being and productivity of dairy cows (Cook et al., 2005; De Palo et al., 2006; Herbut et al., 2018): heat stress (i.e. the sum of external forces acting on an animal that causes an increase in body temperature and evokes a physiological response (Dikmen and Hansen, 2009)) causes many negative consequences in terms of physiological and behavioural disturbances and significant losses in milk production (Herbut et al., 2018) and fertility.

Air temperature and relative humidity are the most important factors in determining the exchange of heat between the animal and its surroundings, but two other relevant microclimate factors influence the heat stress: the air velocity and the solar radiation (Buffington et al., 1981; Shioya et al., 1997; Da Silva et al., 2010). In particular, changes in air velocity influence the convection cooling of cattle determining a significant impact on the regulation of thermal balance of cows (Davis and Mader, 2003), as demonstrated by the presence of the term relative to air velocity in most of the indices used for the heat stress assessment. Specifically, as reported by Bailey et al. (2016), the air velocity recommended for dairy cattle in the USA during heat stress is from 1.8 to 2.8 ms^{-1} (Bailey et al., 2016).

With regard to the contaminant gases…

Due to the increase of human population and of food consumption, global livestock production has expanded intensely in the last years (FAO, 2018). Consequentially, an increased production and productivity to meet demand, structural changes in the livestock sector and more movement and trade in livestock and products were observed. This situation results in an increase of emissions of toxic gases and subsequently leads to a series of environmental problems.

Figure 5. The global livestock sector: drivers and outcomes (FAO, 2018)

The most important gases released in atmosphere from livestock buildings are:

- Ammonia (NH_3) is volatized from manure and depends on cow diet (Aguerre et al., 2010) and environmental conditions (Powell et al., 2008a, 2008b). When NH_3 deposits into terrestrial or aquatic ecosystems, it can cause acidification, over-fertilization, eutrophication, and/or emission of nitrous oxide in these systems. The release of ammonia from manure above floor depends on many factors, such as manure's characteristics, indoor climatic conditions, animal behaviour and livestock management practices (Bjerg et al., 2013a; Bjerg et al., 2013b).
- Methane (CH_4) gas – which represents one of the greenhouse gas emissions – is generated mainly through enteric fermentation. Its production depends on cow genetics and diet (Knapp et al., 2014).

Global anthropogenic atmospheric emission of NH_3 has been valued at some 47 million tonnes, with some 94% produced by the agricultural sector. The livestock sector contributes about 68% of the agriculture part, primarily from deposited and applied manure (Steinfield et al., 2006).

These statistics are in line with what reported by Eurostat, according to which in 2015, the EU agricultural sector emitted a total of 3 751 kilotonnes of ammonia and was responsible for 94 % of total ammonia emissions across the region. (European Environment Agency, 2017).

Total greenhouse gas emissions from global livestock are equal to 7.1 Gigatonnes of Co_2-equiv per year, representing 14.5% of all anthropogenic greenhouse gas emissions (FAO, 2019). This fact is in line FAO's previous assessment (FAO, 2006) although it is based on a much more detailed analysis and improved data sets.

Figure 6: Greenhouse gas emissions from different activities.

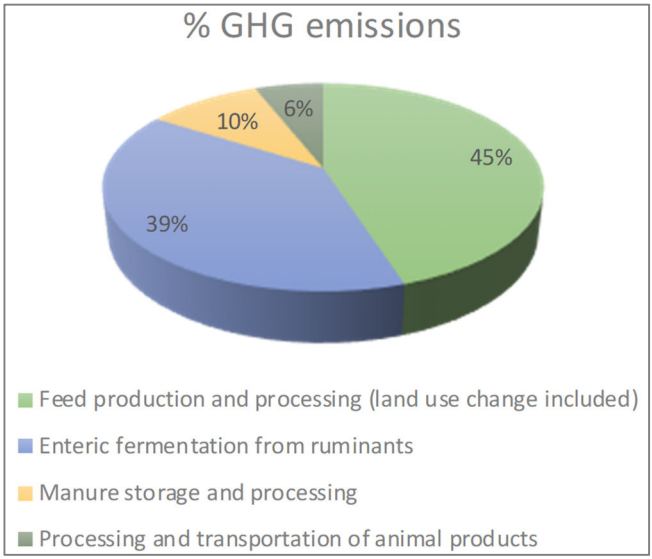

According to the same study (FAO, 2019), cattle (raised for both beef and milk) are responsible for the most greenhouse gas emissions (65% of the livestock sector's emissions).
On a commodity-basis, beef and cattle milk are responsible for the most emissions. They are followed by pig meat, buffalo milk and meat, chicken meat and eggs and small ruminant milk and meat. The remaining emissions are sourced to other poultry species and non-edible products (Figure 7).

Figure 7: Greenhouse gas emissions on a commodity-basis.

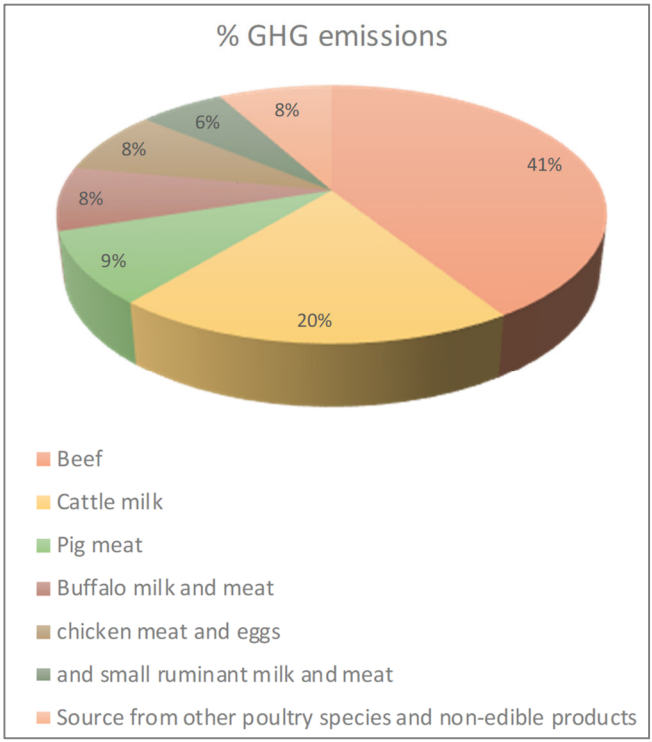

According to the same study (FAO, 2019), livestock supply chains emit:

- Carbon dioxide, corresponding to 5% of anthropogenic CO_2 emissions;
- Methane, corresponding to 44% of anthropogenic CH_4 emissions;
- Nitrous oxide, corresponding to 53% of anthropogenic N_2O emissions.

As reported in Figure 8, the main greenhouse gas produced in agriculture is the enteric CH_4, which is formed by fermentations occurring along the digestive tract of animals.

Figure 8. CH_4 emissions from enteric fermentations (3A); CH_4 and N_2O emissions from leakage management (3B); CH_4 emissions from rice cultivation (3C); direct and indirect emissions of soil management (3D); CH_4 and N_2O emissions from the combustion of crop residues (3F); CO_2 emissions from liming (3G); CO_2 emissions from the urea application (ISPRA, 2016)

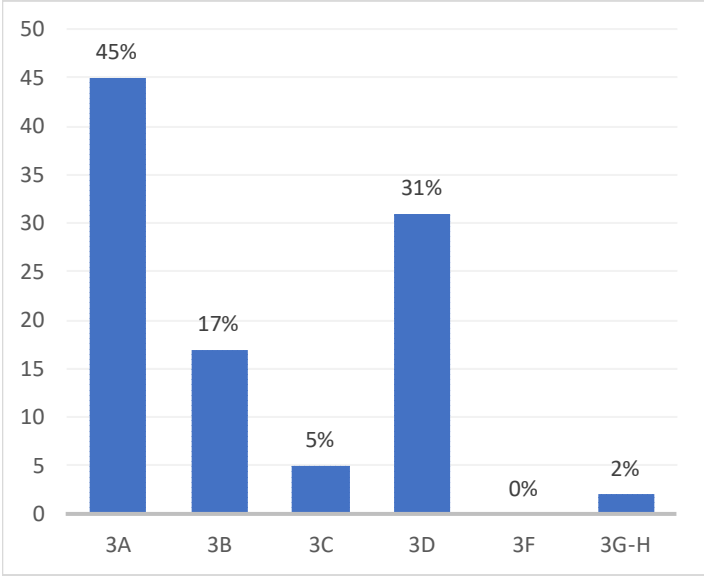

Figure 9. Contribution of the various species to CH_4 emissions in 2014 (ISPRA, 2016)

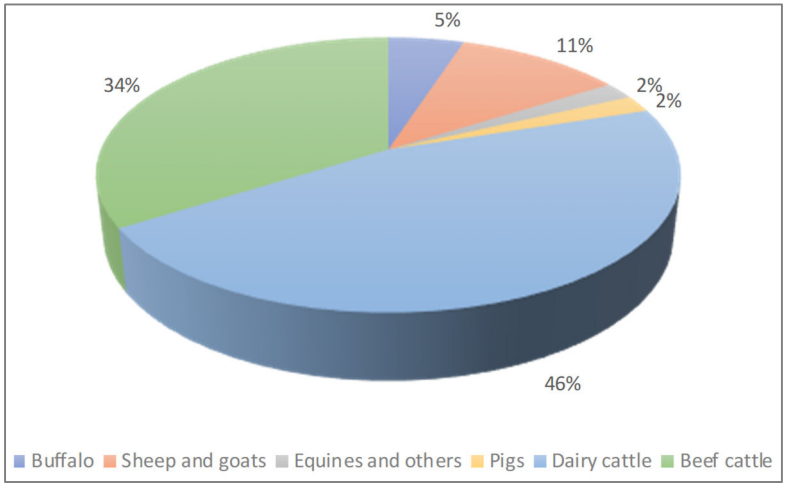

As reported in Figure 9, with regard to the contribution of the various animal species to CH_4 emission in 2014 the highest emissions come from dairy cattle.

Whit regard to the ammonia concentration inside the livestock buildings, the available data concern the buildings located in Northern Europe (Grott Koerkamp et al., 1998; Wathes et al., 2003) (Figure 10-13).

Figure 10. Concentration of ammonia (p.p.m.) for various housing system for cattle, pigs and poultry in England (10.1 °C)

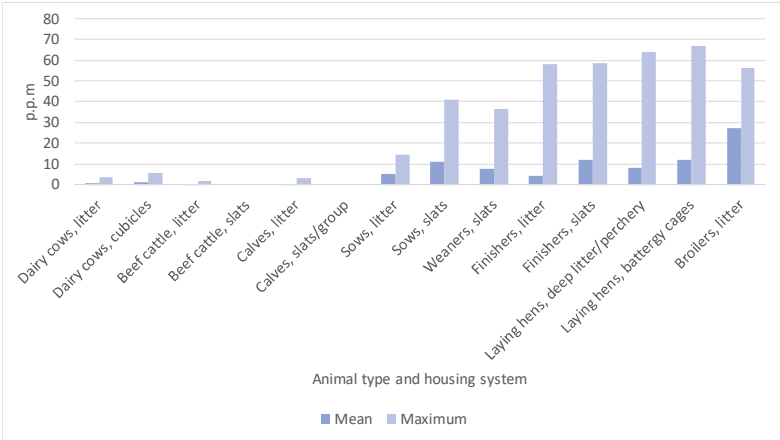

Figure 11. Concentration of ammonia (p.p.m.) for various housing system for cattle, pigs and poultry in The Netherland (9.8 °C)

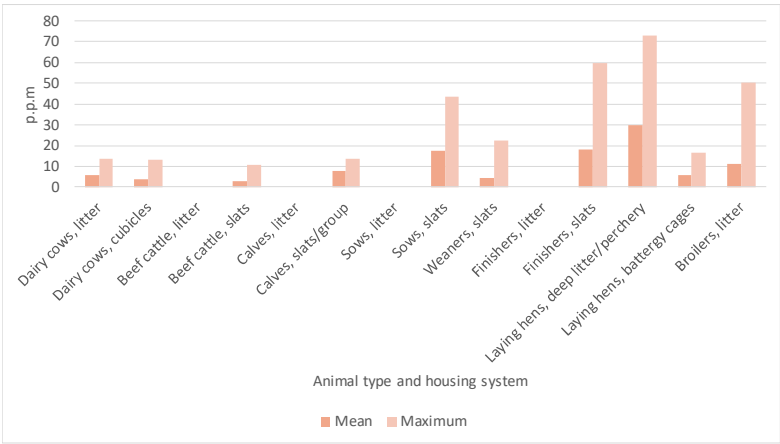

Figure 12. Concentration of ammonia (p.p.m.) for various housing system for cattle, pigs and poultry in Denmark (8.4 °C)

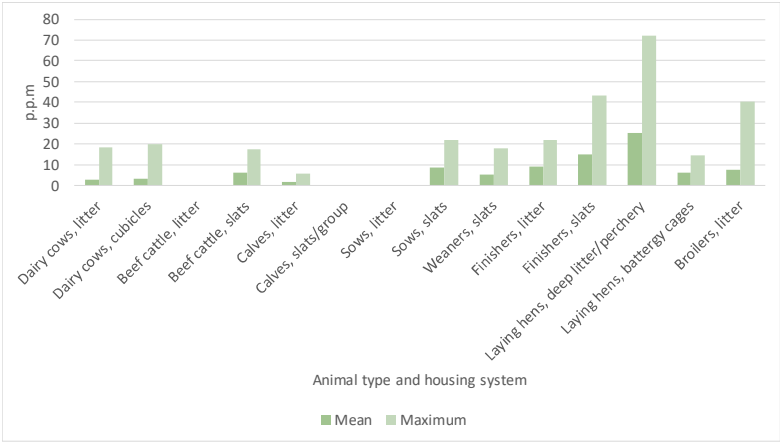

Figure 13. Concentration of ammonia (p.p.m.) for various housing system for cattle, pigs and poultry in Germany (10.5 °C)

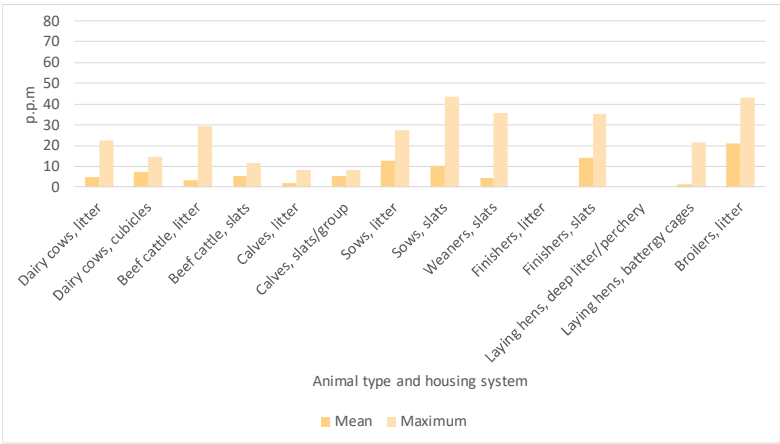

3. Materials and methods

The research has been carried out through experimental trials and numerical models developed over a case study. According to the paragraph 2.10, a livestock building for dairy cows was chosen.

3.1 The study area

Studies carried out on the design of livestock houses in hot climate countries (Cascone, 1991) have shown that in central Mediterranean basin the maximum values of air temperature in summer are largely higher than the upper critical temperatures of the thermo-neutral zones of the various species of livestock. Therefore, in these areas, it is important to find design and management solution that could mitigate the negative effect of high temperature on the animals during the summer season (Arcidiacono and D'Emilio, 2006).
Because of this, and along with the data reported in Figure 14, the barn chosen for the study is located in hot Mediterranean area. In particular, the barn is in Sicily (Southern Italy) in Province of Ragusa, where most of barns present in Sicily are located (Arcidiacono et al., 2015).

Figure 14. Livestock farms for each province of Sicily – detail of livestock (ISTAT 2010)

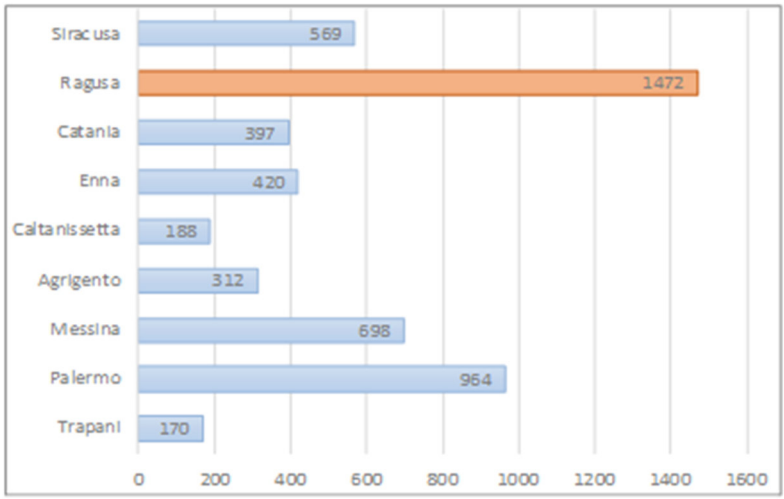

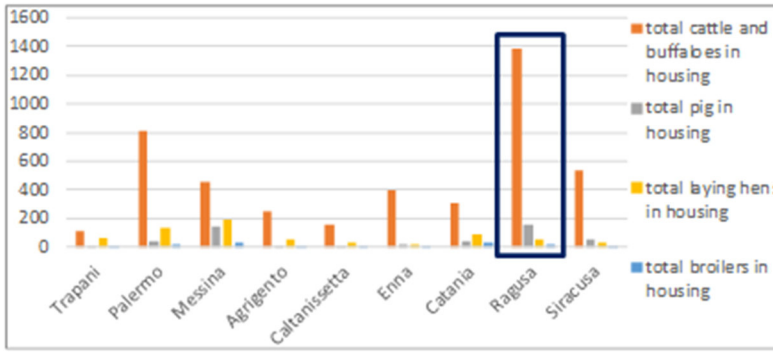

The most widespread type of livestock building in the province of Ragusa (and in Sicily in general) is that for cattle and buffalo (Figure 14). According to this and to the fact that the highest emissions of CH_4 come from dairy cattle, a barn for dairy cows was chosen.

Along with the shown data and motivations, the case study consists in a free-stall barn for dairy cows, located in

Contrada Pozzilli (37.022845°N latitude, 14.534247 °E longitude; Vittoria, Ragusa, Italy), at an altitude of approximately 230 m a.s.l.

3.2 Description of the barn

The barn has a rectangular plan, about 57 m long and about 21 m wide. The height is 5.4 m at the eaves and 6.7 m at the peak (the pitch slope is 12%). The longitudinal axis of the barn was oriented in the North-West-South-East direction. The main functional areas were the feeding area (i.e., feeding alley, feeding passage and the manger), the resting area composed of 64 stalls subdivided in three pens on the same row, and a service alley connected to the feeding area by service passages. The barn had three sides completely open and a wall in South-West side. In this wall there are four doors, which gave access to the pens for calves and heifers. Other two areas along the South-West wall were used as offices for the herd management. Finally, with regard to the main building components, the flooring - having different heights as showed in the section of the barn - was in concrete, the bearing structure consisted of steel pillar and beams, the roof is composed by steel trusses and corrugated fibre cement sheet roofing.
Sensors were positioned inside the resting area, where the animals spend most of their time, so significant with regard to the potential effects of natural ventilation on animal well-being, and outside the barn, above the chimney. The heights of the probes are respectively 2.50 m (inside the barn) and 7.50 m (outside the barn, about 1 m above the chimney).

Figure 15. Section, windward façade and plan of the barn

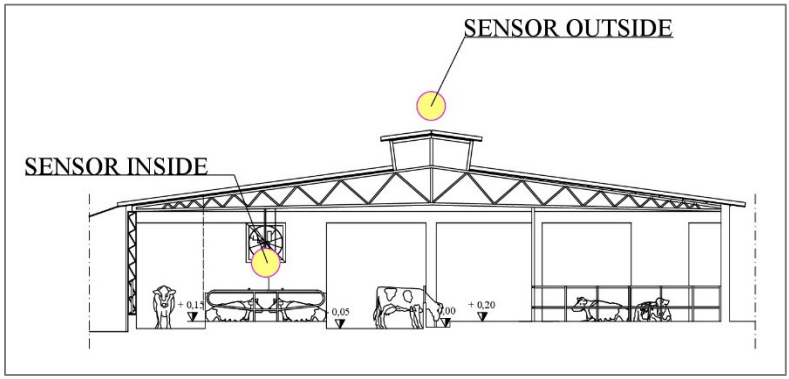

Cross section A-A

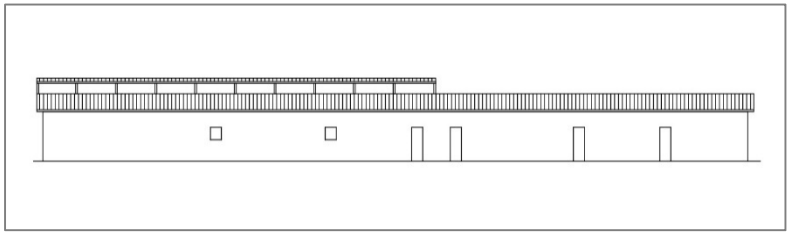

South-West front

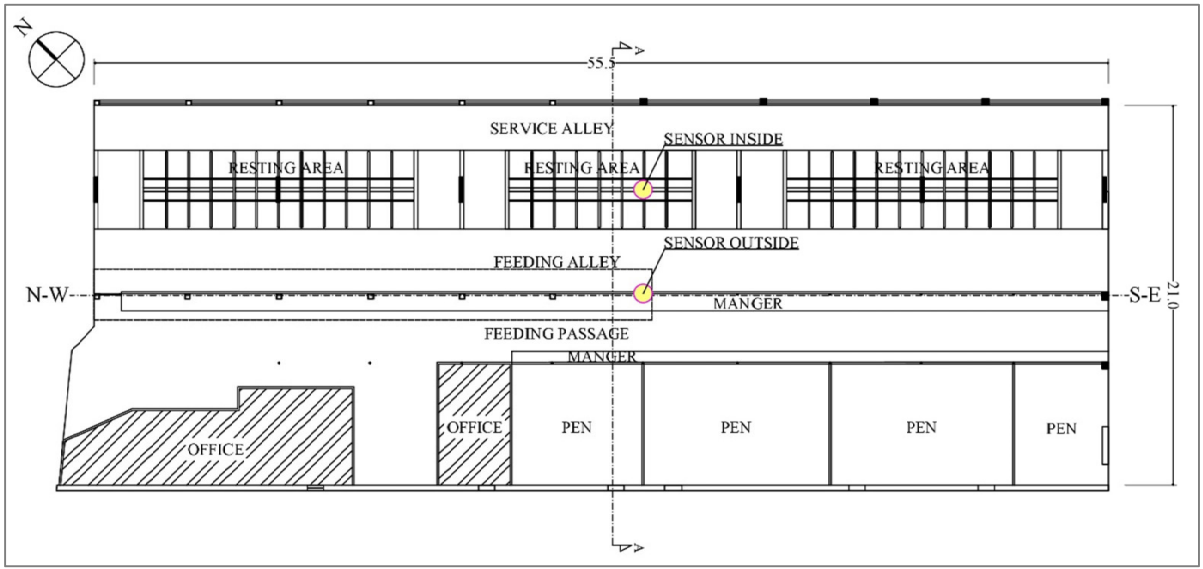
N
A
55.5
A
SERVICE ALLEY
SENSOR INSIDE
RESTING AREA
RESTING AREA
RESTING AREA
SENSOR OUTSIDE
FEEDING ALLEY
N-W
S-E
MANGER
21.0
FEEDING PASSAGE
MANGER
OFFICE
OFFICE
PEN
PEN
PEN
PEN

Plan

Figure 16. Pictures of the barn

North-West front of the barn

South-East front of the barn

Resting area

Figure 17. Render of the barn

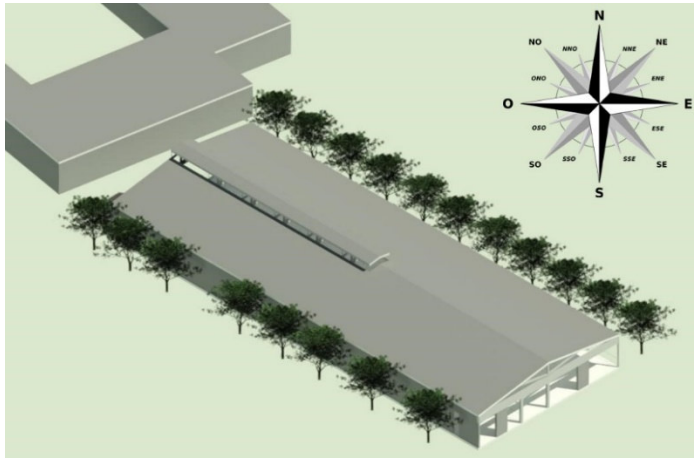

Figure 18. Localization of the barn on map (37.022845°N latitude, 14.534247 °E longitude)

Figure 19. Surrounding trees and rural buildings

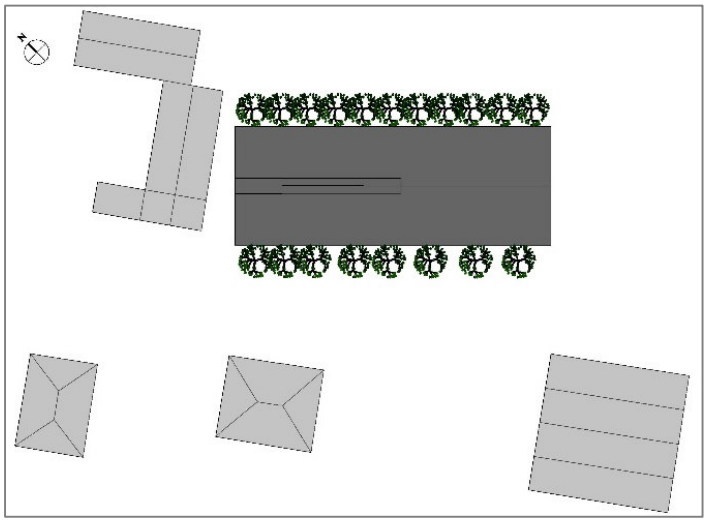

3.3 Data analysis

Many researches in this field were conducted basing on analysis and utilization of wind-rose diagrams and interpretation of climatic zoning requirements (Guo et al., 2015; Chen et al., 2007). It is a must to consider that spatial and temporal variations of wind direction and speed induce highly complex air flows and obstruct the control of internal airflow patterns (Hong et al., 2017; Fiedler et al., 2014)

3.3.1 Data acquired inside the barn

In the barn under study, the measurement system used for indoor microclimate was based on anemometers WindSonic (Gill Instruments Ltd., UK). Probes acquired measurements of air velocity and direction, air temperature and relative humidity at 5-min time sampling.

Figure 20. Sensors inside

Table 5. Sensors specifications

Output		
Units of measure	Metres/second (m/s) Kilometres per hour (kph)	
Parametres	Digital	Analogue
	Polar – Speed and direction or UV- 2 axis, signed Speed	Polar – Speed and Direction Tunnel – U Speed and U Direction
Wind Speed	Digital	Analogue
	0 – 60 m/s	0-30 m/s, 0-50 m/s, 0-60 m/s
Accuracy	± 2 % (12 m/s)	± 2 % (12 m/s)
Resolution	0.01 m/s	0.01 m/s
Wind Direction	Digital	Analogue
Range	0-359°	0-359°
Accuracy	± 3° (20 m/s)	± 3° (20 m/s)
Resolution	1°	1°
Output formats		
0-5 V 4-20 mA	±1% of full scale N.B. Analogue output impedance = 1KΩ	
Output formats		
Gill	Continuous or Polled (output on request by host system)	
Marine – NMEA	NMEA 0183 version 3	
Data Logger	SDI – 12 V1.3	
Communication formats		
Windsonic Option 1	RS232	
Windsonic Option 2	RS232, RS422, RS485	
Windsonic Option 3	RS232, RS422, RS485 and Analogue (0 – 5 V or 4 – 20 mA)	
Windsonic Option 4	SDI – 12, RS232, RS422, RS485	
Anemometer status	Status OK and Error codes included as part of standard output message	

Environmental	
Moisture protection	IP65
Temperature	Operating -35°C to +70°C Storage -40°C to +90°C
Humidity	Operating <5% to 100%
EMC	EN 61000-6 – 3 (Emissions) EN 61000-6 – 2 (Immunity)
Standards	Manufactured within ISO9001:2000 quality system

In order to acquire data about dairy cow behaviour, a multi-camera system - composed of ten cameras positioned in the resting area, which were mounted on steel beams by means of special brackets - was used. Cameras, equipped with HTTP interface and IR sensors for night vision, had a maximum resolution of 1280 × 960 pixels and the ability to capture up to 25 fps.

3.3.2 Outdoor meteorological data

The definition of the wind direction and velocity at a given location is difficult because wind can blow and fluctuate from different direction. Nevertheless, statistical information can be used to determine the prevailing wind direction.

The problem of defining wind data has been studied in past researches. In Norton et al. (2009), wind data was taken with meteorological station and analysed through circular statistics (Jones, 2006). Then, a mast equipped with sensors was installed 5 m South-East of the experimental building, and on the top of the mast (4 m above the ground level) a 2D sonic anemometer was located in order to measure external wind speed. In Wu et al. (2012), external equipment consisting of three-dimensional ultrasonic anemometers was used. The external wind speeds and directions were monitored at 10 m above the ground and the air temperature

was recorded at one position outside the building. In Rong et al. (2015), external three-axis ultrasonic anemometers were located on the West, 10 m high and 30 m away from the sidewall, in order to measure the outdoor wind speed and direction.
In this study, data about the wind direction and velocity between 26 April 2016 and 2 May 2016 have been evaluated in order to obtain the prevailing air direction and the average air velocity. This week was chosen as reference week among those characterised by inactivity of the mechanical ventilation system installed in the barn to mitigate during summer season the effects of hot climate on dairy cows. The available data from the nearby wheater station located in Acate (SIAS, 2016) were used to determine, at 10 m reference height, the average hourly air temperature (°C), the average hourly relative humidity (%), the total hourly solar radiation ($MJmq^{-1}$), the average hourly wind speed (ms^{-1}) and the average hourly wind direction (°).
For the purpose of this study (improvement of the design/current situation of the barn) it was decided to adopt the value of the Acate weather station mainly because Acate is the nearest station to the barn (13.2 km as the crow flies). During the reference week, the predominant wind direction was N-E, perpendicular to the South-West side of the barn, therefore of great relevance for the study.
In this study, to build a wind velocity profile, an equilibrium boundary layer was assumed and data acquired by the weather station were used in the power law reported in the following Equation 26:

$$\frac{U_y}{U_{ref}} = \left(\frac{Y}{Y_{ref}}\right)^{\alpha} \qquad (26)$$

where U_{ref} is the mean velocity at reference height, Y_{ref} is the reference height, and α is the power law exponent.

3.4. CFD analysis

The following methodology was applied in the same way both in the basis configuration - which reflects the real distribution of spaces, openings and context - and in alternative design configurations, which include variations of building elements. A limitation not concerning the modelling process is that the experiment was conducted under isothermal hypotesis. This choice, together with the simplification concerning the model, would not affect the objective of the present study, because all the elements which strongly affect the airflow development and air velocity distribution were taken into account, as reported in some past studies (Rong et al., 2016).

3.4.1 3D modelling with Autodesk Autocad 2016® software

The geometry model was built in a Cartesian coordinate system with Autodesk Autocad 2016® software tool (2016 Autodesk In., San Rafael, CA, USA). The axes of the Cartesian coordinate system were set parallel to the longitudinal axis of the barn. As reported in the guidelines referred to the best practice, in this modelling phase the case study was reproduced with an adequate level of detail. The term “adequate” means that the level of detail should be enough to reflect the real situation, but not too much for not having too many cells in the meshing phase, that would imply an excessive computational cost (Franke et al., 2007).
Many simplifications were made in order to reach this goal. All the small internal elements - such as trusses, fences, fans and steel pillars - were excluded or simplified. The floor was

considered at a single height and the corrugated fibre cement sheet roofing has been simplified and modelled as smooth plan. The barn was modelled as an empty building, i.e. without dairy cows. The surrounding buildings and trees were reproduced as simple geometries, i.e. parallelepiped and prisms; about the trees, only the foliage and not the trunk was considered. Finally, all the solids were reduced to surfaces.
In this phase, also the computational domain was modelled. The choice of the size of computational domain is of utmost importance, in order to consider all the flow structures.
Ideally, where wind data are collected in a site that is distant from the building as in this case, a CFD computational domain should be large enough to include the building and the site where the wind records were made (Etheridge, 2015). Also, the computational domain should be large enough to consider the flow development (and flow re-development behind the wake region) and to not lead to an artificial acceleration of the flow in the region of interest.
Taking as reference one of the most adopted guideline in this research field, i.e. COST guideline (Franke et al., 2007), the following considerations were made.
As minimum requirement, a building with height H has an influence until a distance equal to 6H. By considering a height of the barn approximately equal to 7 m, all the structures considered relevant for the airflow development belonging to a circular area with a diameter of 84 m having as a central point the barn were included in the domain.
The COST guideline gives different rules depending on the number of buildings included in the domain. As in this case five buildings belong to the domain, the rules related to multiple buildings are followed. The tallest building is the barn, so H_{max}=7 m.

- Vertical extension for multiple buildings: for multiple buildings, the top of the computational domain should be at $5H_{max}$ above the roof of the tallest building, with a height equal to H_{max}.
- Lateral extension for multiple buildings: for multiple buildings, the lateral extension of the computational domain should be at $5H_{max}$ to that part of the built area which surrounds the region of interest.

Since the COST guidelines do not give precise rules regarding the distance to be taken in the direction of the airflow, the longitudinal extensions of the domain, i.e. the region in front of (approach flow) and the region behind (wake) the built area, were set equal to $5H_{max}$ and $20H_{max}$ respectively (Santonolini et al., 2018).

Therefore, the computational domain was built as a parallelepiped; taken as reference the height of the building H_{max}, the inlet surface, the vertical and the lateral extensions were set equal to 5 times H_{max} from the building closest to the perimeter of the domain. The outflow boundary is positioned at about at 20 times H_{max} downwind the building.

Figure 21. Case study domain

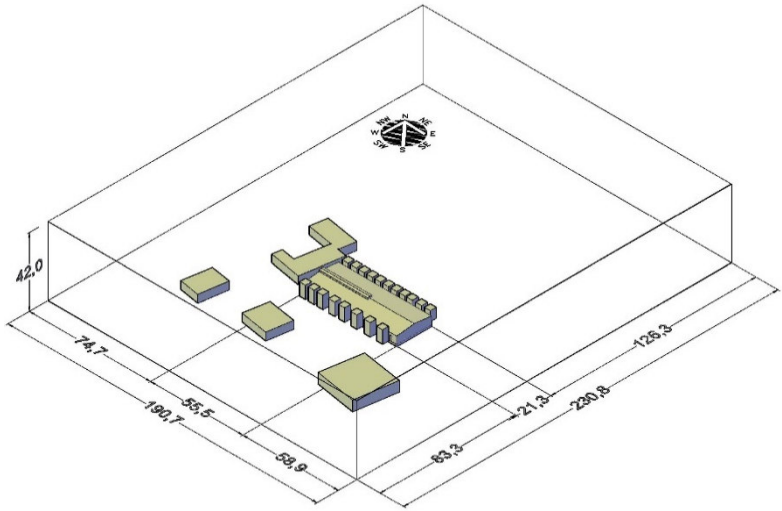

3.4.2 Meshing phase

Figure 22. Mesh nomenclature

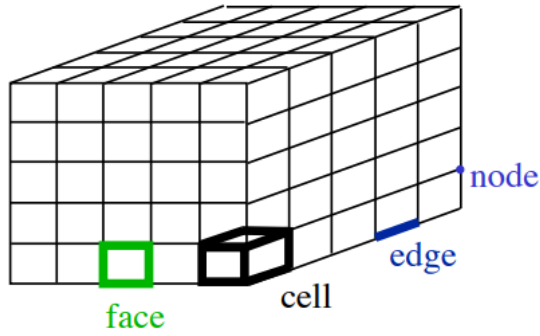

In this context, mesh processing and setting of boundary conditions were conducted by using Ansys CFD 17.1®, where the geometry model was imported. The mesh used was:

- hexahedral: hexahedra shapes are preferable to tetrahedral shapes; in fact, this choice will introduce smaller truncation errors and allow better iterative convergence (Hirsch et al., 2002);
- unstructured, since it was very flexible compared to the structured one for building with complex geometries.

Rules given by literature guidelines were followed to choose the cells parameters (i.e. ratio and spacing). Some computations concerning geometries simpler than the final one were conducted in order to assess the necessary mesh resolution (Blocken et al., 2004). Furthermore, alternative configurations – which include finest meshes – were adopted for comparing and analysing the different outcomes.

The quality of the mesh must be high enough not to affect the results, and its resolution should capture the physical

phenomena (Franke et al., 2007; Casey & Wintergerste, 2000). Ideally, a simulation should be independent by the choice related to the computational grid (Rong et al., 2016), but it is almost impossible due to the computer limitations.
Once the mesh has been created and simulated, other two meshes having different number of cells were created and simulated in order to compare the results. The similarity of the results means the lack of significant grid-dependence on the solution.
Following, the steps made to build the model and the relative mesh are reported.

STEP 1: model import in Ansys ICEM 17.1® and first phases of modelling

The model in .IGES format was imported in Ansys ICEM 17.1® (*File → Import geometry → Legacy → STEP/IGES*).

Figure 23. First phase of modelling

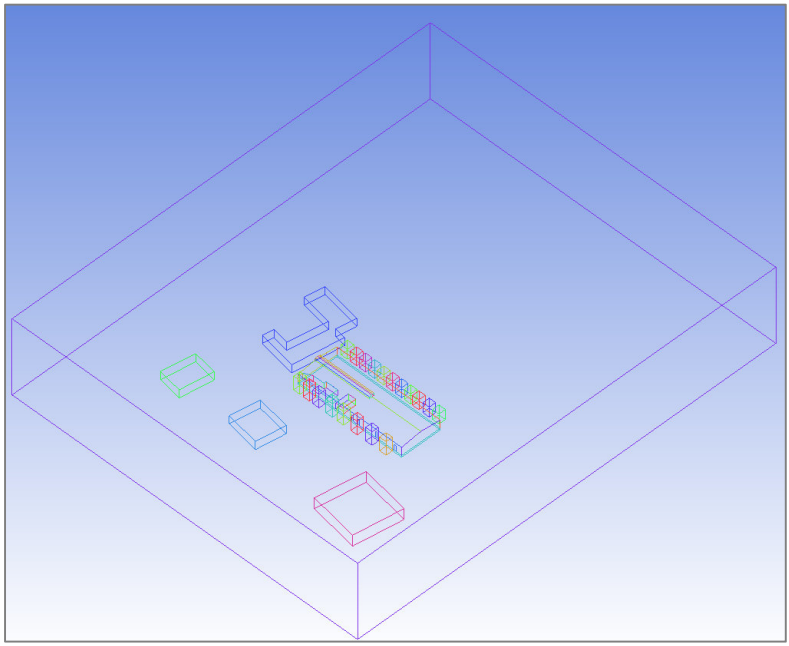

The geometry was “repaired” (*Geometry → Repair Geometry → Build Diagnostic Topology; Tolerance = 0.01*), in order to verify the “correctness” of the imported.

Figure 24. Geometry repair

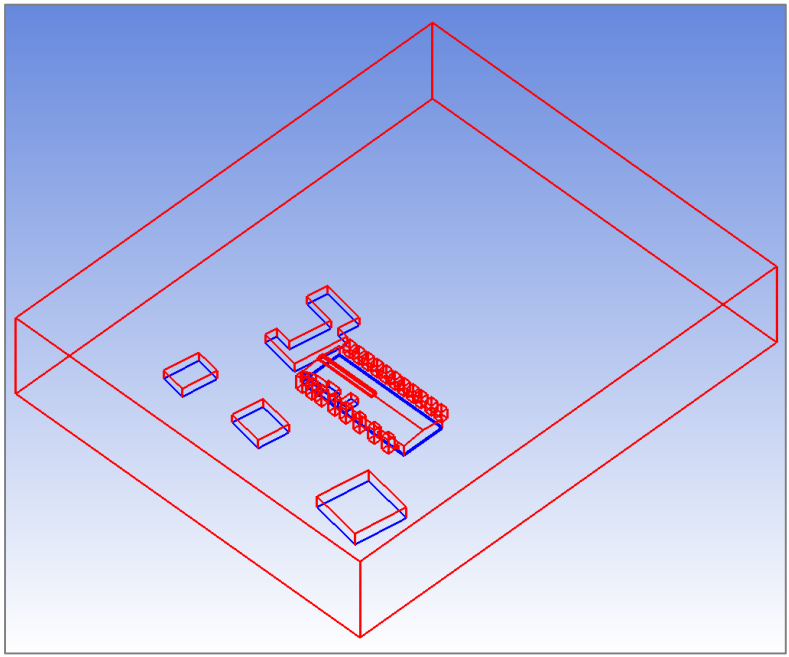

In particular:

- the tolerance is defined in units of the model, and controls how accurately you want to treat surface-to-surface proximity;
- red line = double edge curves (curves adjacent to two surfaces);
  blue line = multiple edge curves (curves adjacent to three or more surfaces) *(Ansys ICEM 17.1 Help).*

All the parts were renamed (*Parts* → *Rename*) and grouped in:

- *openings*, distinguished according to orientation and position (floor level or roof elevation);

- *trees*;
- *surrounding buildings*;
- *wall*, distinguished according to orientation and position (internal or external);
- *roof*, distinguished according to position (first roof or second roof);
- *floor*;
- *domain parts*, distinguished according to position and "rule" in above, below, lateral (2x), inlet and outlet.

The "body" (i.e. the fluid "air") was defined (*Geometry → Create Body → Material Point*).

STEP 2: Geometry "blocking"

This step consisted of Domain Decomposition, i.e. splitting the domain into smaller blocks and then generating separate meshes in each individual block. Because of the complexity of the geometry (part of the domain is slanting for the shape of the roof and the buildings around), this phase was particularly difficult, so many tests were done in order to obtain blocks that were - as far as possible - "regular" from the point of view of the sides and corners. For the creation of blocks - after the creation of the first block - different commands were used, grouping according to purpose:

- Blocks splitting (*Blocking → Split block*, with many *Split Methods*)
- Geometry association (*Blocking → Associate*, in order to associate corners or side using respectively *Associate vertex* and *Associate Edge to Curve*)
- Alignment of parts (*Blocking → Move vertex*, using according to the case *Move vertex*, *Set location*, *Align Vertices* and *Align Vertices in line*).

If necessary, points and curves were also created (*Geometry → Create Points, Create/Modify Curve...*).

Figure 25. Geometry "blocking"

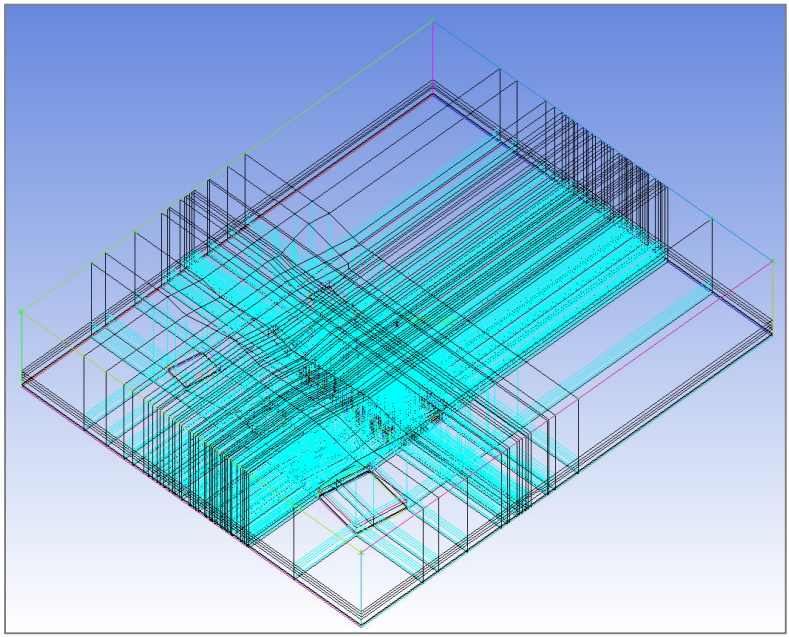

The blocks in correspondence with the internal offices, the raised floor, the surrounding buildings and the trees have been defined and isolated.

STEP 3: Meshing process

This step consisted of meshing process. In *Edge Parameters* (*Blocking – Pre-Mesh Parameters*), the following parameters have been set:

- *Spacing 1-2*
  - = 0.1 close to solids;
  - = 0.0 in the remaining points (as at the ends).
- *Ratio 1-2* = 1.3

In a first setting, the Spacing 1-2 have been set lower than or equal to 0.1 and the Ratio has been set equal to 1.2, as should be done canonically. In fact, in regions with high gradient, the expansion ratio between two consecutive cells should be below 1.3 or 1.2, as reported in Scaperdas and Gilham (2004) and in Bartzis et al. (2004). However, the number of resulting mesh nodes was too high, i.e. about 20 million.

Figure 26. Edge meshing parameters

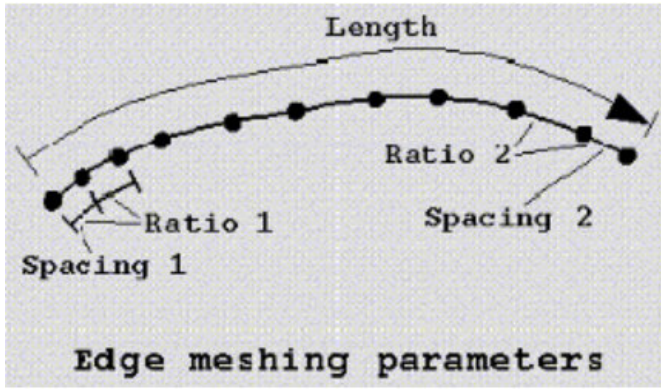

Mesh process was checked during the construction (*Tree – Blocking – Pre-Mesh*). Through *Pre-mesh – Info*, the number of nodes, cells and elements were checked. The result is illustrated in the following figure.

Figure 27. The unstructured mesh

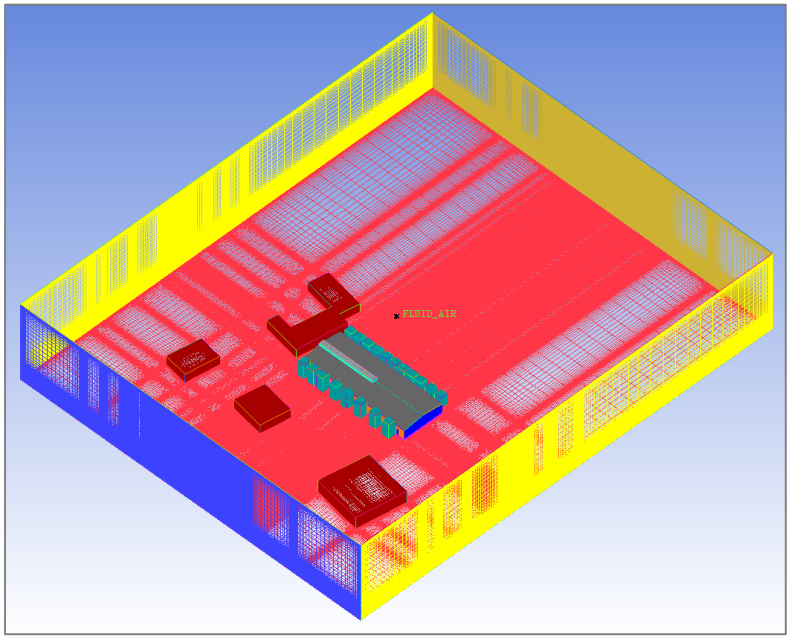

The software Ansys Fluent 17.1® was set as Output solver (*Output Mesh – Select Solver*).

Before to build and export the unstructured mesh, the boundary conditions were defined *(Output Mesh – Boundary Condition)* as reported below:

a. openings and trees→ *interior;*
b. surrounding buildings, walls, roofs, floor and lower part of the domain → *wall;*
c. upper and lateral parts of the domain → *symmetry*

Setting the top boundary conditions is of utmost importance in order to have an equilibrium, generally obtained assuming a constant shear stress over the boundary layer (Franke et al., 2007; Richards & Hoxey,

1993; Hargreaves & Wright, 2006) corresponding to the inflow profiles. Symmetry boundary conditions have been used on the top side of the computational domain to enforce a parallel flow (Shen et al., 2013; Ramponi and Blocken, 2012; Di Sabatino et al., 2007; Horan and Finn, 2008; Perèn et al., 2015; Montazeri et Montazeri, 2018).

d. part of the domain corresponding to the air inlet → *velocity inlet;*
e. part of the domain corresponding to the air outlet → *outflow.* In fact, in order to obtain a fully developed flow (Gromke et al., 2008), in the outlet boundary conditions it should be used a boundary condition in which all flow variables are forced to vanish (Franke et al., 2007), such as “outflow”.

Figure 28. External boundary conditions

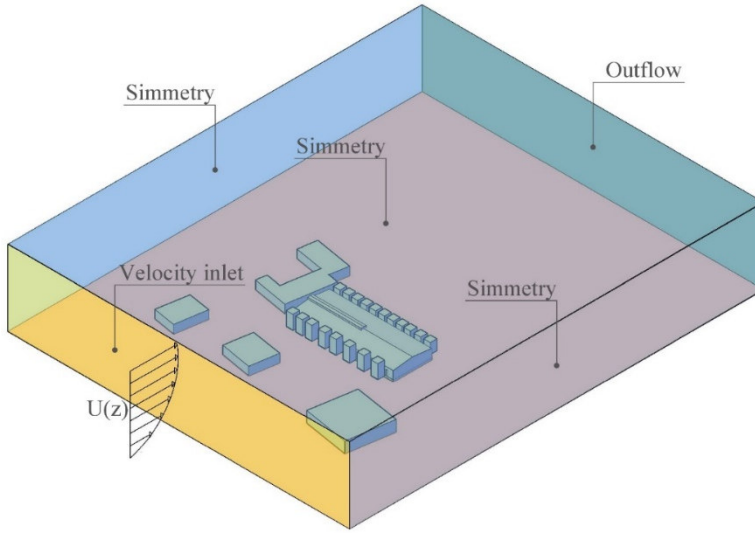

The blocks corresponding to the floor, the internal offices and the surrounding buildings were not exported to Fluent, as the air flow does not pass through them. The air, instead, passes through the crown of the trees, so the relative blocks have been defined and exported.
The unstructured mesh was finally generated (*Tree – Blocking – Convert to Unstructur Mesh,* then *Output mesh – Write input*).
As reported in the workshop "*3D Pipe Junction Using Hexa Meshing*" (©ANSYS, Inc. February 11, 2010): *«The major quality criteria for a hexa mesh are angle, determinant, and warpage».*
In the User's Guide, details on the definitions and the available quality measures are reported:

- ***Angle****: this option checks the maximum internal angle deviation from 90 degrees for each element. If the elements are distorted and the internal angles are small, the accuracy of the solution will decrease. It is always wise to check with the solver provider to obtain limits for the internal angle threshold.*
- ***Determinant (2x2x2 stencil)****: the Determinant, more properly defined as the relative determinant, is the ratio of the smallest determinant of the Jacobian matrix divided by the largest determinant of the Jacobian matrix. In this option, the determinant at each corner of the hexahedron is found. The default range is 0–1 with a Determinant value of 1 indicating a perfectly regular mesh element and 0 indicating an element degenerate in one or more edges. Negative values indicate inverted elements.*

  This determinant is appropriate for 3D linear hexas and calculates more quickly than the 3x3x3 matrix because it does not include the unnecessary mid side nodes.

- ***Warpage:*** *this computes the distortion of a plane, based upon the nodes that compose the surface. The default range is 0–90, where a warpage value of 0 is flat (preferred) while 90 is degenerate.*

These values were checked.

3.4.3 CFD modelling and simulations with Ansys Fluent 2017® software

The numerical simulations, by setting turbulence model, porous media and solver setting, have been carried out by using the Ansys-Fluent 17.1® program.

Step 1. Import of mesh in Ansys Fluent 17.1® and check

The mesh file .msh was imported in Ansys Fluent 17.1 (*File → Read → Mesh*), where the problem dimension was set (*3D*) and the *Double precision* was set (because of the dimension problem and the high value of elements). The *double precision solver* was chosen in order to reduce the round-off error – i.e. *the difference between the calculated approximation of a number and its exact mathematical value due to rounding* (Franke et al., 2007).

As processing option, the *Parallel* one was set; with this option, the solution is calculated using multiple processes that can be performed on the same computer or on different computers of the same network.

The mesh was then checked, ensuring the right shape and the connection between the cells (*Setting Up Domain → Mesh → Check*). The absence of errors has been checked, as well as the absence of a minimum value of the negative cells, which would make it impossible to start the calculation.

As suggested by Fluent, the wall distance was repaired (using the text interface: *Select (enter) → Solve (enter) → Repair-wall-distance*).

For visualization, it was decided to activate only the surfaces and to activate "Edges" and "Outline".
The magnitude of the domain has been checked (*General → Mesh → Scale*).
The quality of the mesh has also been checked (*Setting Up Domain → Mesh → Quality*).
The orthogonality of the cells is an important indicator of the quality of the mesh: its value can vary from 0 to 1, with low values indicating lower quality cells. In general, the minimum orthogonality should not be less than 0.01. In this case, the Minimum Orthogonal Quality is equal to 0.571.
By using (*Setting Up Domain → Mesh → Display*), the elements were "turned on" or “turned off”, as well as suitably distinguished by colour.

Figure 29. The unstructured mesh

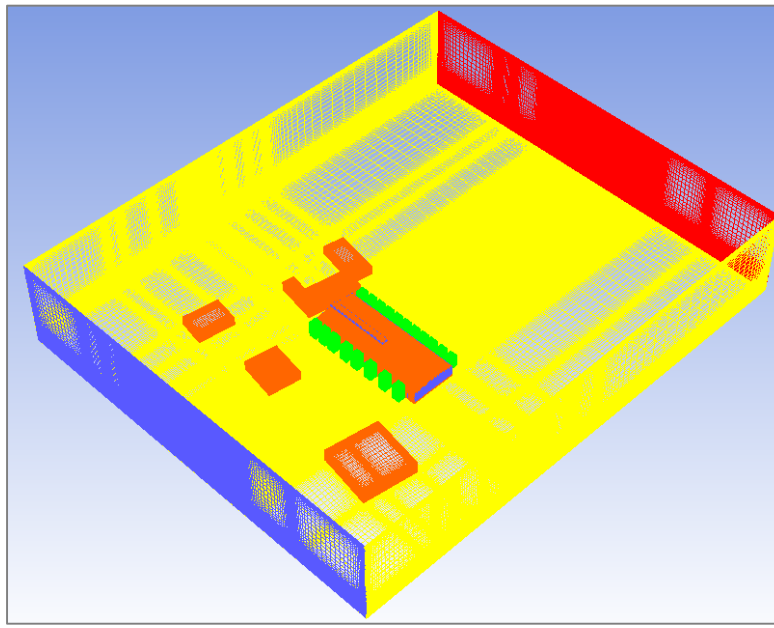

Two control surfaces have been created (*Setting Up Domain → Surface → Create → Plane*): a vertical plane (i.e., Plane A) and one horizontal plane (i.e. Plane B) were defined in relevant location (Fig.7); in detail, the second was considered the most relevant because of its position at a height corresponding to that of the cow's snout.

Figure 30. The analysed plans

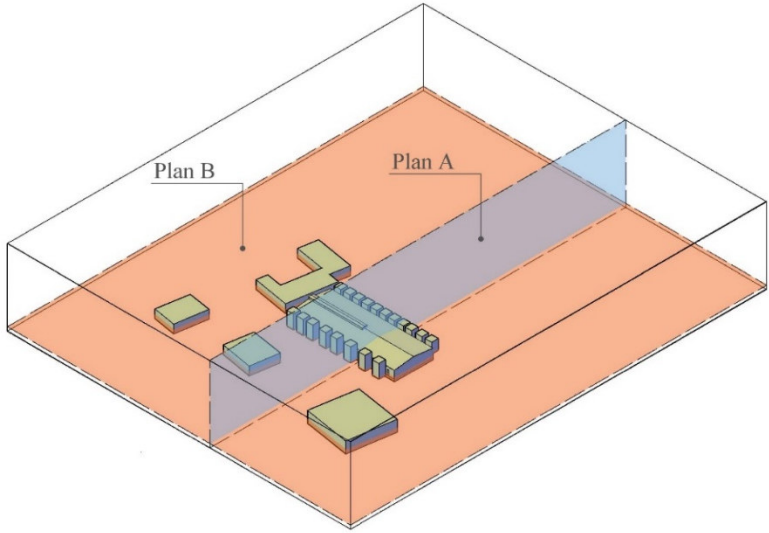

Two control points have been created (*Setting Up Domain → Surface → Create → Point*), in correspondence of the internal and external probes.

Step 2. Definition of solver setting

In this step (*Setting Up Physics → Solver*), the following parameters were set:

- The "time" – ***Steady***, i.e. the simulation has been run in steady-state conditions;
- The "type" of simulation – ***Pressure-based***, used if we want to calculate a spatially periodic flow field with a specific mass flow or with a specific pressure derivative and which activates the *pressure-based Navier-Stokes solution algorithm*.
- The velocity formulation – ***Absolute***.

Step 3. Definition of turbulence model and turbulence parameters/Definition of boundary conditions

During the process of CFD modeling, one important step is to select the appropriate turbulence models which solve to describe the turbulent flow.

The ***Standard k-ε model*** – i.e. a semi-empirical model based on transport equations for the turbulent kinetic energy and its dissipation rate – was set (*Setting Up Physics → Models → Viscous*). Using a Standard k-ε model, turbulence quantities are required, and their profile is obtained assuming that there is an equilibrium boundary layer (therefore, neutral stability conditions). Richards and Hoxey (1993) gave a detailed explanation of the homogenous turbulent flow over rural terrain and defined the mean turbulent kinetic energy and dissipation rate inlet profiles for use in CFD simulations employing k–ε turbulence model. The dissipation rate profile has been specified as:

$$\varepsilon = \frac{u_*^3}{K_v(z + z_0)} \tag{27}$$

where K_v is the von Karman's constant, z_0 is the surface roughness and u_* is the friction velocity, calculated from a specified velocity U_{ref} at a reference height. The turbulence kinetic energy for inlet boundary was derived from:

$$K = \frac{u_*^2}{\sqrt{C_\mu}} \tag{28}$$

where C_μ is an empirical constant.

This turbulence model was chosen due to its simple format and robust performance and because of its favourable

convergence behaviour and reasonable accuracy (Norton et al., 2007; Rong et al., 2016).
The Standard Wall Functions by Launder and Spalding (1974) were chosen as wall treatment for solid surfaces.
The incoming flow profile should consider the effect of changes in wind direction with height (VDI, 2005). Regarding the wind velocity, by assuming an equilibrium boundary layer, the mean velocity has been obtained developing a power-law.
To insert the profiles of v and ε (belonging to a single file), functions have been used, i.e. **User-Defined Function (UDF)**. As reported in "ANSYS FLUENT 12.0: UDF Manual": «*A user-defined function, or UDF, is a function that you program that can be dynamically loaded with the ANSYS FLUENT solver to enhance the standard features of the code (…) ».*
The UDFs used were built with a C programming language, in particular via Notepad ++.
So *«predefined macros and functions supplied by ANSYS FLUENT»*, were not used but were *«executed as interpreted or compiled functions».* In fact, *«Inside ANSYS FLUENT, the source code is compiled into an intermediate, architecture-independent machine code using a C preprocessor. This machine code then executes on an internal emulator, or interpreter, when the UDF is invoked».*
To import the UDF, firstly it was "interpreted" (*User-Defined → Functions → Interpreted → Browse → Interpret).*
The UDFs were then set (*Setting-Up physics → Boundaries → Inlets → Inlet→ Edit).*
For the "Velocity Specification Method", "Components" setting was chosen, which *allows specification in terms of the Cartesian, cylindrical, or local cylindrical velocity components* (Help Fluent). As *Turbolence*, *Specification*

Method, "K e Epsilon Method" was chosen. For v and ε, the profile set through the UDF was chosen.
The turbulence kinetic energy for inlet boundaries was set as a constant value.
For the walls the standard values have been left, that are:

- Wall Motion → **Stationary Wall**, condition which "*specifies that the wall is not moving relative to the adjacent cell zone*" (Help Fluent).
- Shear Condition → **No Slip**, condition which "*specifies that the wall is not moving relative to the adjacent cell zone"* (Help Fluent).

Step 4. Definition of porous media parameters
Because there are porous media, i.e. the trees, additional inputs for the problem setup should be added for each zone (*Setting Up Physics → Zone → Edit*).
The nineteen trees surrounding the building – nine located at North-East side and eleven located at South-West side – were modelled as porous media. In general, porous barriers are wind momentum sinks (i.e., pressure loss) when the surfaces interact with airflow (Guo and Maghirang, 2012).
The porous media were simulated based on the following Equation 29 and 30, i.e. the model of the porous media was added to the fluid flow equation as a momentum sink:

$$S_i = -\left(\frac{\mu}{\alpha}u_i + C_2\frac{1}{2}\rho|u|u_i\right) \quad (29)$$

$$C_2 = \frac{k_r}{W} \quad (30)$$

Where S_i is equivalent to pressure gradient, μ is the air dynamic viscosity (Nm^{-2}), α is the permeability, ρ is the air density (kgm^{-3}), $|u|$ is the magnitude of the air velocity, C_2

is the inertial resistance factor, K_r is the dynamic parameter that depends on porosity and shape of the barrier elements and W is the width of vegetative barrier (m). In particular, the term $\frac{\mu}{\alpha}u_i$ is the viscous loss term and $C_2\frac{1}{2}\rho|u|u_i$ is the inertial loss term.

Step 5. Solver settings

A standard discretization scheme was used for pressure and second order upwind discretization schemes (Barth and Jespersen, 1989) were used for Momentum, Turbolent kinetic Energy and Turbulent Dissipation Rate. These settings were chosen in order to increase the accuracy and reduce numerical diffusion. The SIMPLE scheme was used for the pressure-velocity coupling. The residuals were reduced at four orders of magnitude (Franke et al., 2007). All the simulations have been run in steady-state conditions.

Step 6. Reports settings

The first step that conduct to an appropriate simulation is the selection of target variables, which are chosen according to the sensitivity to numerical treatment and resolution and to the possibility of control during the post-processing. Then, uncertainty of chosen data should be reduced as much as possible by considering only data that have small uncertainties and by evaluating their reliability (Franke et al., 2007; Schlünzen, 1997; Menter et al., 2002).

Two Surface Monitors were created at the sections activated at the beginning.

From the *Tree*, *Solution* → *Monitors* → *Surface* → *New*, were chosen, then:

- *Report Type = Sum;*
- *Field Variable = Velocity-Velocity magnitude*,

by selecting the creating sections. For both, *Plot* and *Print* were set.
Two control surface (to check the *mass flow rate*) were added, at the inlet and outlet.
At the monitoring points, the following values have been set:

- *Report Type = Sum;*
- *Field Variable = Mass flow rate*.

Step 7. Solving: initialization and calculation
First, an initialization was carried out (*Solving* → *Initialization* → *Initialize*): initialization creates the initial solution that the solver will improve in an iterative way. Generally, for a steady state analysis, the same convergent solution is reached regardless of initialization, but convergence will be faster if the starting point is more realistic.
In this case study, the *Hybrid Method* was used. Unlike the Standard method - where the same values are set in all cells - the Hybrid method is based exclusively on the simulation configuration, without requiring further information. This method produces a velocity field conforming to complex domain geometries and a pressure range that fluidly connects high and low pressure values.
For the calculation, *Solving* → *Run Calculation* was selected.

- First, *Check Case* was used to see if, according to Fluent, what has been done can be improved. An inscription that appears indicates *No recommendation to make at this time*.
- In *Iterations*, iterations number was set.

As soon as we have set the parameters, *Calculate* was used.
The solution will stop as soon as the residuals have reached their specific value or after the specified iteration value has been reached.

4. Results and discussion

Results and discussion regard the basis configuration of the barn (real distribution of spaces, openings and context) with data acquired by the Acate weather station are presented in the following paragraphs, except for: the paragraph 4.3, which regard the simulations that consider as input hourly data; the paragraph 4.7, which regards the study of air velocity distribution in alternative design configurations of the barn; the paragraph 4.8, which regards the analysis of the cow behaviour.

4.1 Setting of model parameters by data analyses

A wind rose was used to represent the prevailing wind direction and velocity magnitude during the reference week (SIAS, 2016). Approximately 32.5 % of data recorded between 26 April 2016 and 2 May 2016 revealed a prevailing wind direction from N-E at 10 m height. The logged wind velocities ranged from 0.70 ms^{-1} to 9.60 ms^{-1}, with mean values and standard deviation equal to 3.85 ms^{-1} and 2.59 ms^{-1}, respectively.

Figure 31. Prevailing air velocity and magnitude in the reference week

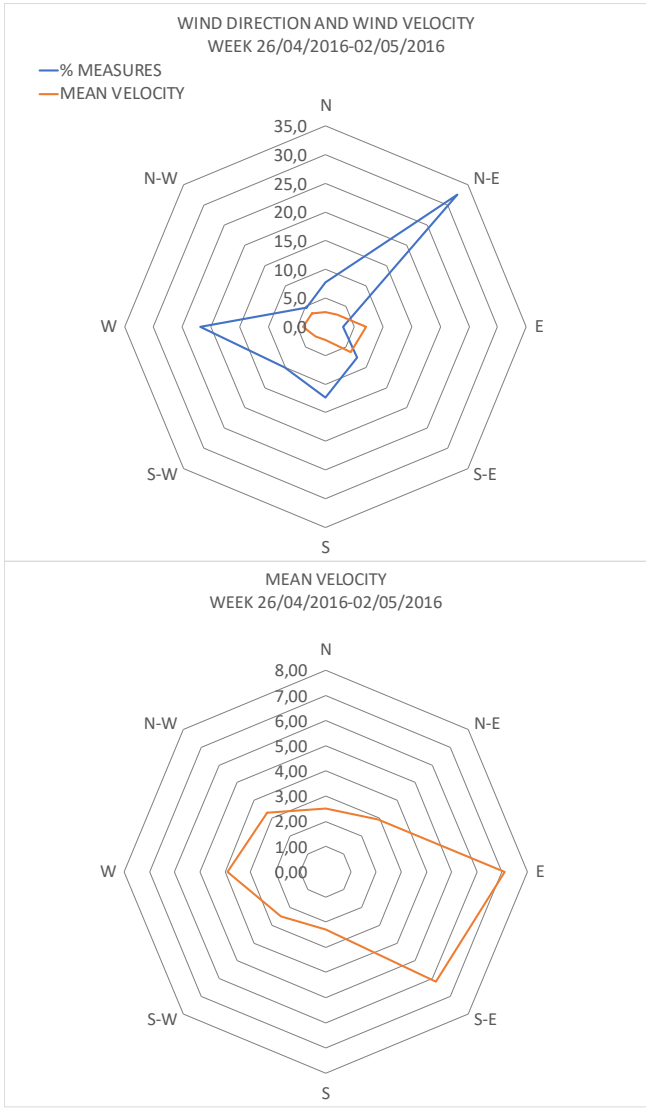

To build the velocity profile by using the Equation 1, the following values of the parameters U_{ref}, Y_{ref} and α were used:
- a mean velocity U_{ref} at reference height equal to 3.85 ms^{-1};
- a reference height Y_{ref} equal to 10 m;
- and a power law exponent α equal to 0.14: that parameter was chosen because in previous research studies it was utilized to obtain the normal profile of the natural wind in open rural field with few trees and buildings (Wu et al., 2012) and because it should be considered indicative of a fully developed turbulence (Sullivan and Greeley, 1993; Schlichting, 1979).

To build the dissipation rate profile by using the Equation 27, the following values were used: by taking as reference the average value of the von Karman's constant k_v studied in previous reviews (Foken, 2006; Hogstrom, 1988; Hogstrom, 1996), it was set equal to 0.385; the surface roughness z_0 was set equal to 0.019 m (Wieringa, 1992) and, by applying the Equation 2, the friction velocity u_* was set equal to 0.236 ms^{-1}, taking as reference a height of 10 m.

The turbulence kinetic energy for inlet boundary was set as a constant value, derived from Equation 28, where C_μ is an empirical constant taken equal to 0.09 (Ramponi et al., 2012).

The incoming wind velocity profile shows wind speed growth along with height increase (VDI, 2005). The created profiles (used as single file, where it was specified at the beginning of each profile the relative name) are:

1) **Velocity at inlet_power law**

```
# include "udf.h"

DEFINE_PROFILE(inlet_velocity, thread, index)
```

```
{
   real p[ND_ND];
   real y, u0=3.85, yref=10.0;
   face_t f;
   begin_f_loop (f, thread)
   {
     F_CENTROID (p,f,thread);
     y=p[1];
     F_PROFILE(f,thread,index)=-u0*pow(y/yref,0.14);
   }
   end_f_loop(f, thread)
}
```

2) Dissipation ε at the inlet

```
# include "udf.h"

DEFINE_PROFILE(inlet_epson, thread, index)
{
   real p[ND_ND];
   real y, y0=0.019, u0=0.278;
   face_t f;
   begin_f_loop (f, thread)
   {
     F_CENTROID (p,f,thread);
     y=p[1];

F_PROFILE(f,thread,index)=(1/0.385)*pow(u0,3.0)/(y
+y0);
   }
   end_f_loop(f, thread)
}
```

The porosity has not been directly estimated. According to Gan and Salim (2014), the porosity value of 0.96 was assumed. According to Guo and Maghirang (2012), viscous loss term in Equation 29 was ignored, so the viscous resistance was set as 0. According to previous researches (Jeanjean et al., 2015), C_d was set equal to 0.25 and Leaf Area Density (LAD) was set equal to 1.6 m^{-1}, so the final pressure loss coefficient is 0.4 m^{-1}.
Finally, model convergence was not assumed to be reached until both the velocity magnitude at the monitoring points and the residual has stabilized (Rong et al., 2016). After the simulation was completed, the balance of mass has been checked.

4.2 Convergence study

The convergence was not assumed to be reached until both the velocity magnitude at the monitoring points – i.e. at the points corresponding to the sample ones – and the residual have stabilized (Rong et al., 2016). The iteration steps necessary to reach a convergent solution were about 1500. After the simulation was completed, the balance of mass has been checked.

Figure 32. Residuals

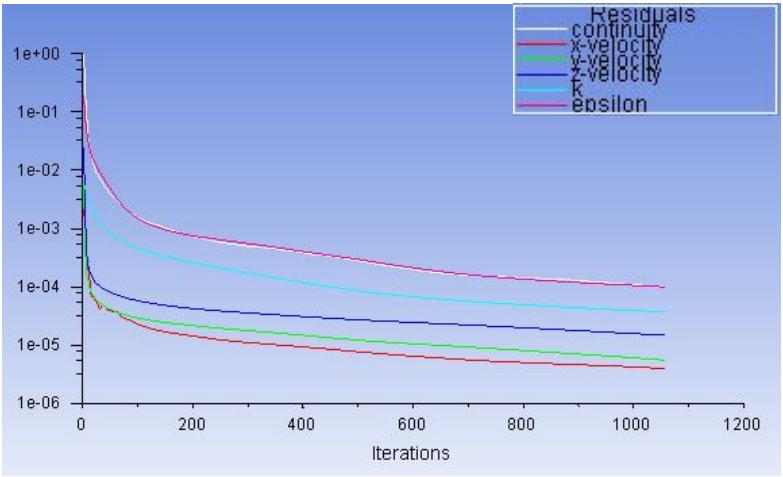

Through *Postprocessing* → *Reports* → *Fluxes* → *Flux Reports* → *Mass Flow Rate*, by setting Inlet and Outlet, the following results are obtained:

Table 6. Mass flow rate

Mass Flow Rate (kg/s)	
Inlet	40511.027
Outlet	-40511.027
Net	-3.3469405e-10

Figure 33. Mass flow rate

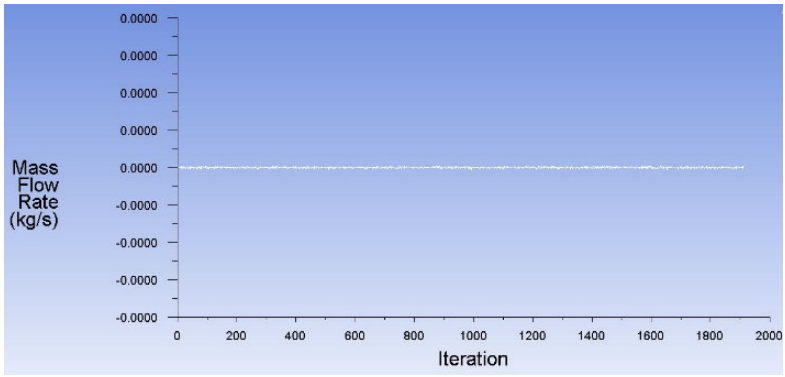

4.3 Validation of the model

Through *Postprocessing* → *Reports* → *Surface integrals*, the velocity magnitude (*Velocity* → *Velocity magnitude)* was calculated in the sample points.

The validation of the model was carried out through the comparison between air velocity hourly data measured inside the barn and air velocity hourly data obtained after the simulations in the same point (i.e., sensor inside and outside the model, Figure 15).

Twenty simulations are reported in the present study, taking into consideration the hours of the reference week in which the prevailing wind direction was N-E both at the Acate weather station and at the measurement point located above the roof (Table 7). The chosen hours were all nocturnal also because of the absence of buoyancy forces (i.e. because the natural ventilation is only wind driven). In fact, the aim of the research is to study only the natural ventilation induced by wind.

Table 7. Data comparison between measurements and simulations

N. simulation	Air velocity at weather station (H=10 m) (ms^{-1})	Air velocity in sensor outside the barn (ms^{-1})			Air velocity in sensor inside the barn (ms^{-1})		
		MEASURED	SIMULATED	RELATIVE ERROR %	MEASURED	SIMULATED	RELATIVI ERROR %
1 (27/04-22:00)	1.90	1.14	1.38	18.84	0.24	0.29	16.90
2 (28/04-02:00)	2.90	1.83	2.08	13.02	0.40	0.45	12.31
3 (28/04-06:00)	2.70	2.04	1.89	7.56	0.44	0.44	0.32
4 (28/04-07:00)	2.70	1.96	1.89	3.64	0.46	0.44	5.00
5 (28/04-19:00)	6.40	3.94	4.59	15.31	0.98	0.98	0.08
6 (28/04-20:00)	6.00	3.43	4.31	22.82	0.79	0.91	14.70
7 (28/04-21:00)	7.80	3.38	5.58	49.21	0.89	1.19	29.13
8 (28/04-22:00)	7.90	4.51	5.66	22.65	1.07	1.20	11.36
9 (29/04-00:00)	5.80	4.06	4.17	2.68	0.95	0.88	7.71
10(29/04-01:00)	6.80	4.27	4.89	13.45	1.10	1.03	6.35
11(29/04-02:00)	8.20	5.50	5.89	6.89	1.23	1.26	2.07
12(29/04-03:00)	6.80	4.45	4.89	9.48	1.02	1.03	0.98
13(29/04-05:00	8.50	3.97	6.08	42.04	0.89	1.29	36.98
14(29/04-06:00)	8.50	4.13	6.08	38.17	0.87	1.29	39.22
15(30/04-00:00)	2.00	1.16	1.44	21.30	0.32	0.31	4.23
16(30/04-01:00)	2.50	1.45	1.80	21.65	0.27	0.38	35.59
17(30/04-02:00)	2.00	1.34	1.44	7.48	0.32	0.31	1.98
18(01/05-01:00)	2.80	2.00	2.01	0.54	0.45	0.43	4.72
19(01/05-02:00)	2.00	1.99	1.44	32.04	0.39	0.31	23.36
20(01/05-05:00)	1.40	0.93	0.98	5.43	0.32	0.24	29.61

For each pair of values measured and simulated, the absolute error (i.e. the absolute value of the difference between measured and simulated data), the average value (i.e. the sum of the values divided by the number of values) and the relative error (i.e. the ratio between absolute error and average value) were calculated. The relative error is often used for the comparison between measured and simulated data (Zhang et al., 2007; Valenti et al., 2018) due to its precision in estimating the "tolerability" of the error: a low relative error corresponds to a greater precision in the measurement carried out. With relation to the air velocity outside the barn, the validation of the CFD model can be considered good (relative error <10%) in 40 % simulations, acceptable (relative error <30%) in 40% simulations and marginal (relative error <50%) in 20% simulations carried out. With relation to the air velocity inside the barn, the validation of the CFD model can be considered good (relative error <10%) in 50% simulations, acceptable (relative error <30%) in 35% simulations and marginal (relative error <50%) in 15% simulations carried out.

In general, the air velocity at weather station in Acate is higher than the air velocity measured in the sensor located above the chimney outside the barn. This is due to the obstacles located between the weather station and the barn that reduce the air velocity.

Figure 34. Wind profile

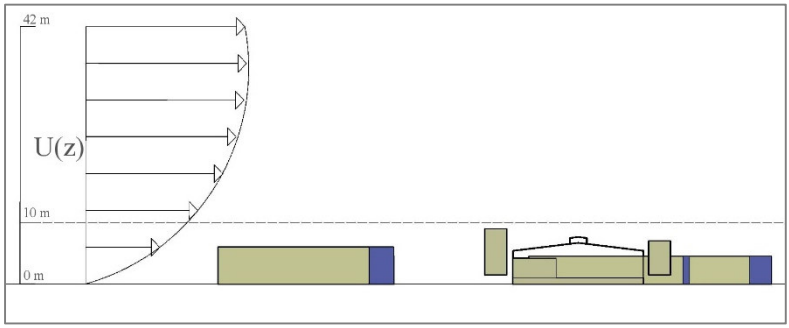

As expected, the air velocity measured in the sensor located inside the barn is lower than the air velocity measured in the sensor above the chimney, because at a lower height the airflow intercepts more obstacles and because of the south-west wall of the barn, located in front of the trees and having only four small openings (2.75 m^2 each) (Figure 35).

Figure 35. Comparison between air velocity at weather station, air velocity measured outside the barn and air velocity measured inside the barn

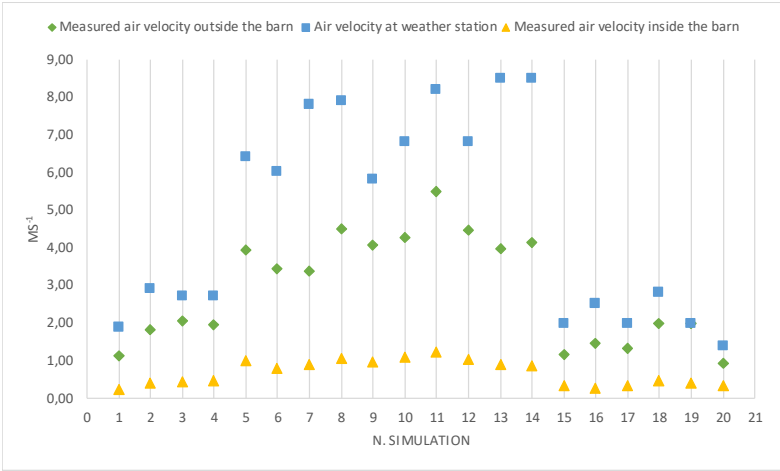

At a height of 10 m, the average air velocity at weather station in Acate is 4.8 ms^{-1}.

For values of air velocity at weather station lower than 4.8 ms^{-1}:

- the simulated air velocity outside the barn is overestimated in 70% of the simulation. The relative error is <10 % in 50% simulations, <30 % in 40% simulations and <50 % in 10% simulations (Figure 36);
- the simulated air velocity inside the barn is overestimated in 30% of the simulation. The relative error is <10 % in 50% simulations, <30 % in 40% simulations and <50 % in 10% simulations (Figure 37).

Figure 36. Comparison between measured and simulated air velocity outside the barn (V<4.8 ms^{-1})

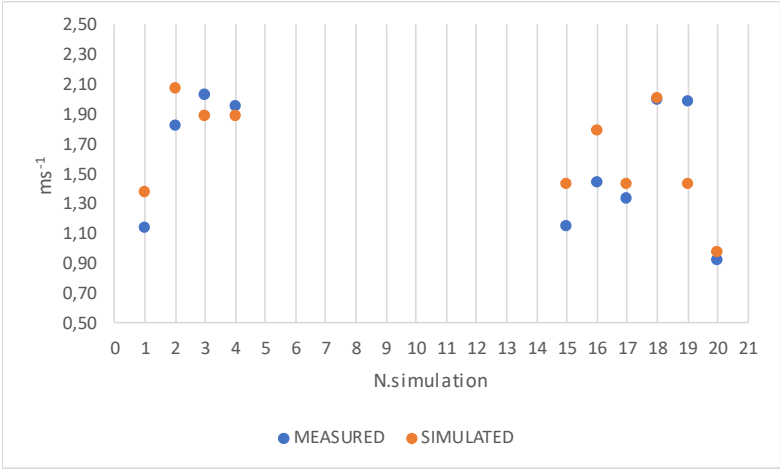

Figure 37. Comparison between measured and simulated air velocity inside the barn (V<4.8 ms^{-1})

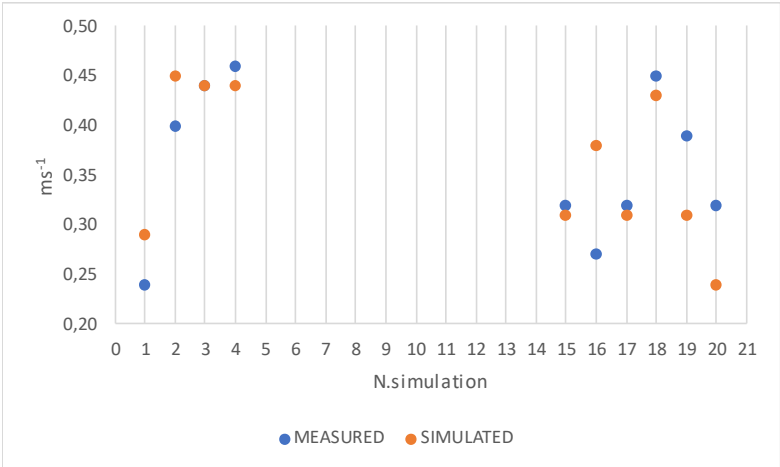

For values of air velocity at weather station higher than 4.8 ms^{-1}:

- the simulated air velocity outside the barn is overestimated in 100% of the simulation. The relative error is <10 % in 20% simulations, <30 % in 50% simulations and <50 % in 30% simulations (Figure 38);
- the simulated air velocity outside the barn is overestimated in 70% of the simulation. The relative error is <10 % in 50% simulations, <30 % in 30% simulations and <50 % in 20% simulations (Figure 39).

Figure 38. Comparison between measured and simulated air velocity outside the barn (V>4.8 ms^{-1})

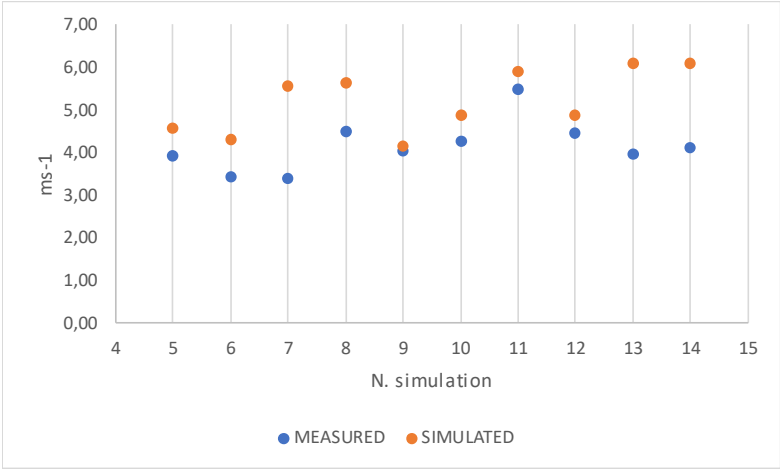

Figure 39. Comparison between measured and simulated air velocity inside the barn (V>4.8 ms^{-1})

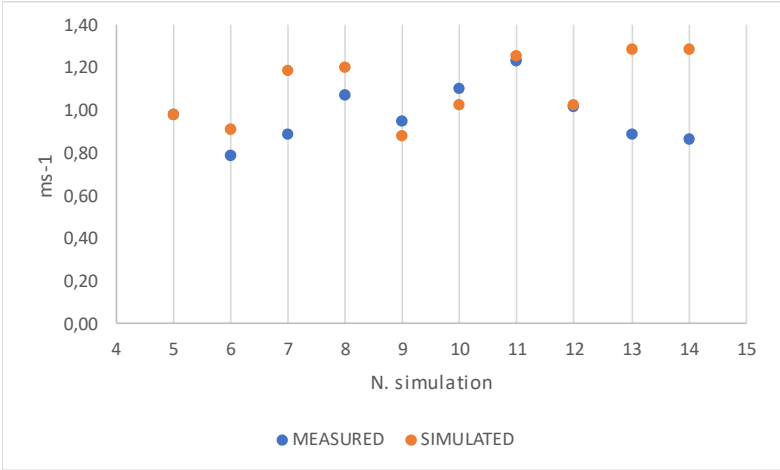

As shown by the graphs and the data, the model reflects better the real condition inside the barn for values of air velocity at the weather station lower than 4.8 ms^{-1}. This happens because turbulence increases with increasing air velocity and the standard k-ε turbulence model – adopted for these simulations because of robust performance, favourable convergence behaviour and reasonable accuracy – does not accurately simulate phenomena like rotation, separation and recirculation.

With the aim of verifying the possibility of improving the accuracy of simulations, the realizable and the standard k-ε turbulence model were both simulated, because the author recognizes that the realizable k-ε turbulence model has an improved equation for dissipation of turbulent kinetic energy, in which the coefficient C_μ is variable instead of constant. Compared to standard k–ε model, realizable k–ε model has

also improvements on the prediction of rotation, boundary layers under strong pressure gradient, separation and recirculation.
Anyway, it was observed that the simulated results from standard k–ε turbulence model and realizable k–ε model were very close to each other, so the standard k–ε model was adopted due to the less computational costs in comparison with the realizable k–ε model.

4.4 Mesh sensitivity

To obtain a high quality CFD model, the grid should be refined to get a grid-independent solution (He et al., 2017). In order to identify the independence of the results from mesh dimension, a grid-convergence study was performed by comparing the results of three different meshes. In addition to the mesh built and simulated for the basis configuration (below called *basis mesh*) having a number of nodes equal to 8.15 million, two more meshes have been analysed. In order to build these meshes, the basis mesh was decreased of a factor equal to 1.1 and 1.2, that led to have two meshes having respectively 7.1 and 5.3 million number of nodes (obtained through Ansys ICEM CFD 17.1, *Blocking* → *Pre-Mesh Params* → *Scale Sizes*). As reported in previous research studies (Rong et al., 2016), the basis mesh should be increased or decremented of a factor equal to 2.
The choice adopted in this study, even if does not follow what is reported in reference (Rong et al., 2016), was due with respect to the mesh having a doubled number of nodes to the computational costs and the power machine, that have been considered during the improving process (Norton et al., 2007; Hong et al., 2017), and with respect to the mesh having a

halved number of nodes – simulated before the others – to the fact that the difference was excessive.
In order to analyse the results of the three meshes, horizontal velocity profiles – respectively downwind, inside the barn and upwind – have been extracted and compared.

Figure 40. Position of straight lines considered for the mesh comparison

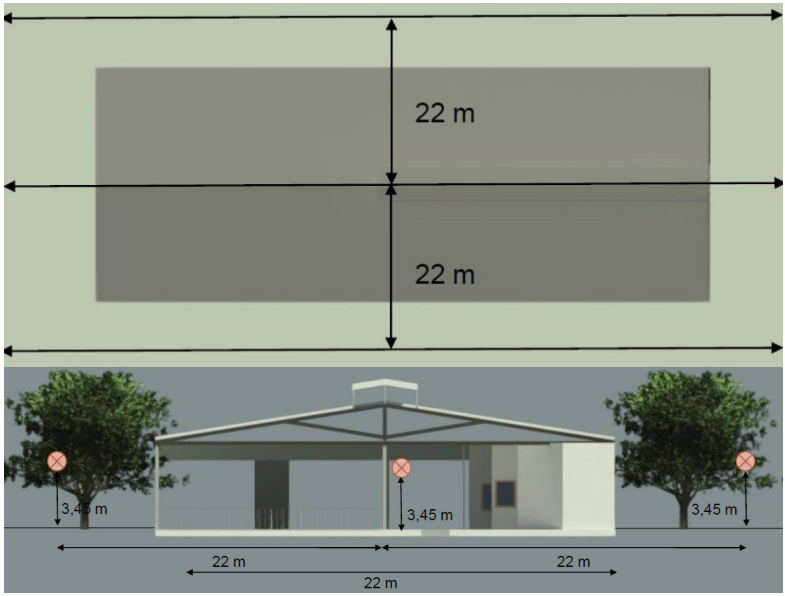

The graphs reported in Figure 41-42-43 show that the results obtained with the meshes decreased of a factor equal to 1.1 and 1.2 are similar to the ones obtained by simulating the basis configuration. This means that the results related to air velocity are independent of the used mesh. Thanks to the power of the used PC, the mesh with the highest number of nodes (i.e. the basis mesh) has been simulated.

Figure 41. Downwind mesh comparison

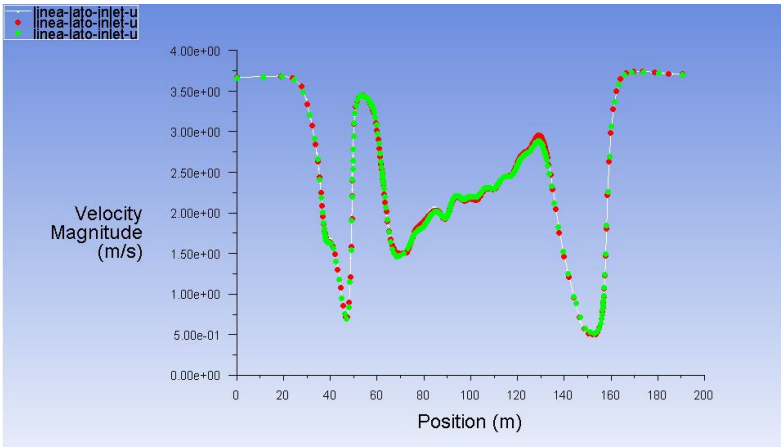

Figure 42. Mesh comparison inside the barn

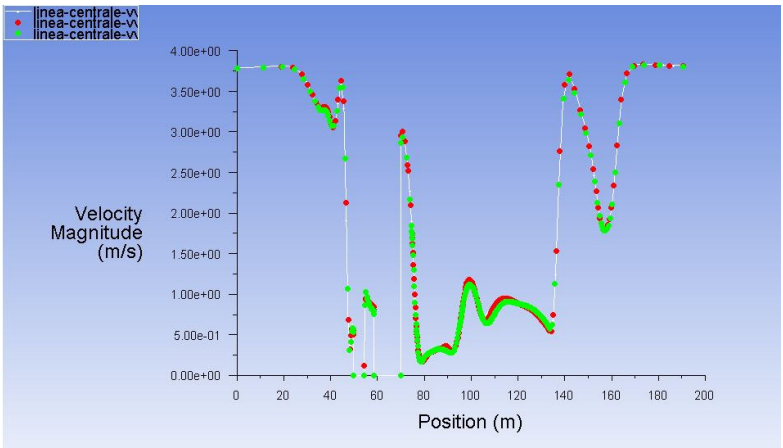

Figure 43. Upwind mesh comparison

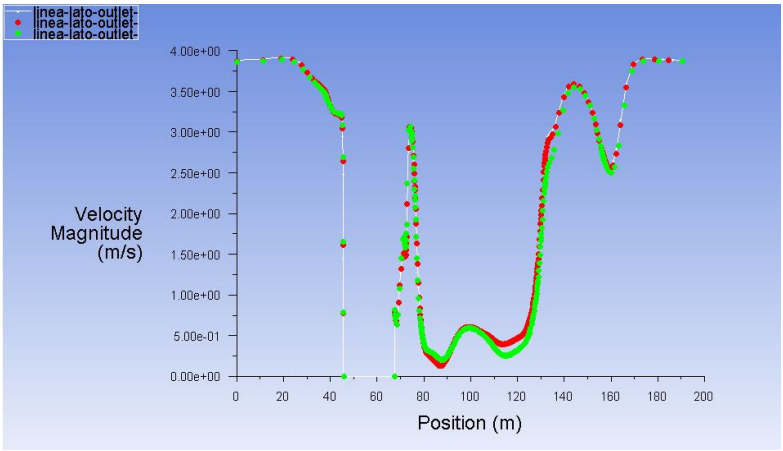

By following the methodology proposed by He et al. (2017), where indoor average temperature and average velocity were compared for eight meshes, the indoor average velocity was compared for the three considered meshes. The results are showed in Figure 44.

Figure 44. Indoor average velocity comparison for the three meshes

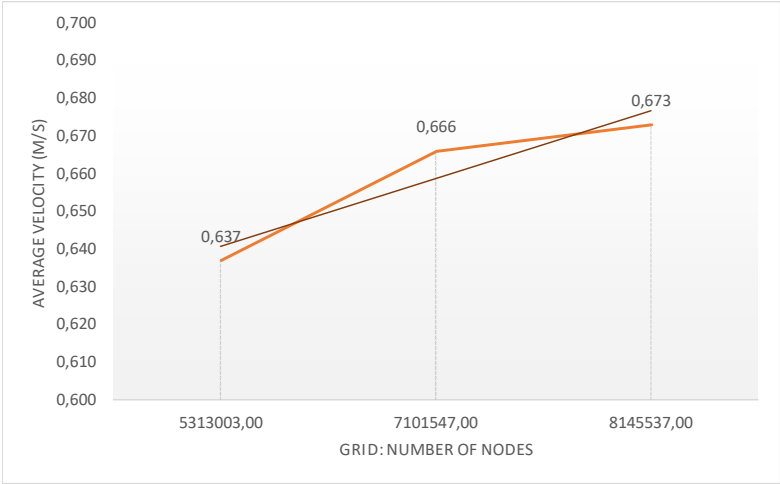

The results show that the solutions corresponding to decreases equal to 1.1 and 1.2 are similar to the ones of the basis configuration. Since the computational cost is sustainable, the mesh with 8.15 million nodes was used.

4.5 The impossibility to use GCI index

As reported in Rong et al. (2016), once the mesh has been created, a grid-convergence study should be conducted by running simulations of different structured meshes and by using a Grid Convergence Index (GCI), proposed by Roache (1994). This method is based on a grid refinement error estimator derived from the theory of generalized Richardson Extrapolation and it should be conducted at least on two mesh, even if it provides a better error estimation when used with three mesh solutions.

The equation is given by:

$$GCI = 3|\mathcal{E}|(r^P - 1)$$
$$\mathcal{E} = \frac{(f_2 - f_1)}{f_1} \quad (31)$$
$$r = \frac{h_2}{h_1}$$

where:

- f_1 is the variable value at a point with fine grid;
- f_2 is the variable value at the same point with coarse grid; h_1 is the representative grid size of fine grid;
- h_2 is the representative grid size of coarse grid;
- p denotes the numerical scheme order of accuracy, which is 2 for second order scheme.

This method should be used for grids with number of elements doubled or halved. However, it is not possible to double as a matter of PC power. Similarly, it is not possible to halve as there is a noticeable difference of the results. For this reason, we proceeded with a graphic comparison, as reported in the previous paragraph.

4.6 Study of air velocity distribution in the barn

The study focuses on the barn, so only the related results – and not the ones regard the context – will be discussed.
With regard to the plane A (Figure 30), an increase in air velocity with increasing height can be observed. The air velocity at 7.5 m height is very different from that at 10 m height and this difference was already detected with the comparison between the air velocity at the weather station (10 m height) and the air velocity measured by the sensor

positioned about 1 m above the chimney (7.5 m height). In particular, the air velocity increases after passing the obstacle represented by the barn roof.

Figure 45. Wind profile

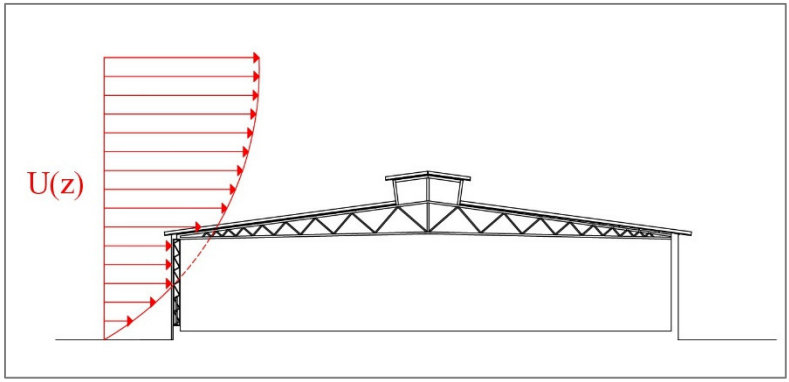

Figure 46a. Plane A – air velocity distribution (ms^{-1})

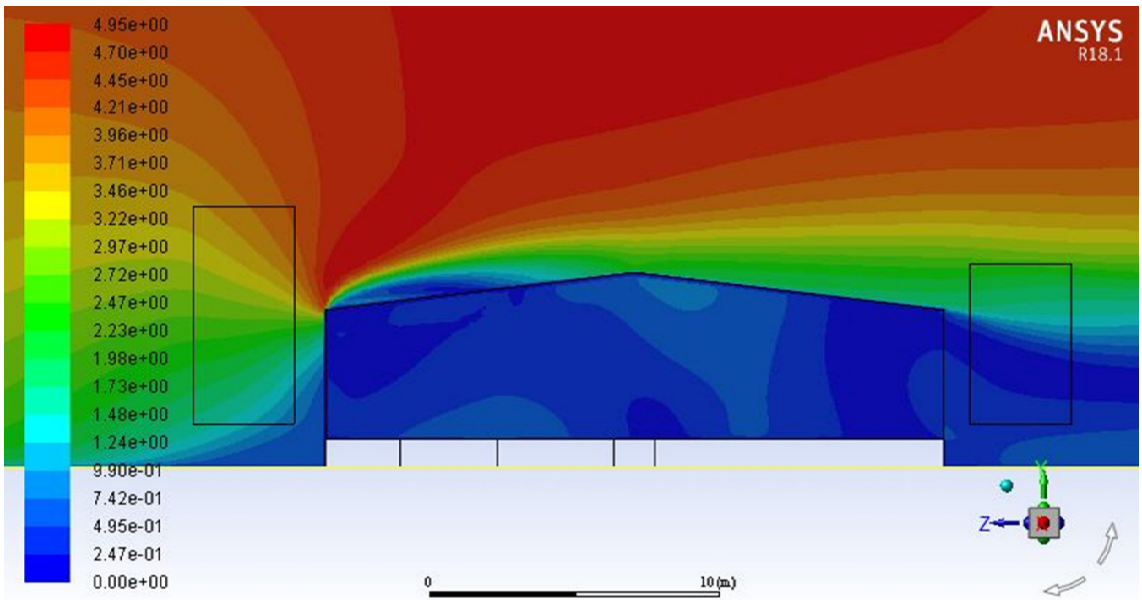

Figure 46b. Plane A – air velocity vectors distribution (ms^{-1})

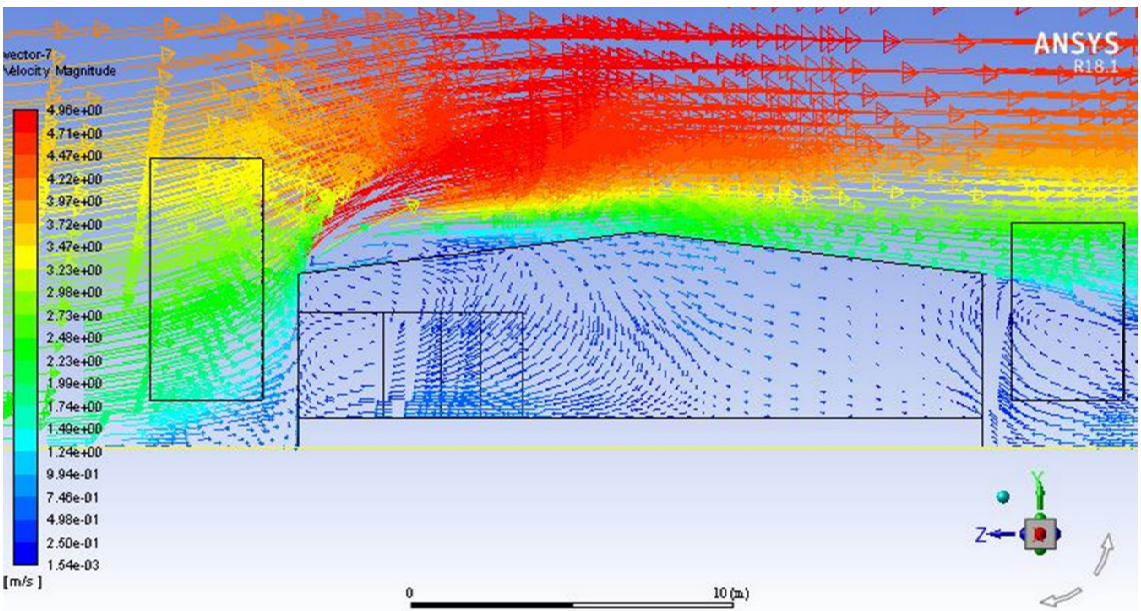

The air velocity in North-East direction (that is the prevalent one as set) has a decrease due to the presence of the barn. The air velocity inside the barn is clearly lower than the external one, as can be seen from the previous Table 7; this is due to the presence of the obstacles that the airflow intercepts and to the South-West wall, having only four small openings (2.75 m^2 each). The chimney causes an increase of air velocity and a vortex nearby the chimney – due to the crossing of the airflow coming from the barn openings with the airflow coming from the chimney – can be observed. A recirculation of the air is shown next to the South-West opening, because of the cross-ventilation generated by the presence of two airflows (i.e. the one coming from North-West and the one coming from South-West) (Figure 46).
With regard to the plane B (Figure 30), the influence of the surrounding buildings – that causes a decrease in the air velocity – can be observed. The influence of trees on the airflow is instead minimal. The vortices are located in the North, in the South and South-West of the barn, because of the airflows coming from the several openings. Air velocity peaks are higher near the South-West openings, due to the narrowing of the airflow passage area. The lowest air velocity values are detected in front of the office and between them. Also in this graph it can be observed that the air velocity in North-East direction has a decrease due to the presence of the barn (Figure 47).
The distribution of the air velocity well reflects the real conditions, where the internal distribution of the spaces and the position of the openings have a strong impact on the airflow.

Figure 47a. Plane B – air velocity distribution (ms^{-1})

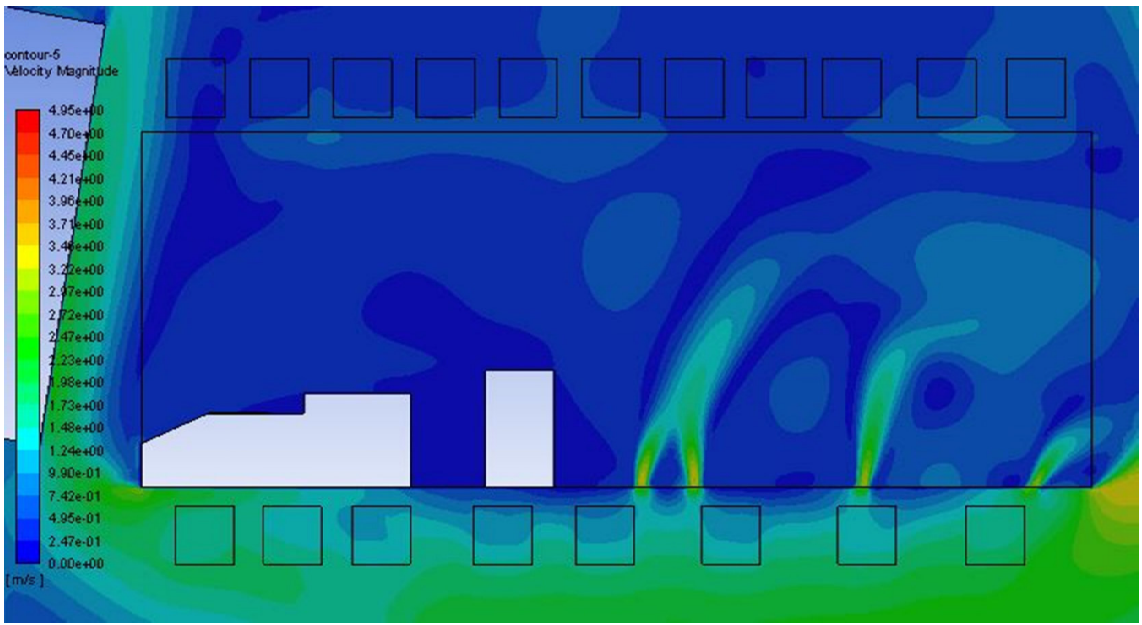

Figure 47b. Plane B –air velocity vectors distribution (ms^{-1})

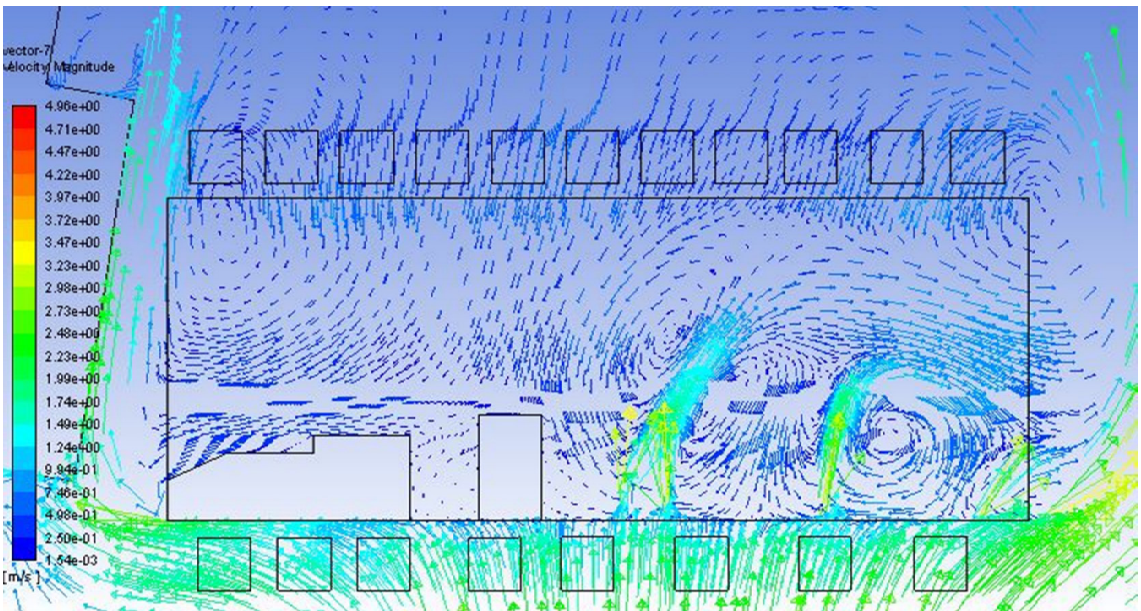

The data analysed were those regarding the areas considered more relevant for animal housing. In detail, average air velocity was equal to 0.42 ms^{-1} in the resting areas, service alley and feeding alley which housed dairy cows. Regarding pens for calves, average air velocity was equal to 0.67 ms^{-1}.

Figure 48. Plane B - average velocity in the areas considered more relevant for animal housing (ms^{-1})

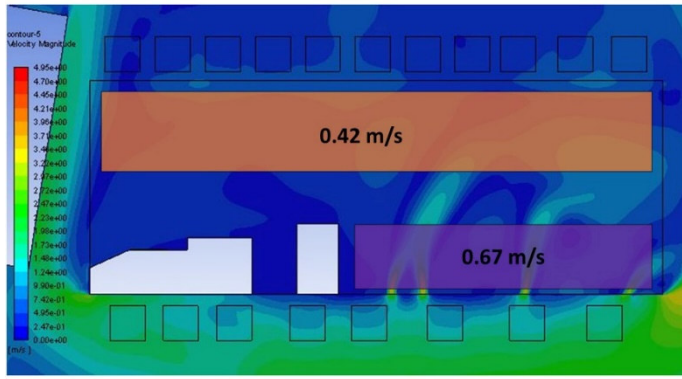

The data reported in the Table 7 and in Figure 48 showed that the air velocities detected inside the barn, both measured and simulated, are too low, even in accordance with what reported by Bailey et al. (2016). This results in high discomfort in cows, as also demonstrated by the analysis of the cow's behaviour reported in the following paragraph 4.7. Consequently, alternative design configurations have been studied in order to increase the air velocity in the resting areas, as reported in the paragraph 4.8.

4.7 Analysis of the cow behaviour

Dairy cow behaviour was studied by visual examination of time-lapse video-recordings obtained thanks to a multi-camera system composed of ten cameras located in the resting area (Figure 49).

Figure 49. Location of the cameras inside the barn

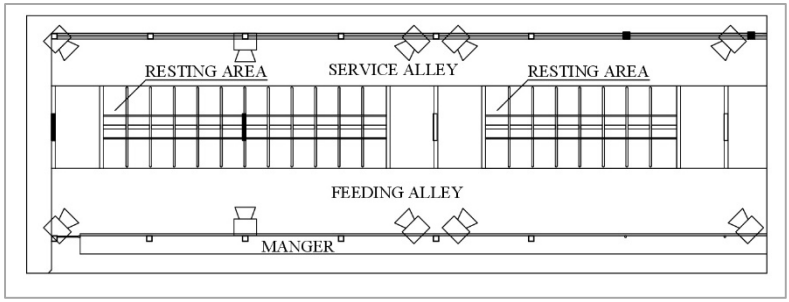

The analysis of dairy cow behaviour was carried out by visual recognition of the obtained video sequence at ten-minute scan sampling interval. Visual analysis of selected images permitted five different behaviours to be analysed among those most frequently studied for their high relation to the comfort of dairy cows (Bava et al., 2012; DeVries et al., 2003; Fregonesi et al., 2007; Overton et al., 2002; Provolo and Riva, 2009; D'Emilio et al., 2018):

- lying, which refers to all the possible decubitus positions inside the cubicle;
- feeding, which refers to the position standing still in the feeding alley;
- standing, which refers to the standing still in the alleys or to the deambulation;

- perching, which refers to the position standing inside the stall;
- drinking, which refers to the position with the head over the drinking trough.

The Table 8 shows the analysis of the cow behaviour in the resting area during the hours for which simulations were carried out in the validation phase, i.e. the hours in which the prevailing wind direction was N-E both at the Acate weather station and at the measurement point located above the roof (see paragraph 4.3). The hours during which other activities, such as milking, were carried out have not been taken into consideration, as the behaviour of the cows was influenced by these activities.

Figure 50. Multi-camera system

Table 8. Analysis of the cow behaviour in the resting area

N. simulation	Air velocity at weather station (10 m height) (ms^{-1})	Air velocity measured inside the barn (ms^{-1})	Cows *lying* in cubicles (%)	*Feeding* cows (%)	*Standing* cows (%)	*Perching* cows (%)	*Drinking* cows (%)
1 (27/04-22:00)	1.90	0.24	24.80	34.67	22.77	13.21	4.55
2 (28/04-02:00)	2.90	0.40	30.30	31.69	22.70	11.92	3.39
3 (28/04-06:00)	2.70	0.44	52.18	28.24	11.57	1.76	6.26
4 (28/04-07:00)	2.70	0.46	10.67	80.48	0.48	8.36	-
5 (28/04-19:00)	6.40	0.98	36.15	54.34	3.79	2.21	3.51
6 (28/04-20:00)	6.00	0.79	73.74	15.65	4.55	5.58	0.48
7 (28/04-21:00)	7.80	0.89	79.30	9.60	5.55	2.52	3.03
8 (28/04-22:00)	7.90	1.07	65.15	22.42	7.07	4.14	1.21
9 (29/04-00:00)	5.80	0.95	67.68	18.28	4.04	7.88	2.12
10 (29/04-01:00)	6.80	1.10	61.11	26.77	0.51	7.07	4.54
11 (29/04-02:00)	8.20	1.23	67.24	18.94	5.33	6.69	1.79
12 (29/04-03:00)	6.80	1.02	74.24	5.56	9.40	9.29	1.52
13 (29/04-05:00	8.50	0.89	54.55	18.18	9.09	18.18	-
14 (29/04-06:00)	8.50	0.87	/	/	/	/	/
15 (30/04-00:00)	2.00	0.32	50.17	32.49	6.24	7.38	3.71
16 (30/04-01:00)	2.50	0.27	41.92	43.93	7.08	5.04	2.02
17 (30/04-02:00)	2.00	0.32	45.95	41.42	6.56	5.05	1.01
18 (01/05-01:00)	2.80	0.45	66.16	18.68	10.10	5.06	-
19 (01/05-02:00)	2.00	0.39	50.33	32.66	10.94	6.06	0.00
20 (01/05-05:00)	1.40	0.32	30.30	54.55	6.06	9.09	0.00

Below, the graphs related to the analysis of cow behaviour in the resting area are reported.

Figure 51. Analysis of the cow behaviour in the resting area

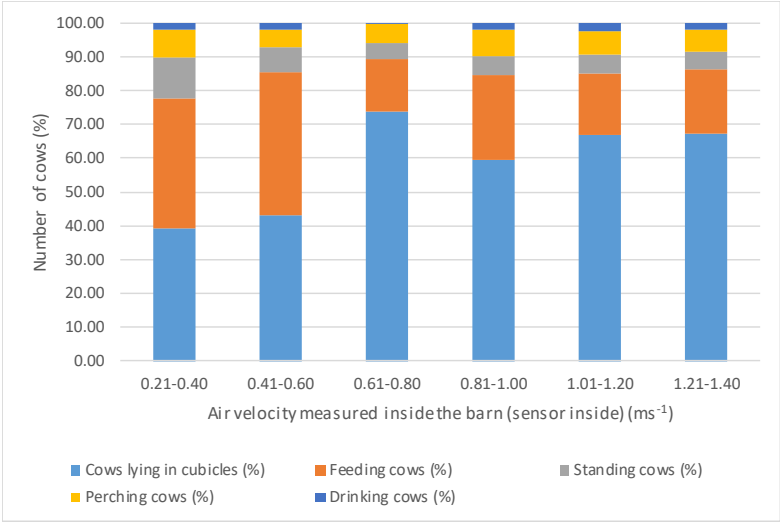

The graph reported in Figure 51 shows, by dividing the air velocity measured inside the barn in six ranges, the behaviour of the cows when the air velocity changes.
The following graphs described respectively, to vary of air velocity, the percentages of cows lying in cubicles (Figure 52), the percentages of feeding cows (Figure 53), the percentages of standing cows (Figure 54), the percentages of perching cows (Figure 55) and the percentages of drinking cows (Figure 56), in order to find the correlation between the air velocity measured inside the barn and the behaviour of the cows in the resting area and to check for heat stress in cows.

Figure 52. Relation between cows lying behaviour and air velocity measured inside the barn in the resting area

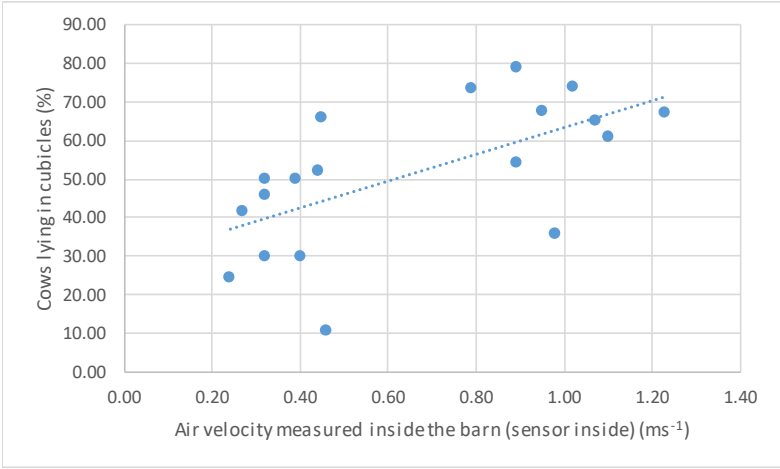

Figure 53. Relation between cows feeding behaviour and air velocity measured inside the barn in the resting area

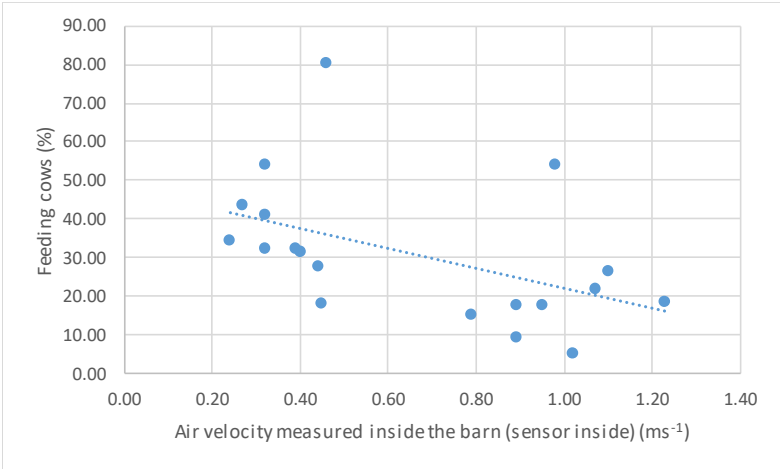

Figure 54. Relation between cows standing behaviour and air velocity measured inside the barn in the resting area

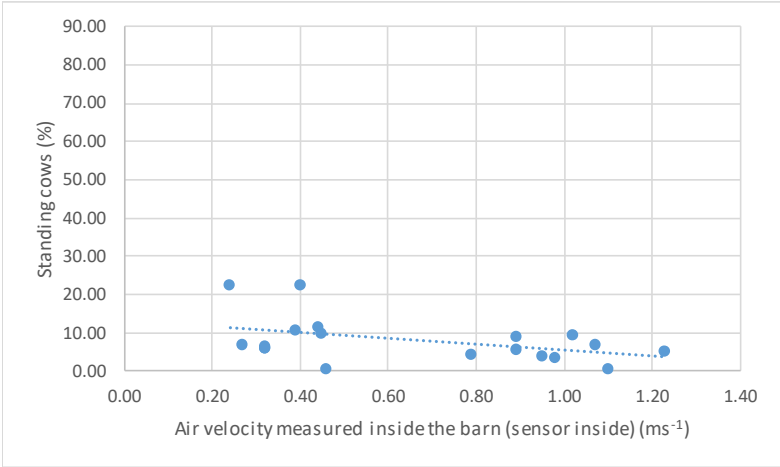

Figure 55. Relation between cows perching behaviour and air velocity measured inside the barn in the resting area

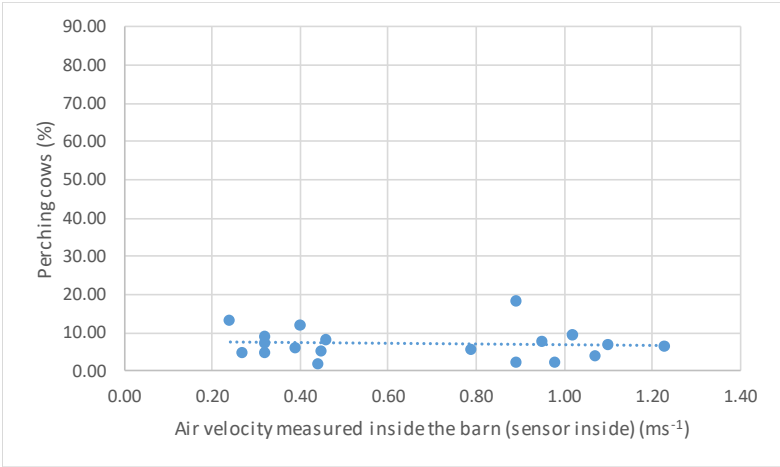

Figure 56. Relation between cows drinking behaviour and air velocity measured inside the barn in the resting area

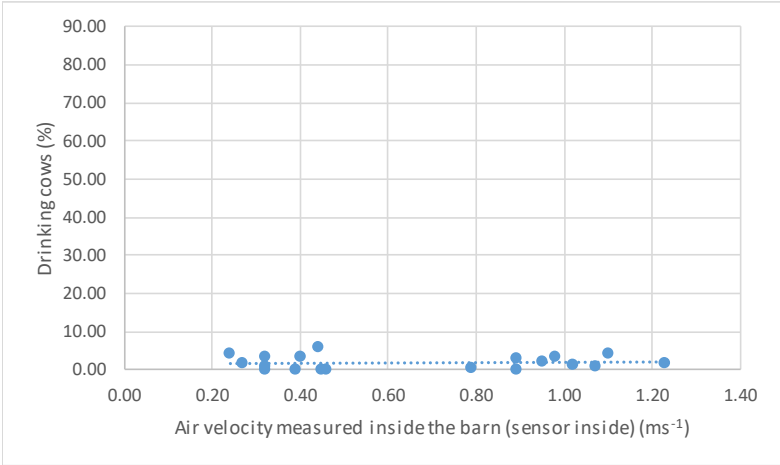

4.8 Study of air velocity distribution in alternative design configurations

By following the same methodology used to build and simulate the airflow in the basis configuration, alternative design configurations of the barn have been modelled and simulated.

Figure 57. Alternative design configurations

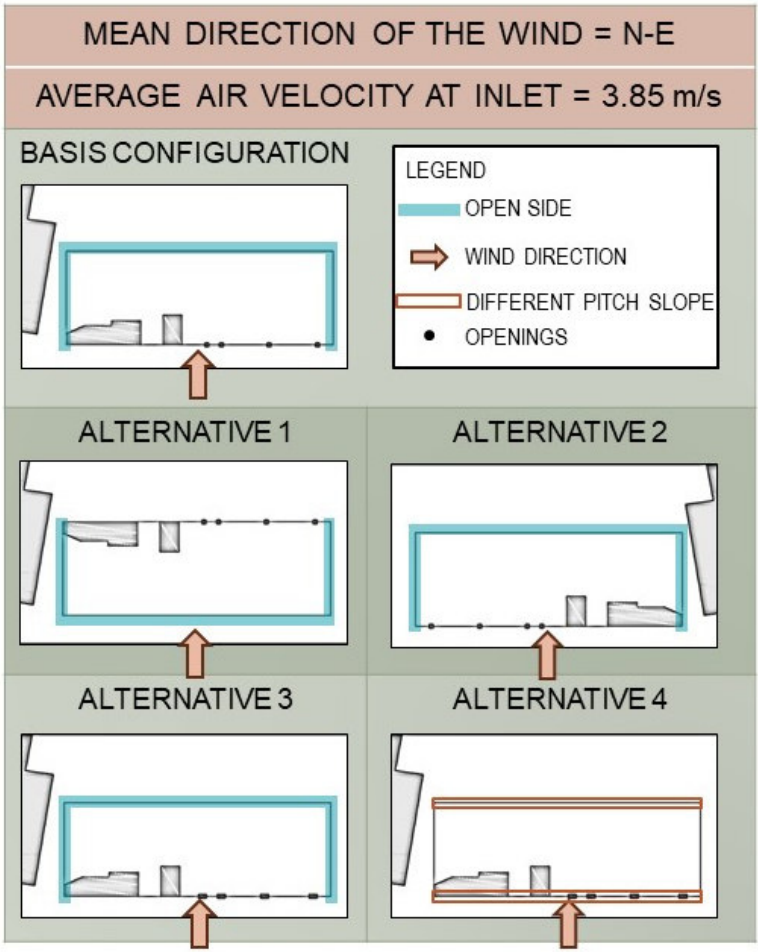

The input data were the same used for the basis configuration, in order to compare the alternative design solutions under the same external conditions. The surrounding trees have not

been moved, instead the buildings around were moved only in an alternative design configuration.
After having performed the simulations, the alternative design configurations have been analysed in order to evaluate the best in terms of natural ventilation, i.e. the one that allows a greater natural ventilation of the areas inside the barn intended for cows and calves.
The results of the simulations regarding the alternative design configurations, showed in the planes A and B as in the basis configuration (Figure 30), are reported below.

4.8.1 Alternative 1

In alternative 1, the office areas and the North-Western wall with openings were mirrored along the longitudinal axis of the barn. When the barn was built, the connection between internal and external places was thought to optimally perform the related productive activities (for example, the milking activity). In order to maintain this relationship unchanged, the surrounding buildings have not been moved.
Regarding the plane A, as in the basis configuration, an increase in air velocity with increasing height can be observed. However, due to the displacement of the wall from South-West to North-East, the air speed decreases near the North-East side of the barn. Part of the airflow passes through the chimney, while the remaining part is hampered by the pitch of the roof. A vortex nearby the pavment – due to the crossing of the airflows coming from the barn openings in the South-East and North-West sides – can be observed, as well as a vortex in the upwind region is shown by the graph (Figure 58).

Figure 58a. Alternative 1, Plane A – air velocity distribution (ms^{-1})

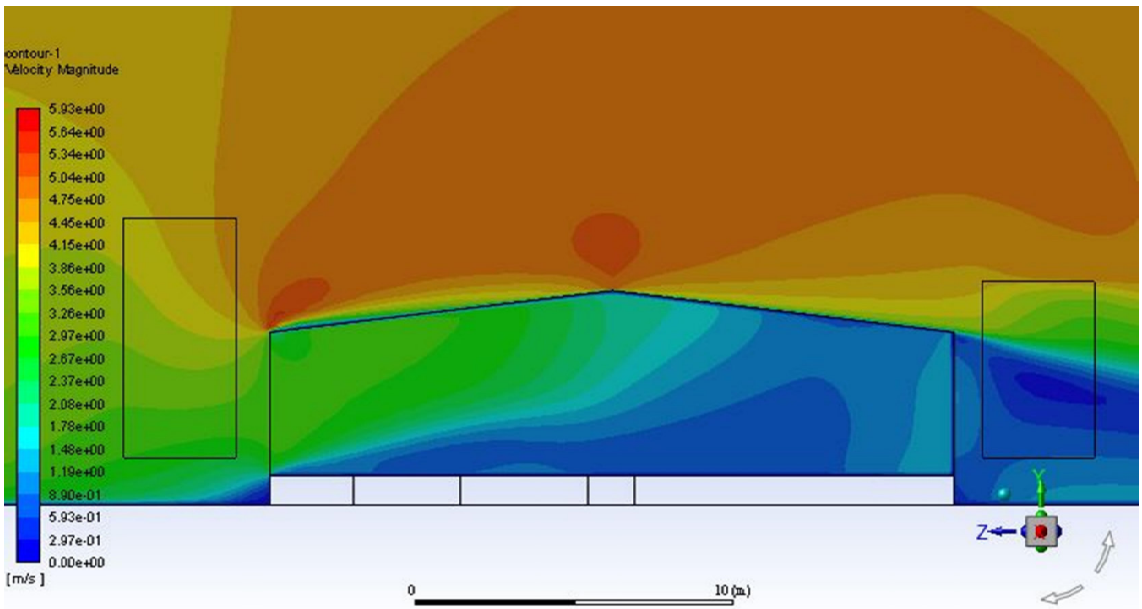

Figure 58b. Alternative 1, Plane A – air velocity vectors distribution (ms^{-1})

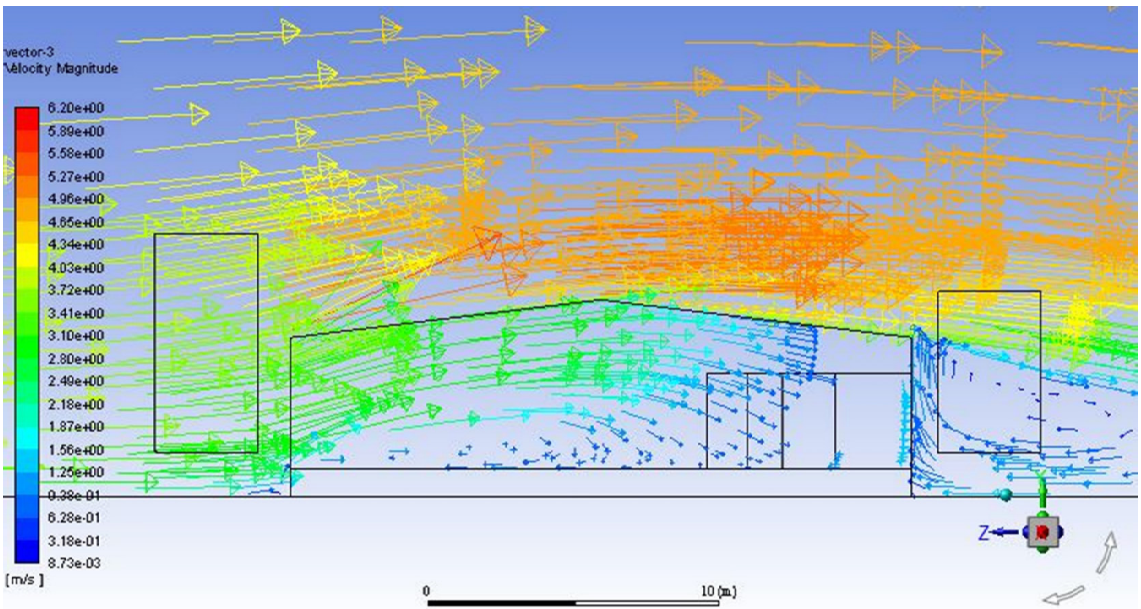

Figure 59a. Alternative 1, Plane B –air velocity distribution (ms^{-1})

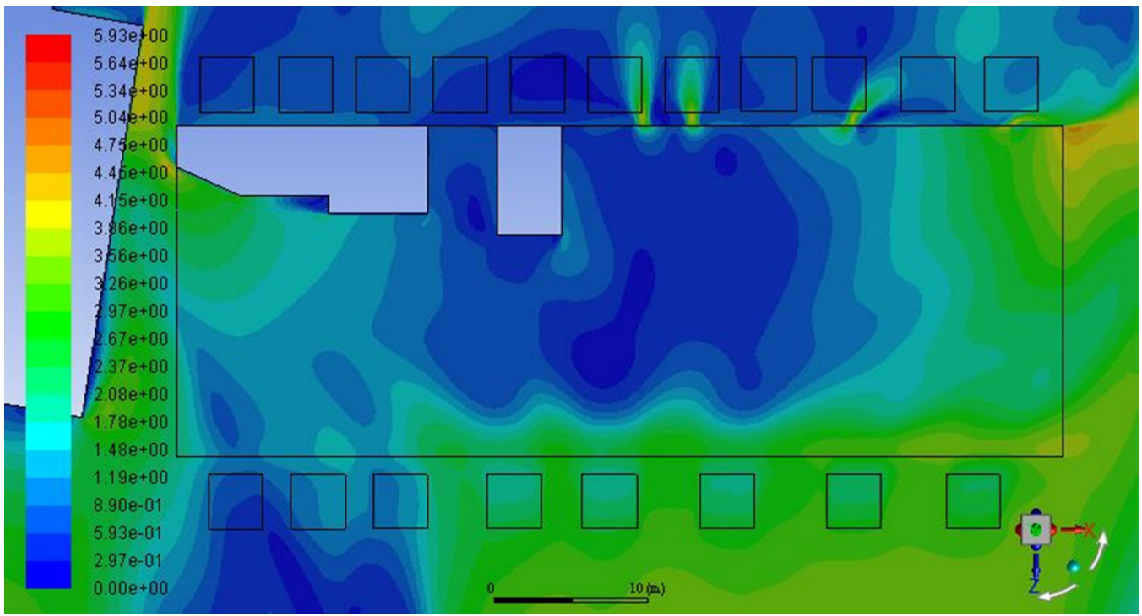

Figure 59b. Alternative 1, Plane B –air velocity vectors distribution (ms^{-1})

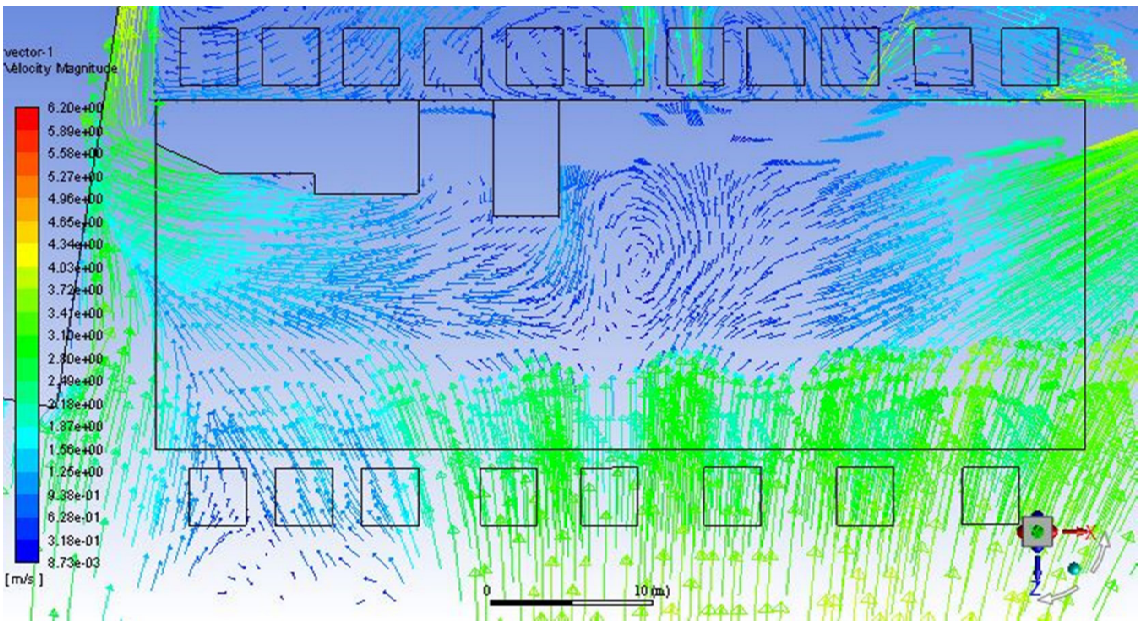

With regard to the plane B, the vortices are located in the central part of the barn, because of the airflows coming from the three open sides. In particular, it can be observed that the airflow coming from South-West goes to North-West and South-East to reach the two open sides of the barn avoiding the obstacle represented by the wall. Air velocity peaks are higher in correspondence of the three open sides, while the lowest air velocity values are detected next to the offices and between them. The influence of the building in the South-West is in this case greater than that in the basis configuration: the air flow from the South-West, in fact, is in this case greater due to the absence of the windward wall (Figure 59).
Also for the alternative design configuration 1, the data analysed were those regarding the areas considered more relevant for animal housing. In detail, average air velocity was equal to 1.42 ms^{-1} in the resting areas, service alley and feeding alley. Regarding pens for calves, average air velocity was equal to 1.27 ms^{-1} (Figure 60).

Figure 60. Alternative 1, Plane B - average velocity in the areas considered more relevant for animal housing (ms^{-1})

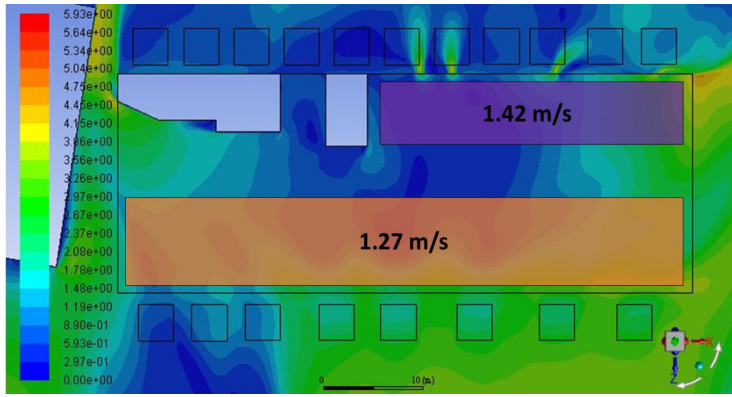

4.8.2 Alternative 2

In alternative 2, the office areas and the openings of North-West wall were mirrored along the transversal axis of the barn. As in the alternative 1, in order to maintain the connection between internal and external places unchanged, the surrounding buildings have been moved.

With regard to plane A, also in this case an increase in air velocity with increasing height can be observed. The air velocity increases after passing the obstacle represented by the barn roof (Figure 61).

In the alternative 2, the air velocity inside the barn is higher than the air velocity inside the barn in the basis configuration, due to the different design configuration that allows the formation of vortices inside the barn.

Regarding the plane B, the vortices are located in the North-West, in the South-East and in the central part of the barn, because of the airflows coming from the three open sides. The vortex located in South-East part of the barn has an air velocity higher than the one of the North-West part of the barn: the space, in fact, is smaller, so the velocity increases.

Air velocity peaks are higher at the two extremes of North-East opened side and in correspondence of the South-West openings, while the lowest air velocity values are detected close to the offices and between them (Figure 62).
In the alternative design configuration 2, the average air velocity was equal to 1.38 ms^{-1} in the resting areas, service alley and feeding alley. Regarding pens for calves, average air velocity was equal to 1.42 ms^{-1} (Figure 63).

Figure 61a. Alternative 2, Plane A –air velocity distribution (ms^{-1})

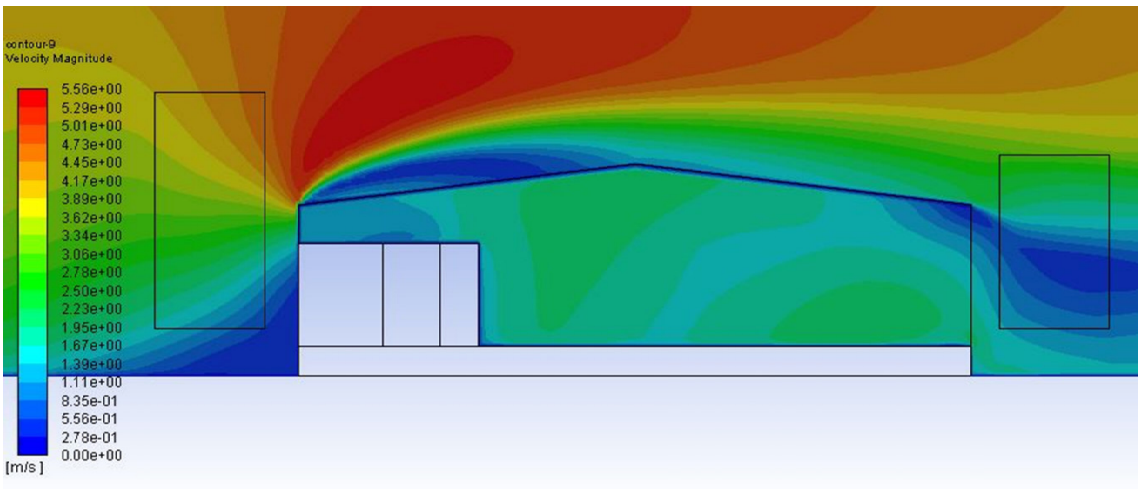

Figure 61b. Alternative 2, Plane A –air velocity vectors distribution (ms^{-1})

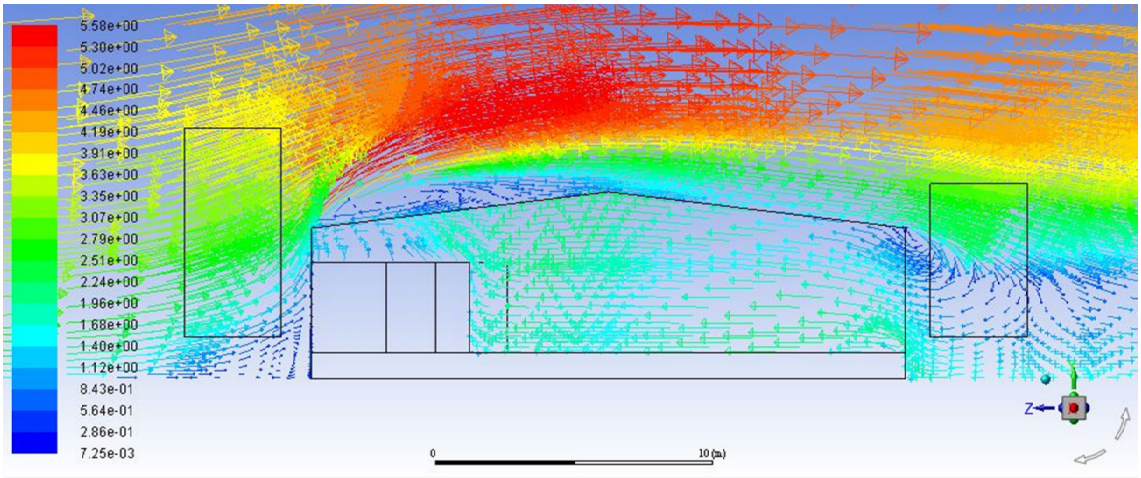

Figure 62a. Alternative 2, Plane B –air velocity distribution (ms^{-1})

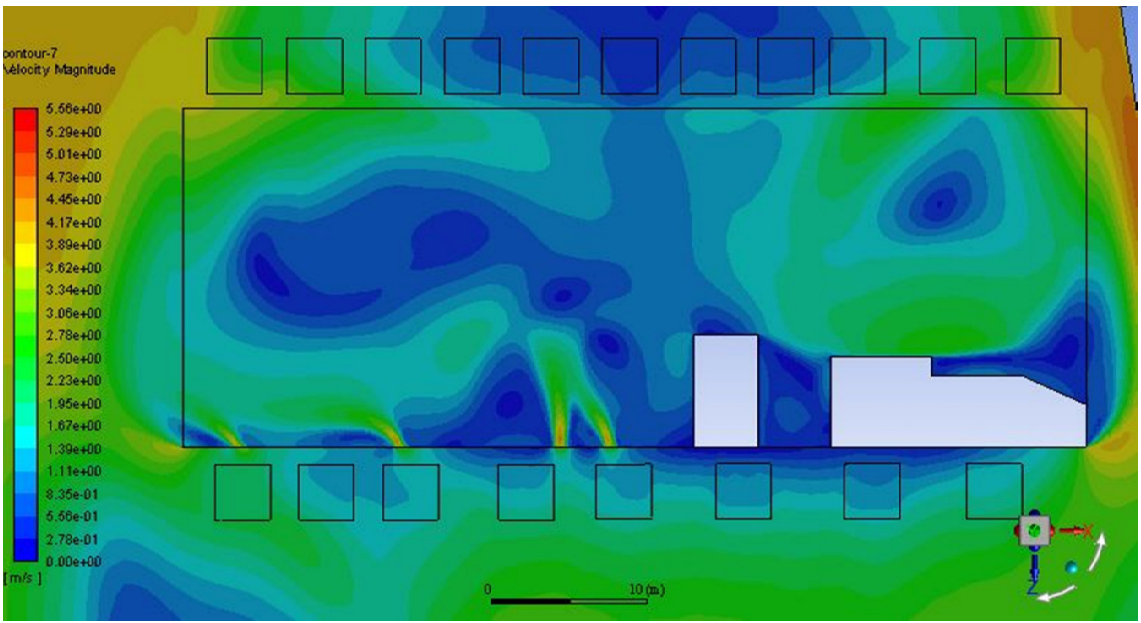

Figure 62b. Alternative 2, Plane B –air velocity vectors distribution (ms^{-1})

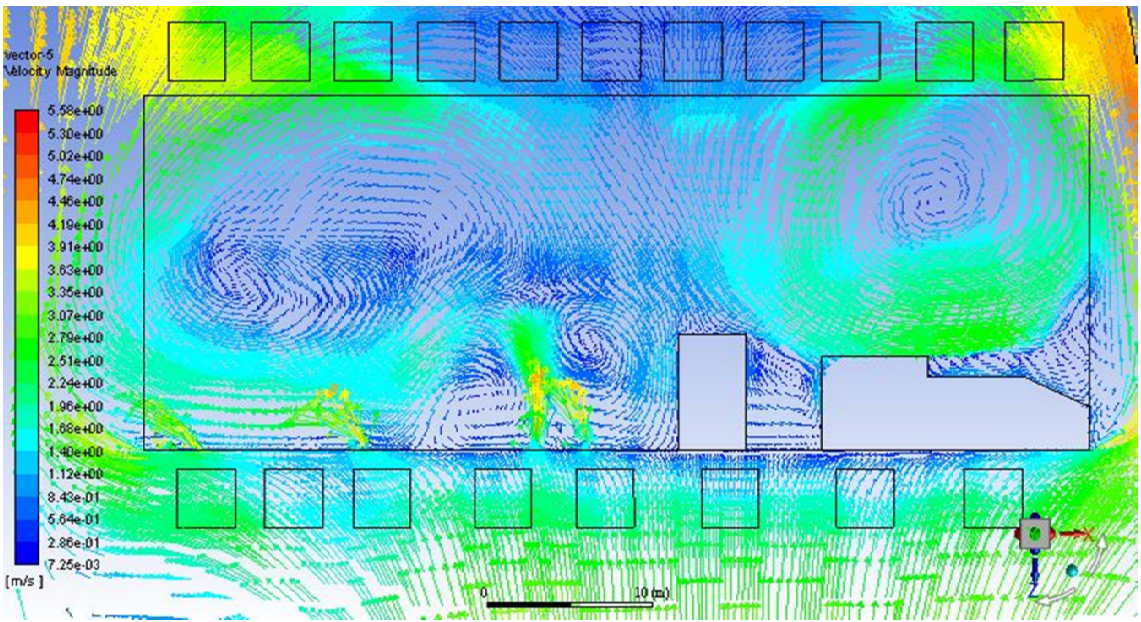

Figure 63. Alternative 2, Plane B - average velocity in relevant areas (ms^{-1})

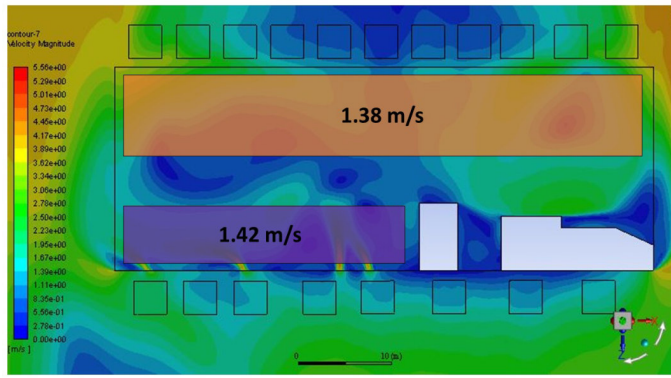

4.8.3 Alternative 3

In alternative 3, each opening in the South-West wall was doubled, reaching an area of about 5.5 m^2. The surrounding buildings and the office areas inside the barn have not been moved.

The plane A is located between two openings, where the air velocity is low next to the South-West wall. The velocity increases in the central part of the barn, where the airflows coming from the openings in the South-West wall and from the North-East and South-East side cross the barn, generating a vortex. After, in North-East direction, the air velocity decreases, especially close to the barn roof. Also in this case, outside the barn, the air velocity increase with the height, reaching is maximum after passing the barn roof (Figure 64).

Figure 64a. Alternative 3, Plane A –air velocity distribution (ms^{-1})

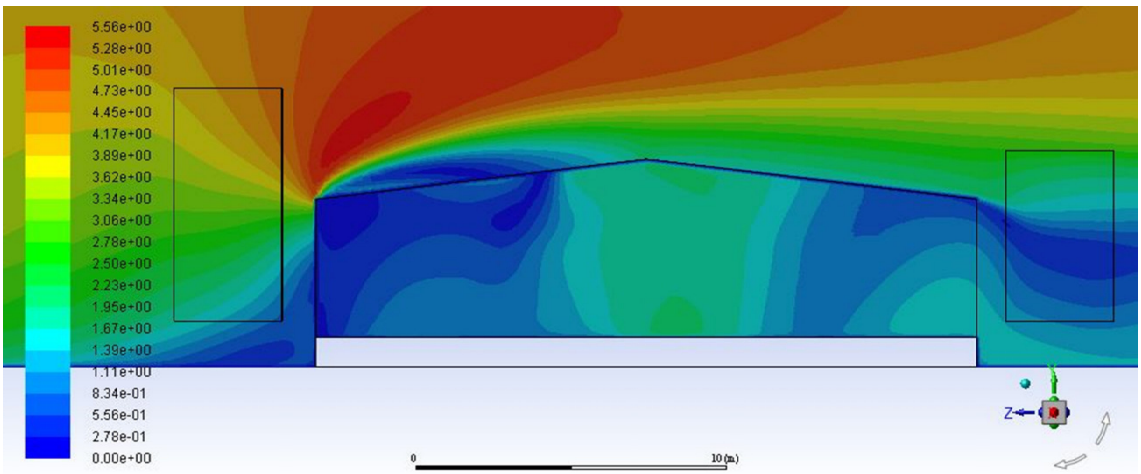

Figure 64b. Alternative 3, Plane A –air velocity vectors distribution (ms^{-1})

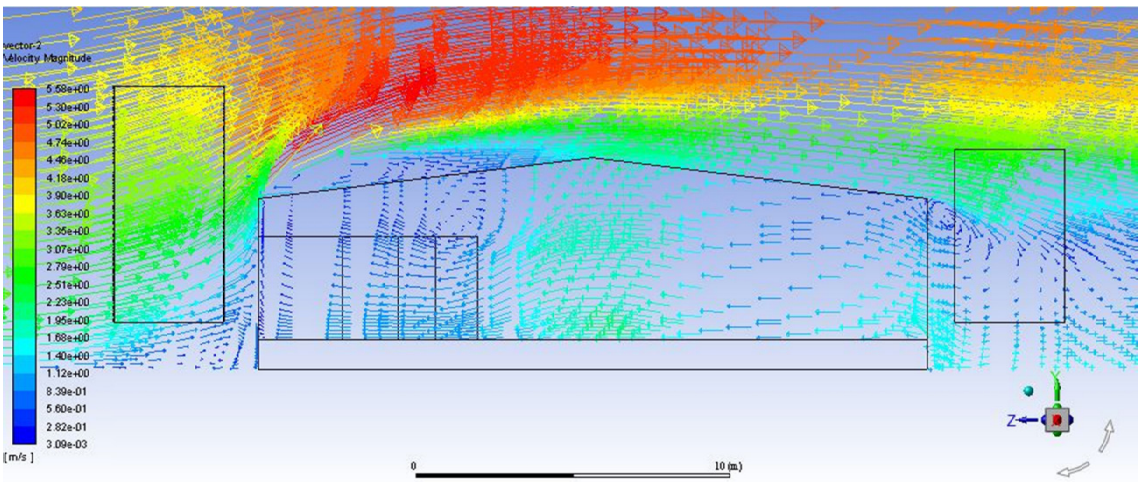

Regarding the plane B, the above-mentioned vortex can be observed in the East part of the barn. Another vortex is located in the North part of the barn, due to the crossing of airflows coming from North-West and North-East. As expected, air velocity peaks are higher in correspondence of the South-West openings, while the lowest air velocity values are detected close to the office, between them and between the openings (Figure 65).
As in the basis configuration, the influence of the surrounding buildings and trees on the airflow is minimal: the airflow, decelerated by the South-West building, diverts next to the South-West wall and the air velocity increases after overcoming obstacles.

Figure 65a. Alternative 3, Plane B – air velocity distribution (ms^{-1})

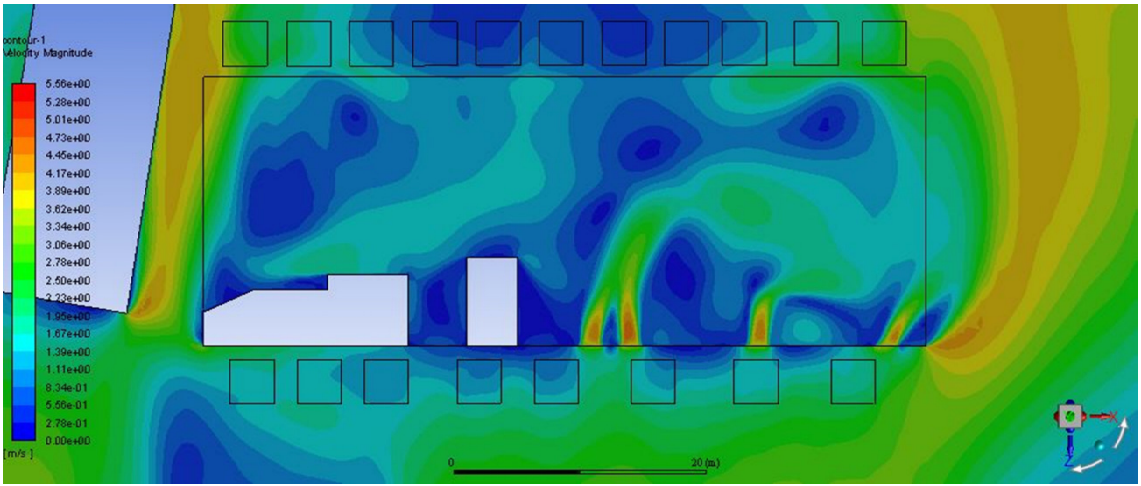

Figure 65b. Alternative 3, Plane B – air velocity vectors distribution (ms^{-1})

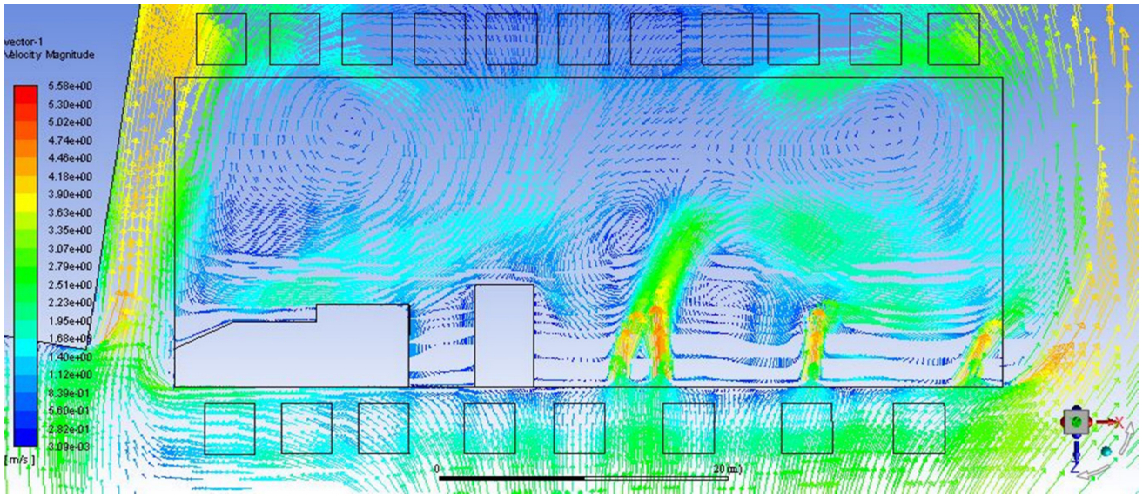

In the alternative design configuration 3, the average air velocity was equal to 1.18 ms^{-1} in the resting areas, service alley and feeding alley. With regard to pens for calves, average air velocity was equal to 1.29 ms^{-1} (Figure 66).

Figure 66. Alternative 3, Plane B - average velocity in relevant areas (ms^{-1})

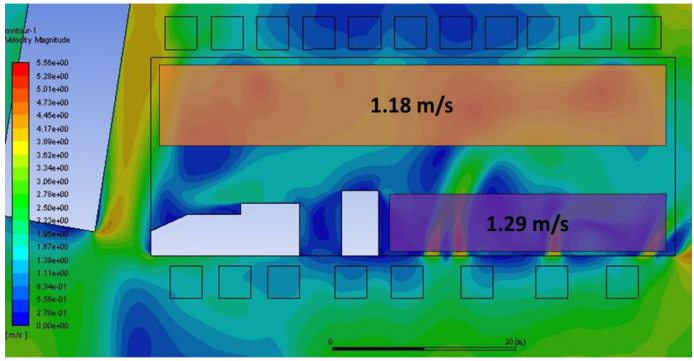

4.8.4 Alternative 4

In alternative 4, the pitch slope was changed from 12% to 25%. The surrounding buildings and the office areas inside the barn have not been moved.

As shown in the vertical section of the barn (Plane A), the air velocity inside the barn is lower than outside, due to the south-west wall1. The airflow outside, after passing the obstacle represented by the barn itself, tends to regain velocity upwards. In the leeward area, due to the open North-East side, the air recirculates, generating a vortex (Figure 67). As shown in the horizontal section (Plane B), the vortices are located in the North and in the East parts of the barn, because of the airflow coming from the three open sides. Air velocity peaks are higher at the two extremes of North-East opened

side and at the openings located on the south-west wall, while the lowest air velocity values are detected close to the office and between them. Also in this case, the influence of the surrounding buildings and trees on the airflow does not change comparing with the basis configuration and the airflow tends to decrease next to the obstacles and regain velocity after passing them. The airflow diverts next to the South-West wall, near which its velocity decreases (Figure 68).

Figure 67a. Alternative 4, Plane A –air velocity distribution (ms^{-1})

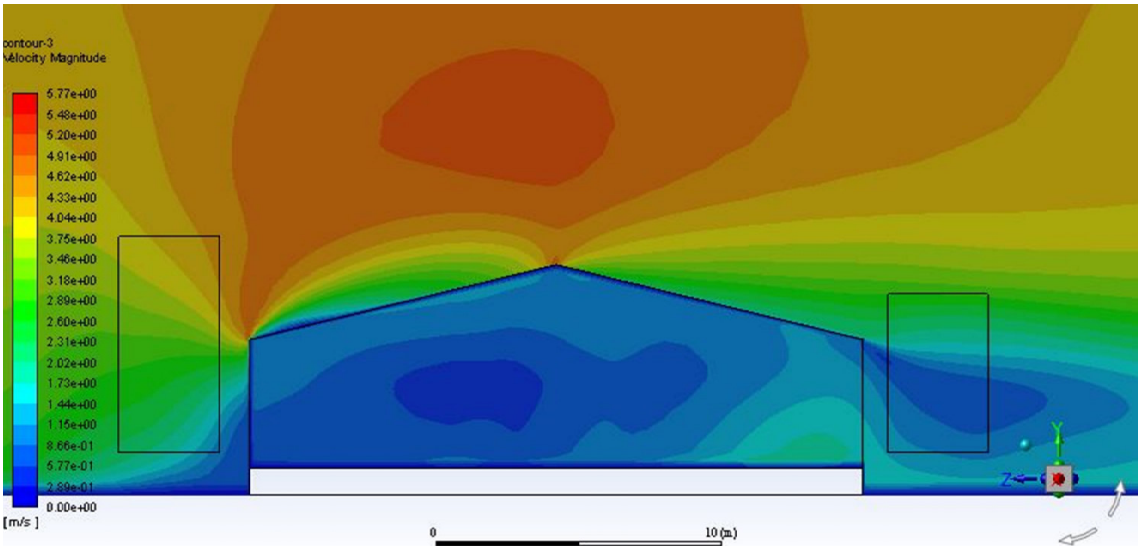

Figure 67b. Alternative 4, Plane A –air velocity vectors distribution (ms^{-1})

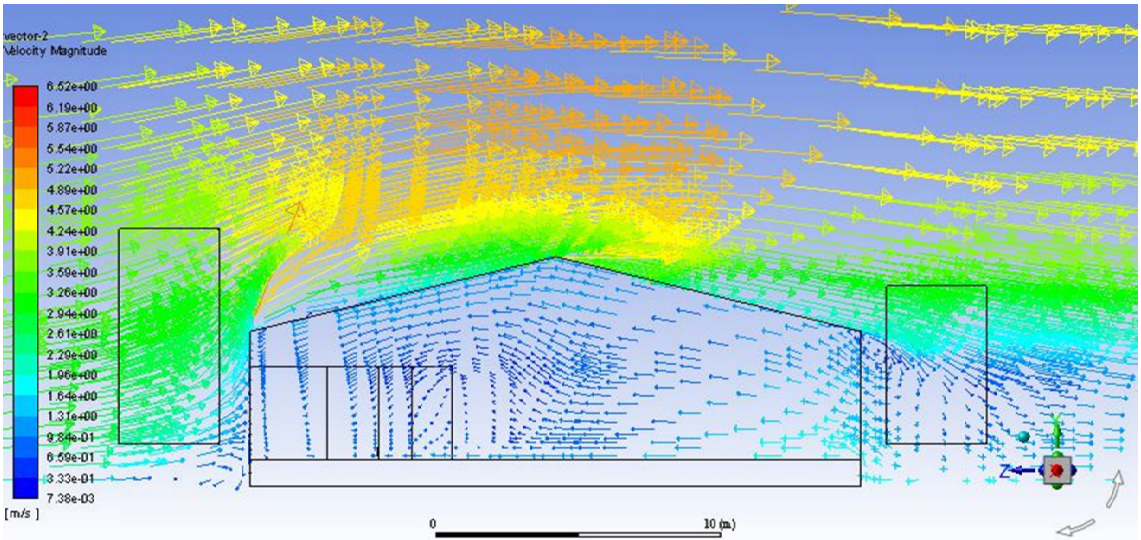

Figure 68a. Alternative 4, Plane B –air velocity distribution (ms^{-1})

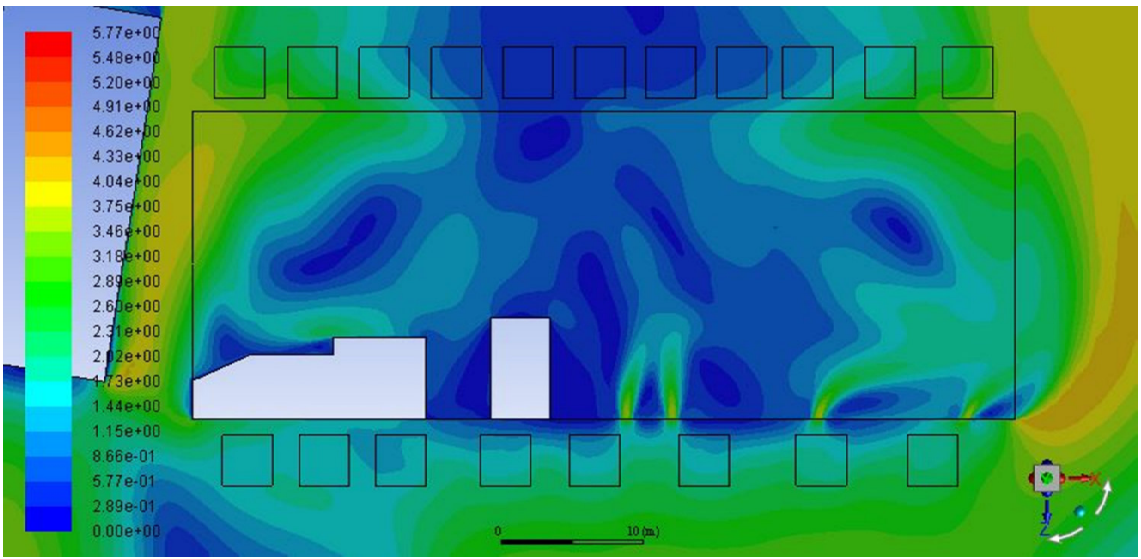

Figure 68b. Alternative 4, Plane B –air velocity vectors distribution (ms^{-1})

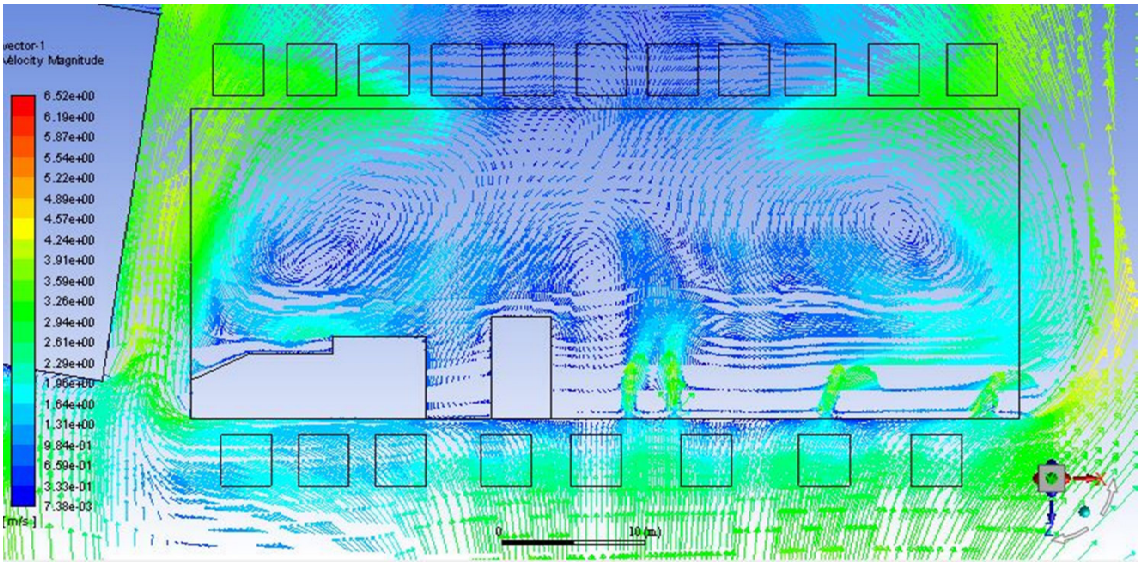

In the alternative design configuration 4, the average air velocity was equal to 1.26 ms^{-1} in the resting areas, service alley and feeding alley. About pens for calves, average air velocity was equal to 1.20 ms^{-1} (Figure 69).

Figure 69. Alternative 4, Plane B - average velocity in relevant areas (ms^{-1})

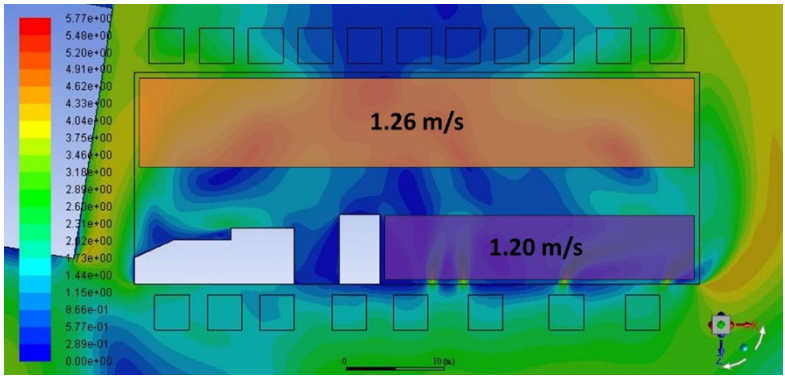

4.8.5 Comparison between the alternative design configurations

As reported in the introduction, a comparison between the results related to the air velocity in resting area, the service alley and feeding alley for dairy cows and in the pens for calves was conducted in order to find the best configuration, i.e. the one associated with a greater degree of natural ventilation, important for the well-being of animals (Table 9).

Table 9. Comparison between the results related to the air velocity in the two areas

Configuration	Average air velocity in the resting area and alleys for dairy cows (ms^{-1})	Average air velocity in the pens for calves (ms^{-1})
Basis	0.66	0.76
Alternative 1	1.27	1.25
Alternative 2	1.38	1.42
Alternative 3	1.18	1.29
Alternative 4	1.26	1.20

The configuration that allows to obtain the greater average air velocity in the two areas considered was the alternative 2.

5. Conclusions

Natural ventilation through large openings often characterizes semi-open buildings for dairy cows in hot climate regions, as they can guarantee an air change adequate to ensure the animal's well-being. Nevertheless, currently only few researches regarded the study of natural ventilation through large openings, due to the difficulty given by bidirectional flows through large openings and the high turbulence that characterizes the airflow.

The main objective of this study was to analyse the air velocity distribution inside a semi-open free stall barn located in Southern Italy, in a region highly characterised by hot climate conditions during summer that could induce animal heat stress, in order:

- to know the air velocity in areas considered most sensitive for the presence of animals;
- to analyse the dairy cow behavior by carrying out a visual examination;
- to find, based on the first results of the study, alternative design configurations with the aim to discovery the best condition for the well-being of users and animals.

The first objective was achieved in this study by developing and validating a CFD model. Air velocity was measured in different indoor and outdoor points at different heights by using a Campbell system, with 15 min acquisition time. The 3D model was made by using Autodesk Autocad 2016®, then it was imported into Ansys ICEM CFD 17.1® to build the unstructured mesh and to assign the boundary condition. Finally, the numerical simulations have been carried out by using the Ansys-Fluent 17.1® program, both by considering hourly data, in order to compare simulated data to those obtained from a measuring system previously installed within

the barn, both for the basis configuration, i.e. the configuration that considers as input the average data taken from the meteorological station nearby the barn.
By using the described CFD methodology, a representation of the airflow distribution was given. It was considered good because it reflects the real condition inside the barn – where the internal distribution of the spaces and the position of the openings strongly impact the air velocity – and because of the comparison between measured and simulated data carried out. Therefore, the model was considered validated.
After the simulation of the basis configuration, average air velocities of the two areas considered relevant for animal housing, were analysed. The air velocity was too low, and that condition leads to discomfort in cows. This fact was also confirmed by the analysis of the dairy cow behaviour in the reference period, carried out through visual examination of time-lapse video-recordings obtained from a multi-camera system. Therefore, the need for adequate ventilation during the analysed period (i.e. spring/summer) was not taken into account in the design and construction phases of the barn. A better ventilation could have been obtained thanks to the prevailing winds coming from the north-east.
Since the modelled air velocity distribution in the barn fit the real one with a good accuracy, alternative design configurations were analysed with the aim to find the best condition for the well-being of animals. In *alternative 1*, the office areas and the North-Western wall with openings were mirrored along the longitudinal axis of the barn. In *alternative 2*, the office areas and the openings of North-Western wall were mirrored along the transversal axis of the barn. The buildings for milking have been moved, in order to maintain the "logical connection" between the internal and external activities. In *alternative 3*, the openings of North-Western

wall were doubled, reaching an area of about 5.5 m^2. In *alternative 4*, the pitch slope was changed from 12 % to 25%. By comparing the results related to the air velocity in the two areas housing the animals, it was discovered that the configuration that allows to obtain the greater average air velocity in these areas was the *alternative 2*.

The CFD model can be considered reliable to study other transversal and longitudinal sections, by adding other anemometers. Future implementations should also regard the increase of the geometry complexity, the study of gases distribution according with the airflow distribution and the analysis of the ventilation of the barn during daylight hours, also taking into account the other wind directions and the different seasons of the year.

Furthermore, the methodology applied in this thesis represents an example for study the natural ventilation of livestock buildings having similar characteristics.

References

Aguerre, M.J.; Wattiaux, M.A.; Hunt, T.; Larget, B.R. (2010) Effect of dietary crude protein on ammonia - N emission measured by herd nitrogen mass balance in a freestall dairy barn managed under farm-like conditions. *Animal* 4(8), 1390-1400.

Ahmed, A.Q.; Gao, S.; Kareem, A.K. (2017) Energy saving and indoor thermal comfort evaluation using a novel local exhaust ventilation system for office rooms. *Appl. Therm. Eng.* 110, 821-834.

AIC. Air infiltration instrumentation and measuring techniques. In: 1st AIC Conference, Windsor, Berkshire, UK, 6-8 October, 1980.

Allocca, C.; Chen, Q.; Glicksman, L. R. (2003) Design analysis of single-sided natural ventilation. *Energy Build* 35(8), 785-795.

Anderson, J.D. (1995) Computational Fluid Dynamics. Springer.

Arcidiacono, C.; D'emilio, A. (2006) CFD analysis as a tool to improve air motion knowledge in dairy houses. *Rivista di ingegneria agraria* 1, 35-42.

Arcidiacono C.; Porto S.M.; Cascone G. (2015) On ammonia concentrations in naturally ventilated dairy houses located in Sicily. *AgricEngInt: CIGR Journal*, 294-309.

Asfour, O.S. (2015) Natural ventilation in buildings: An overview. In book: Natural Ventilation: Strategies, Health Implications and Impacts on the Environment, Edition 1.

ASHRAE Fundemental Handbook (1985). Ch. 22. Natural ventilation and infiltration. American Society of Heating, Refrigeration and Air-Conditioning Engineers, Atlanta, GA.

Aynsley, R.M.; Melbourn, W.; Vickery, B.J. (1977). Architectural Aereodynamics. *Applied Science Publisher*, London.

Bailey, T., Sheets, J., McClary, D., Smith, S. Bridges A. (2016) Heat abatement. Elanco Dairy Business Unit.

Barth, T.J.; Jespersen, D.C. (1989) The Design and Application of Upwind Schemes on Unstructured Meshes. *Technical Report AIAA-89-0366. In: AIAA 27th Aerospace Sciences Meeting, Reno, Nevada*.

Bartzis, J.G.; Vlachogiannis, D.; Sfetsos, A. (2004) Thematic area 5: Best practice advice for environmental flows. The QNET-CFD Network Newsletter 2(4), 34-39.

Bava, L.; Tamburini, A.; Penati, C.; Riva, E.; Mattachini, G.; Provolo, G.; Sandrucci, A. (2012) Effects of feeding frequency and environmental conditions on dry matter intake, milk yield and behaviour of dairy cows milked in conventional or automatic milking systems. *ITAL J ANIM SCI* 11(3), 230-235.

Berg-Munch, B.; Clausen, P.; Fanger, P.O. (1984) Ventilation requirements for the control of body odour in

spaces occupied by women. Proceedings of the 3rd Int. Conference on Indoor Air Quality, Stockholm, Sweden, v. 5.

Bjerg, B.; Norton, T.; Banhazi, T.; Zhang, G.; Bartzanas, T.; Liberati, P.; Cascone, G.; Lee, I.B.; Marucci A. (2013a) Modelling of ammonia emissions from naturally ventilated livestock buildings: Part 1, ammonia release modelling. *Biosyst. Eng.* 116(3), 232-245.

Bjerg, B.; Liberati, P.; Marucci, A.; Zhang, G.; Banhazi, T.; Bartzanas, T.; Cascone, G.; Lee, I.; Norton, T. (2013b) Modelling of ammonia emissions from naturally ventilated livestock buildings: Part 2, air change modelling. *Biosyst. Eng.* 116(3), 246-258.

Bjerg, B.; Cascone, G.; Lee I.; Bartzanas, T.; Norton, T.; Hong, S.; Seo, I.; Banhazi, T.; Liberati, P.; Marucci, A.; Zhang, G. (2013c) Modelling of ammonia emissions from naturally ventilated livestock buildings. Part 3: CFD modelling. *Biosyst. Eng.* 116(3), 259-275.

Blocken, B.; Roels, S.; Carmeliet, J. (2004) Modification of pedestrian wind comfort in the Silvertop Tower passages by an automatic control system. *J WIND ENG IND AEROD* 92, 849-873.

Boussinesq, J. (1877) Essai sur la théorie des eaux courantes, Memoires present par divers savants à l'Académie des Sciences XXIII: 1, 1-680.

Bournet, P.E.; Boulard, T. (2010) Effect of ventilator configuration on the distributed climate of greenhouses: a

review of experimental and CFD studies. *Comput. Electron. Agric.* 94, 47-57.

Bruce, J. M. (1974) Wind tunnel study: Suckler cow building. *Farm Building Progress* 38, 15-17.

Bruce, J. M. (1977) Natural ventilation - Its role and application in the bio-climatic systems. Farm Building R&D Studies.

Bruce, J. M. (1978) Natural convection through openings and its application to cattle building ventilation. *J. Agric. Eng. Res.* 23, 151-167.

Bruce, J. M. (1982) Ventilation of a model livestock building by thermal buoyancy. *Transactions of the American Society of Agricultural Engineers* 25, 1724-1726.

BS 5925 (1980). Code of Practice for Design of Buildings: Ventilation principles and designing for natural ventilation. British Standards Institution, London.

Buffington, D.E.; Collazo-Arocho, A.; Canton, G.H.; Pitt, D.; Thatcher, W.W.; Collier, R.J. (1981) Black globe humidity index (BGHI) as comfort equation for dairy cows. *Trans ASAE* 24, 711-714.

Cain, W.S.; Leaderer, B. P.; Isseroff, R.; Berglund, L.G.; Huey, R.J.; Lipsitt, E.D.; Perlman, D. (1983) Ventilation requirements in buildings. *Atmos Environ* 17(6).

Cascone, G. (1991) Sistemi passivi ed impianti attivi per il controllo ambientale degli edifici per l'allevamento nei paesi a clima caldo. *Medit* 4, 43-52.

Casey, M.; Wintergerste, T. (editors) (2000) ERCOFTAC SIG "Quality and Trust in Industrial CFD": Best Practice Guidelines, ERCOFTAC.

Centre Scientifique et Technique du Batiment (CSTB) (1992). Guide sur la Climatisation naturelle de l'habitat en climat tropical humide – Methodologie de prise en compte des parametres climatiques dens l'habitat et conseils pratiques. Tome 1 (in French). CSTB, 4 Avenue du Recteur Poincarè, 75782 Paris Cedex 16, France.

Chen, F.; Cai, Z.Y.; Wang, F. (2007) Generation and significance of building form under wind environment concept. *Architectural Journal* 7, 29-33.

CIBSE (1997) Natural ventilation in non-domestic buildings. Application manual AM10. London: the Chartered Institution of Building Services Engineers.

Clarke, J.; Hand J.; Strachan P. (1990) ESP – A building and plant energy simulation system. ERSU Manual U90/1, Energy Stimulation Research Unit, Dept. of Mechanical Engineering, University of Strathclyde.

Cook, N.B.; Bennett, T.B.; Nordlund, K.V. (2005) Monitoring indices of cow comfort in free-stall-housed dairy herds. *J Dairy Sci* 88(11), 3876-3885.

Darliel, S.B.; Lane –Serff, G.F. (1991) The Hydraulics of Doorway Exchange Flows. *BUILD ENVIRON* 26(2), 121-135.

Da Silva, R.G.; Guilhermino, M.M.; Morais, D.A.E.F. (2010) Thermal radiation absorbed by dairy cows in pasture. *Int J Biometeorol.* 54, 5-11.

Davis, S.; Mader, T.L. (2003) Adjustments for Wind Speed and Solar Radiation to the Temperature-Humidity Index. *Nebr Beef Cattle Rep* 224.

D'Emilio, A.; Cascone, G.; Lanteri, P.; Porto, S.M.C. (2018) Effects of Different Cooling Systems on Heat Stress and Behaviour of Dairy Cows, CIGR Journal.

De Gidds, W.; Phaff H. (1982) Ventilation Rates and Energy Consumption due to Open Windows. *Air Infiltration Review* 4(1), 4-5.

De Palo, P., Tateo, A., Zezza, F., Corrente, M., Centoducati, P. (2006) Influence of free-stall flooring on comfort and hygiene of dairy cows during warm climatic conditions. *J Dairy Sci* 89, 4583-4595.

DeVries, T.J.; von Keyserlingk, M.A.G.; Weary, D.M.; Beauchemin, K.A. (2003) Technical Note: Validation of a System for Monitoring Feeding Behavior of Dairy Cows. *J Dairy Sci* 86(11), 3571-3574.

Dikmen, S.; Hansen, P.J. (2009) Is the temperature-humidity index the best indicator of heat stress in lactating dairy cows in a subtropical environment? *J Dairy Sci* 92, 109-116.

Di Sabatino, S.; Buccolieri, R.; Pulvirenti, B.; Britter, R. (2007) Simulations of pollutant dispersion within idealised urban-type geometries with CFD and integral models. *ATMOS ENVIRON* 41, 8316-8329.

Down, M.J.; Foster, M.P.; MacMahon, T.A. (1985). The design of livestock buildings for natural ventilation: The theoretical basis and a rational design method. Victoria: University of Melbourne.

Down, M.J.; Foster, M.P.; McMahon, T.A. (1990) Experimental verification of a theory for ventilation of livestock buildings by natural convection. *J. Agric. Eng. Res*. 45, 269-279.

Ernest, D.R. (1991). Predicting Wind-Induced Air Motion, Occupant Comfort and Cooling Loads in Naturally Ventilated Buildings. Phd Thesis, University of California at Berkeley.

Etheridge, D. (2015) A perspective on fifty years of natural ventilation research. *Build Environ* 91, 51-60.

Ferziger, J.H.; Perić, M. (2002) Computational Methods for Fluid Dynamics, Springer Verlag, Berlin Heidelberg New York, 3rd edition.

Feustel, H (1990) Fundamentals of the Multizone Air Flow Model – COMIS (Conjuction of Multizone Infiltration Specialist), AIVC Technical Note 29.

Fiedler, A.; Fischer, J.; Hempel, S.; Saha, C. K.; Loebsin, C.; Berg, W.; Amon, B.; Brunsch, R.; Amon, T. (2014) Flow

fields within a dairy barn - Measurements, physical modelling and numerical simulation. In: International Conference of Agricultural Engineering AgEng 2014, Zurich, Switzerland.

Foken, T. (2006). 50 years of the Monin-Obukhov similarity theory. *Boundary-Layer Meteorology* 119, 431-447.

Foster, M.P.; Down, M.J. (1987) Ventilation of livestock buildings by natural convection. *J. Agric. Eng. Res.* 37, 1-13.

Franke, J.; Hellsten, A.; Schlünzen, H.; Carissimo, B. (2007) Best practice guideline for the CFD simulation of flows in the urban environment. In COST action.

Fregonesi, J. A.; Leaver. J.D. (2001) Behaviour, performance and health indicators of welfare for dairy cows housed in straw yard or cubicle systems. *Livest Sci* 68(2-3), 205-216.

Gan, C.; Salim, S. (2014) Numerical Analysis of Fluid-Structure Interaction between Wind Flow and Trees. *Proc. World Congr. Eng.*

Givonni, B. (1978). L'Homme, l'Architecture et le Climat. Eyrolles, Paris (French Edition).

Gromke, C.; Buccolieri, R.; Di Sabatino, S.; Ruck, B. (2008) Dispersion study in a street canyon with tree planting by means of wind tunnel and numerical investigations - evaluation of CFD data with experimental data. *Atmosph. Environ.* 42, 8640-8650.

Grosso, M. (1992) Wind pressure distribution around buildings: a parametrical model. *ENERG BUILDINGS* 18, 101-131.

Groot Koerkamp, P.W.G.; Metz, J.H.M; Uenk, G.H.; Phillips, V.R.; Holden, M.R.; Sneath, R.W.; Short, J.L.; White, R.P.; Hartung, J.; Seedorf, J.; Schroder, M.; Linkert, K.H.; Pedersen, S.; Takai, H.; Johnsen, J.O.; Whates, C.M. (1998) Concentrations and emissions of ammonia in Livestock buildings in Northern Europe. *J. agric. Engng. Res.* 70, 79-95.

da Graça, G.C.; Linden, P. (2016) Ten questions about natural ventilation of non-domestic buildings. *BUILD ENVIRON*. 107, 263-273.

Guo, W.; Liu, X.; Yuan, X. (2015) Study on Natural Ventilation Design Optimization Based on CFD Simulation for Green Buildings. *Procedia Engineering* 121, 573-581.

Guo, L.; Maghirang, R.G. (2012) Numerical simulation of airflow and particle collection by vegetative barriers. *Eng. Appl. Comput. Fluid Mech*. 6, 110-122.

Gürdil, G. A. K. (2009) Numerical simulation of natural ventilation rates in laying hen houses. *J ANIM VET ADV* 8, 624-629.

Hargreaves, D.M.; Wright, N.G. (2006) On the use of the k-Ɛ model in commercial CFD software to model the neutral atmospheric boundary layer, J WIND ENG IND AEROD.

Hawendi, S.; Gao, S. (2017) Impact of an external boundary wall on indoor flow field and natural cross-ventilation in an isolated family house using numerical simulations. *Journal of Building Engineering* 10.

He, X.; Wang, J.; Guo, S.; Zhang, J.; Wei, B.; Sun, J.; Shu, S. (2018) Ventilation optimization of solar greenhouse with removable back walls based on CFD, *Comput. Electron. Agric.* 149, 16-25.

Hempel, S.; Saha, C.K.; Fiedler, M.; Berg, W.; Hansen, C.; Amon, B.; Amon, T. (2016) Non-linear temperature dependency of ammonia and me-thane emissions from a naturally ventilated dairy barn. *Biosyst. Eng.* 145, 10-21.

Herbut, P., Angrecka, S., Godyń, D. (2018) Effect of the duration of high air temperature on cow's milking performance in moderate climate conditions. *Ann Anim Sci.* 18(1), 195–207.

Hirsch, C.; Bouffioux, V.; Wilquem F. (2002) CFD simulation of the impact of new buildings on wind comfort in an urban area, in G. Augusti, C. Borri, and C. Sacré, editors, Impact of Wind and Storm on City life and Built Environment, Proceedings of the Workshop, 164-171, CSTB, Nantes.

Hogstrom, U. (1988). Non-dimensional wind and temperature profiles in the atmospheric surface layer-a re-evaluation. *Boundary Layer Meteorology* 42, 55-78.

Hogstrom, U. (1996). Review of some basic characteristics of the atmospheric surface layer. *Boundary-Layer Meteorology* 78, 215-246.

Hong, SW; Exadaktylos, V; Lee, I.B.; Amon, T.; Youssef, A.; Norton, T; Berckmans, D. (2017) Validation of an open source CFD code to simulate natural ventilation for agricultural buildings, *Comput. Electron. Agric.* 138, 80-91.

Horan, J.M.; Finn, D.P. (2008) Sensitivity of air change rates in a naturally ventilated atrium space subject to variations in external wind speed and direction. *ENERG BUILDINGS* 40, 1577-1585.

Jeanjean, A. P. R.; Hinchliffe, G.; McMullan, W. A.; Monks, P. S.; Leigh, R. J. (2015) A CFD study on the effectiveness of trees to disperse road traffic emissions at a city scale. *Atmos. Environ.* 120, 1-14.

Janssen J.E.; Woods, J.E.; Hill, T.J.; Maldonado, E. (1982) Ventilation for control of indoor air quality: a case study. *ENVIRON INT.* 8.

Janssen, J.E. (1986) Ventilation for acceptable indoor air quality. Proceedings of CIBSE/ASHRAE Conference: The Engineered Environment. Dublin, Ireland.

Jones, T.A. (2006) MATLAB functions to analyze directional (azimuthal) data - I: single-sample inference. *Computational Geoscience* 32, 166-175.

Khodr Mneimne, H. (1990) Transferts Thermo-aerouliques entre Pieces à travers les grandes ouvertures. PhD Thesis, Nice University.

Knapp J.R.; Laur, G.L.; Vadas, P.A.; Weiss, W.P.; Tricarico, J.M. (2014) Invited review: enteric methane in dairy cattle production: quantifying the opportunities and impact of reducing emissions. *J. Dairy Sci.* 97(6), 3231-3261.

Launder, B.E.; Spalding, D.B. (1974) The numerical computation of turbulent flows. *Comput. Methods Appl. Mech. Eng.* 3, 269-289.

Liberati, P.; Zappavigna, P.A. (2007) Dynamic computer model for optimization of the internal climate in swine housing design. Transactions of the ASABE 50(6), 2179-2188.

Limam, K.; Innard, C.; Allard, F. (1991) Etude Experimentale des Transferts de masse et de chaleur a travers les grandes ouvertures verticals. Conference Groupe d'Etude de la Ventilation et du Renouvellement d'Air, INSA, Lyon, 98-111.

Linden, P.F. (1999) The fluid mechanics of natural ventilation, *Annu. Rev. Fluid Mech.* 31, 201-238.

Melaragno, M. (1982) Wind in Architectural and Environmental Design. Van Nostrand Reinhold, New York.

Menter, F.; Hemstrom, B.; Henrikkson, M.; Karlsson, R.; Latrobe, A.; Martin, A.; Muhlbauer, P.; Scheuerer, M.; Smith, B.; Takacs, T.; Willemsen, S. (2002) CFD Best Practice Guidelines for CFD Code Validation for Reactor-

Safety Applications, Report EVOLECORA- D01, Contract No. FIKS-CT-2001-00154.

Montazeri, H.; Montazeri, F. (2018) CFD simulation of cross-ventilation in buildings using rooftop wind catchers: Impact of outlet openings. *RENEW ENERG.*, 502-520.

Norton, T.; Sun, D.W.; Grant, J.; Fallon, R.; Dodd, V. (2007) Applications of computational fluid dynamics (CFD) in the modelling and design of ventilation systems in the agricultural industry: A review. *Bioresour Technol.* 98(12), 2386-414.

Norton, T.; Grant, J.; Fallon, R.; Sun, D.W. (2009) Assessing the ventilation effectiveness of naturally ventilated livestock buildings under wind dominated conditions using computational fluid dynamics. *Biosyst. Eng.* 103(1), 78-99.

Norton, T.; Grant, J.; Fallon, R.; Sun, D.W. (2010) Assessing the ventilation performance of a naturally ventilated livestock building with different eave opening conditions. *Comput. Electron. Agric.* 71(1), 7-21.

Omrani, S; Garcia-Hansen, V.; Capra, B.; Drogemuller, R. (2017) Natural ventilation in multi-storey buildings: Design process and review of evaluation tools. *BUILD ENVIRON*. 116, 182-194.

Overton, M.W.; Sischo, W.M.; Temple, G.D.; Moore, D.A. (2002) Using time-lapse video photography to assess dairy cattle lying behavior in a free-stall barn. *J Dairy Sci* 85(9), 2407-2413.

Pelletret, R.; Allard, F.; Haghigat, F.; Van der Maas, J., (1991) Modeling of large openings. In: Proceedings of the 12th AIVC Conference, Canada, AIVC, University of Warwick.

Perén, J.I.; vah Hooff, T.; Leite, B.C.C.; Blocken, B. (2015) CFD analysis of cross-ventilation of a generic isolated building with asymmetric opening positions: Impact of roof angle and opening location. *BUILD ENVIRON.* 85, 263-276.

Powell, J.M.; Broderick, G.A.; Misselbrook, T.H. (2008a). Seasonal diet affects ammonia emissions from tie-stall dairy barns. *J. Dairy Sci.* 91(2), 857-869.

Powell, J.M.; Misselbrook, T.H.; Casler, M.D. (2008b). Season and bedding impacts on ammonia emissions from tie-stall dairy barns. *J. Environ. Qual.* 37(1), 7-15.

Provolo, G.; Riva, E. (2009) One year study of lying and standing behaviour of dairy in frestall barn in Italy. J. *agric. eng.* 40(2), 27-33.

Ramponi, R.; Blocken B. (2012) CFD simulation of cross-ventilation for a generic isolated building: impact of computational parameters. *BUILD ENVIRON* 53, 34-48.

Richards, P.J.; Hoxey, R.P. (1993) Appropriate boundary conditions for computational wind engineering models using the k-ε turbulence model. *Computational Wind Engineering* 1, 145-153.

Roache, P.J. (1994) Perspective: a method for uniform reporting of grid refinement studies. *J. Fluids Eng. Trans.* ASME 116(3), 405-413.

Rong, L.; Liu, D.; Pedersen, E.F.; Zhang, G. (2015) The effect of wind speed and direction and surrounding maizeon hybrid ventilation in a dairy cow building in Denmark. *ENERG BUILDINGS* 86, 25-34.

Rong, L.; Bjerg, B.; Batzanas, T.; Zhang, G. (2016) Mechanisms of natural ventilation in livestock buildings: Perspectives on past achievements and future challenges. *Biosyst. Eng.* 151, 200-217.

Rong, L.; Nielsen, P.V.; Bjerg, B.; Zhang, G. Summary of best guidelines and validation of CFD modeling in livestock buildings to ensure prediction quality. *Comput. Electron. Agric.* 121, 180-190.

Santamouris, M. (1992) Natural Convection Heat and Mass Transfer throught large openings - Internal report, PASCAL Research Program, European Commission DGX11.

Santamouris, M.; Alvarez, S.; Daskalaki, E.; Guarracino, G.; Maldonado, E.; Sciuto, S.; Vandaele, L. (1998) Natural ventilation in buildings: a design handbook. Science Publisher Ltd, 35-37 William Road, London NW1 3ER, UK.

Sapounas, A.; Dooren, H.J.C.; Smits, M.C.J. (2013) Natural Ventilation of Commercial Dairy Cow Houses: Simulating the Effect of Roof Shape Using CFD, In: Proceedings of the 1st IS on CFD Applications in Agriculture, 221 - 228.

Scaperdas, A.; Gilham, S. (2004) Thematic Area 4: Best practice advice for civil construction and HVAC, The QNET-CFD Network Newsletter 2(4), 28-33.

Seo, I.H.; Lee, I.B.; Moon, O.K.; Kim, H.T.; Hwang, H.S.; Hong, S.W.; Bitog, J.P.; Yoo, J.I.; Kwon, K.S.; Kim, Y.H.; Han, J.W. (2009) Improvement of the ventilation system of a naturally ventilated broiler house in the cold season using computational simulations. *Biosyst. Eng.* 104(1), 106-117.

Schrade, S.; Zeyer, K.; Gygax, L.; Emmenegger, L.; Hartung, E.; Keck, M. (2012) Ammonia emissions and emission factors of naturally ventilated dairy housing with solid floors and an outdoor exercise area in Switzerland. *Atmos Environ* 47, 183-194.

Schlichting, H. (1979) Boundary Layer Theory, McGraw-Hill, New York, 7th ed., 578-595.

Schlünzen, K.H. (1997) On the validation of high-resolution atmospheric mesoscale models. J. *Wind Engineering and Industrial Aerodynamics* 67-68, 479-492.

Shen, X.; Zhang, G.; Wu, W.; Bjerg, B. (2013) Model-based control of natural ventilation in dairy buildings. *Comput. Electron. Agric.* 94, 47-57.

Shioya, S., Terada, F., Iwama, Y. (1997) Physiological responses of lactating dairy cows under hot environments. Eiyoseirikenkyukaiho 41(2), 61-68.

Shuzo, M. (2007) CFD and Building Environment Design, Beijing: China Architecture & Building Press.

Dati SIAS (2016): www.sias.regione.sicilia.it http://www.sias.regione.sicilia.it/frameset_dati.htm

Steinfeld, H.; Pierre, G.; Wassenaar, T.; Castel, V.; Rosales, M.; de Haan, C. (2006) Livestock's 1872 Long Shadow. *Environmental issues and options, FAO*.

Sullivan, R.; Greeley, R. (1993) Comparison of aerodynamic roughness measured in a field experiment and in a wind tunnel simulation. *J WIND ENG IND AEROD* 48(1), 25-50.

Tiller, T.R. (1973) ASHRAE Transactions, v. 79.

Valenti, F.; Porto, S.M.C.; Tomasello, N.; Arcidiacono, C. (2018) Enhancing Heat Treatment Efficacy for Insect Pest Control: A Case Study of a CFD Application to Improve the Design and Structure of a Flour Mill. *Buildings* 8(48), 1-18.

VDI 3783 Part 9: 2005, Environmental meteorology – Prognostic microscale wind field models – Evaluation for flow around buildings and obstacles. Beuth Verlag, Berlin.

Wathes, C.M.; Charles, D.R. (1994) Air and Surface Hygiene. Livestock Housing, *CAB International, Wallingford*, 123-148

Wathes, C.M.; Demmers, T.G.M.; Xin, H. (2003) Ammonia concentrations and emissions in livestock production facilities: guidelines and limits in the USA and UK. In: Proceeding of 2003 ASAE Annual International Meeting, Las Vegas, Nevada, USA, 27-30 July 2003.

Wieringa, J. (1992) Updating the Davenport roughness classification. *J WIND ENG IND AEROD,* 357-358.

Wu, W.; Zhai, J.; Zhang G.; Nielsen, P.V. (2012) Evaluation of methods for determining air exchange rate in a naturally ventilated dairy cattle building with large openings using computational fluid dynamics (CFD). *Atmos. Environ.* 63, 179-188.

Yang, L.; Ye, M.; He, B.J. (2014) CFD simulation research on residential indoor air quality. *Sci Total Environ* 472, 1137-1144.

Zhang, Y. (1999) Engineering control of dust in animal facilities. In: Proceedings of Dust Control in Animal Production Facilities.

Zhang, Z.; Zhang, W.; Zhai, Z.; Chen, Q. (2007) Evaluation of various turbulence models in predicting airflow and turbulence in enclosed environments by CFD: Part-2—Comparison with experimental data from literature. *HVAC&R Res.* 13, 871-886.

Zhiqiang, Z.; Mankibib, M.; Zoubirb, A. (2015) Review of natural ventilation models, *Energy Procedia* 78, 2700-2705.